



Department of Pure and Applied Chemistry

**Peptide Nanomaterials: Characterisation of Enzyme-Assisted
Self-Assembly**

By

Meghan Hughes

A thesis is presented to the Department of Pure and Applied Chemistry, University of Strathclyde, in fulfilment of the requirements for the degree of Doctor of Philosophy.

2012

This thesis is the result of the author's original research. It has been composed by the author and has not been previously submitted for examination which has led to the award of a degree. The copyright of this thesis belongs to the author under the terms of the United Kingdom Copyright Acts as qualified by University of Strathclyde Regulation 3.50. Due acknowledgement must always be made of the use of any material contained in, or derived from, this thesis.

Signed:

Date:

Acknowledgements

I would like to take this opportunity to thank everyone who helped with the work described in this thesis. In particular, I would like to thank Pim W.J.M. Frederix, Daniel Cannon and Dr. Tell Tuttle for providing molecular modelling, Dr. Neil T. Hunt for his invaluable expertise with regards to FTIR analysis; Dr. Louise S. Birchall for synthesis and help with analysis of Fmoc-Yx-OMe; Dr. Sisir Debnath for synthesis of phosphorylated Fmoc-Yx-OH precursors; Christopher Hamilton for allowing me to use fluorescence microscope in the Dept. of Bioengineering; Dr. Laurence Tetley and Margaret Mullen for TEM imaging; Dr. Fiona C. Coomer and Dr. Edmund Cussen for the use of the XRD; Stephen Furzeland and Derek Aitken for the use of their cryoTEM; Dr. Dave J. Adams and Jacklyn Raeburn for their hospitality, use of and guidance with the rheometer, and; Dr. Charles Knapp for providing E.coli samples and allowing me to use all the equipment in his lab.

Thank you to all the members of the Ulijn group, past and present – your chemistry chats and motivational talks have been invaluable. I would particularly like to acknowledge all those who have helped me keep my sanity over the years, Dr. Louise Birchall, Lynsey A. Aitken, Pim W.J.M. Frederix, Dr. Jan W. Sadownik and Pier F. Caponi.

Thanks to all my family and friends for their emotional and financial support over the last few years; particularly, my parents, Ellis, Lauren, Kieran, Jordon, Malcolm and Antonia.

Finally, I would like to thank Prof. Rein V. Ulijn for giving me this opportunity. His time, guidance, support and enthusiasm throughout the last three and a half years have been invaluable.

Abstract

Aromatic peptide amphiphiles have emerged as molecular building blocks which form a variety of supramolecular peptide nanostructures by molecular self-assembly. These are short peptide chains, generally less than five amino acids in length, chemically modified at the N-terminus with an aromatic group to aid assembly. In aqueous environments, they form supramolecular structures by π -stacking of aromatic moieties and hydrogen bonding between peptide chains, typically in a β -sheet fashion, with additional stabilisation possible from the amino acid side chains. Enzymes have been employed to control the assembly process by converting non-assembling precursors into self-assembling molecules, thus initiating molecular self-assembly. Variation of the peptide sequence has allowed for access to a range of nanoscale architectures including tubes, fibres,^{1, 2} twisted ribbons, tapes, sheets, spheres and rings. The morphology is influenced by both the route of assembly and the amino acid sequence within the peptide chain. Therefore, by understanding the amino acid sequence/structure relationships, may allow rational design and tailoring of the materials for purpose.

By utilising thermolysin triggered self-assembly of Fmoc-SF-OMe by condensation of the amino acid precursors, a system which operates under thermodynamic control, the production of the first micron sized two-dimensional peptide nanostructures from chiral molecular building blocks was demonstrated. The lateral self-assembly is enabled by the reversible nature of the system, favouring the thermodynamic product (extended sheets) over kinetically favoured 1 dimensional structures. Furthermore, the use of a fully reversible system allows for the thermodynamically favoured product to be formed reproducibly. In turn, by direct comparison of four self-assembling aromatic peptide amphiphiles, Fmoc-SF-OMe, Fmoc-SL-OMe, Fmoc-TF-OMe and Fmoc-TL-OMe, it is possible to monitor the influence of small changes in the molecular structure within the peptidic tail on nanoscale architecture.

As the hydrophobic effect is known to be a major driving force in molecular self-assembly, typically aromatic peptide amphiphiles have been designed to be hydrophobic in nature, and contain aromatic amino acid residues. In order to introduce a new chemical functionality to peptide nanostructures, terminating hydrophilic amino acid residues are

introduced to the peptide chain. Subtilisin triggered self-assembly of Fmoc-YT-OH, Fmoc-YS-OH, Fmoc-YN-OH and Fmoc-YQ-OH is monitored in order to rationalise the influence of different amino acid residues within the peptide chain on nanoscale structure.

Finally, as the enzymes employed to triggered self-assembly are present in biological systems, it was possible to convert non-assembling precursors into self-assembling aromatic peptide amphiphiles *in vivo*. *E. Coli* was cultured with an over expression of the enzyme alkaline phosphatase. By addition of the self-assembly precursors, it was then possible to monitor the anti-microbial effects of five different aromatic peptide amphiphiles; Fmoc-FY-OH, Fmoc-YT-OH, Fmoc-YS-OH, Fmoc-YN-OH and Fmoc-YQ-OH. A differential anti-microbial response was observed for *E. Coli* after treatment with the aromatic peptide amphiphiles.

Contents

Acknowledgements	III
Abstract	IV
Contents	VI
1.0 Introduction	1
1.1 Introduction to thesis	2
1.2 Motivation of the project	3
1.3 Layout of the thesis	3
2.0 Literature Review	6
2.1 Peptide Nanostructures	7
2.2 Generating Nanomaterials	7
2.3 Peptide Design	8
2.3.1 Creating the chain – Using amino acids as building blocks	8
2.3.2 Supramolecular Assembly	10
2.3.3 Chemical Modification to Aid Assembly	14
2.3 Desgined Peptide Nanomaterials	15
2.3.1 β -sheet Assemblies	15
2.3.2 β -hairpins	17
2.3.3 α -helical and coiled coils	17
2.3.4 Peptide Amphiphiles	19
2.3.5 Aromatic Peptide Amphiphiles	20
2.4 Self-Assembly On Cue	21
2.5 Biocatalytic Self-Assembly of Aromatic Peptide Amphiphiles	22
2.5.1 Enzyme Controlled Self-Assembly of Aromatic Peptide Amphiphiles	23
2.5.2 Enzyme Controlled Disassembly of Peptide Hydrogels	28
2.6 Kinetic Vs Thermodynamic Control of Enzyme Assisted Self-Assembly	30
2.6.1 Self-Assembly Under Kinetic Control	30
2.6.2 Self-Assembly Under Thermodynamic Control	32
2.7 Spatiotemporal Control Over Nucleation and Structure Growth	33
3.0 Biocatalytic Self-Assembly of 2D Peptide-Based Nanostructures	34
3.1 Introduction	35
3.1.1 Background	35
3.1.2 Thermolysin and Reversed Hydrolysis	36
3.2 Results and Discussion	38
3.2.1 Preparation of Fmoc-SF-OMe	38
3.2.2 Nanoscale Morphology	39
3.2.3 Molecular Association	42
3.2.4 Molecular Modelling	46
3.2.5 Hierarchical Assembly	49
3.3 Conclusions	51

4.0 Sequence/structure relationships in aromatic dipeptide hydrogels formed under thermodynamic control by enzyme-assisted self-assembly	53
4.1 Introduction	54
4.1.1 Background	54
4.2 Results and discussion	55
4.2.1 Composition	55
4.2.2 Nanoscale Morphology	57
4.2.3 Mechanical Properties	58
4.2.4 Supramolecular Structure	60
4.2.5 Molecular Modelling	64
4.3 Conclusions	65
5.0 Differential supramolecular organisation of Fmoc-dipeptides with hydrophilic terminal amino acid residues by biocatalytic self-assembly	67
5.1 Introduction	68
5.1.1 Background	68
5.1.2 Subtilisin and Ester Hydrolysis	69
5.2 Results and Discussion	71
5.2.1 Composition	71
5.2.2 Supramolecular structure	73
5.2.3 Nanoscale Morphology	76
5.2.4 Mechanical Properties	78
5.2.5 Characterisation of the thermodynamically favoured state	80
5.3 Conclusions	84
6.0 Differential antimicrobial properties of enzymatically triggered self-assembling aromatic peptide amphiphiles <i>in vivo</i>	86
6.1 Introduction	87
6.1.1 Background	88
6.1.2 Alkaline Phosphatase	88
6.2 Results and Discussion	90
6.2.1 <i>In vitro</i> self-assembly studies of alkaline phosphatase triggered self-assembly of Fmoc-FY-OH	90
6.2.2 <i>In vivo</i> alkaline phosphatase triggered self-assembly of Fmoc-FY-OH using <i>E. Coli</i>	92
6.2.3 <i>In vitro</i> self-assembly studies of alkaline phosphatase triggered self-assembly of Fmoc-Yx-OH	96
6.2.4 Monitoring differential anti-microbial response <i>In vivo</i> of alkaline phosphatase triggered self-assembly of Fmoc-Yx-OH using <i>E. Coli</i>	99
6.3 Conclusions	101
7.0 Conclusions and Future Work	103
7.1 Conclusions	104
7.2 Future Work	105
8.0 Materials and Methods	107

8.1 Methods and Materials associated with the study of Fmoc-SF-OMe (discussed in chapter 3.0)	108
8.1.1 Thermolysin catalysed condensation of amino acid residues to form Fmoc-SF-OMe	108
8.1.2 Monitoring the conversion of Fmoc-S to Fmoc-SF-OMe using HPLC	108
8.1.3 Fluorescence	108
8.1.4 Infra-red spectroscopy	108
8.1.5 WAXS	109
8.1.6 TEM	109
8.1.7 CryoTEM	109
8.1.8 Optical Microscopy	109
8.1.9 Synthesis of Fmoc-SF-OMe	110
8.1.10 Computer Modelling	111
8.2 Methods and Materials associated with the comparative study of thermolysin catalysed self-assembly of Fmoc-SF-OMe, Fmoc-SL-OMe, Fmoc-TF-OMe and Fmoc-TL-OMe (discussed in chapter 4.0)	111
8.2.1 Thermolysin catalysed condensation of amino acid fragments	111
8.2.2 Monitoring the conversion of amino acid fragments to Fmoc-dipeptide using HPLC	111
8.2.3 Fluorescence Spectroscopy	112
8.2.4 FTIR Spectroscopy	112
8.2.5 TEM	112
8.2.6 CryoTEM	112
8.2.7 WAXS	113
8.2.8 Rheometry	113
8.2.9 Computer modeling	113
8.3 Methods and Materials associated with the comparative study of subtilisin catalysed self-assembly of Fmoc-YT-OH, Fmoc-YS-OH, Fmoc-YN-OH and Fmoc-YQ-OH (discussed in chapter 5.0)	114
8.3.1 General reagents and analytical methods used in the synthesis of non-assembling precursors	114
8.3.2 Synthesis of Fmoc-YS-OMe	114
8.3.3 Synthesis of Fmoc-YT-OMe	115
8.3.4 Synthesis of Fmoc-YN-OMe	116
8.3.4 Synthesis of Fmoc-YQ-Ome	118
8.3.5 Subtilisin catalysed hydrolysis of Fmoc-peptide methyl ester protected starting materials	119
8.3.6 Reaction progress by HPLC	119
8.3.7 Fluorescence spectroscopy	120
8.3.8 Circular dichroism	120
8.3.9 Infra-red spectroscopy	120
8.3.10 Rheology	120
8.3.11 Transmission electron microscopy	121
8.3.12 Dynamic light scattering	121
8.3.13 Heat/Cool Cycles	122

8.4 Methods and materials associated with the comparative <i>In vivo</i> studies of alkaline phosphatase catalysed self-assembly of aromatic peptide amphiphiles (discussed in chapter 6.0).	122
8.4.1 Synthesis of Fmoc-YpT-OH	122
8.4.2 Synthesis of Fmoc-YpS-OH	123
8.4.3 Synthesis of Fmoc-YpN-OH	124
8.4.4 Synthesis of Fmoc-YpQ-OH	126
8.4.5 alkaline phosphatase catalysed dephosphorylation of phosphorylated Fmoc-dipeptide protected starting materials <i>in vitro</i>	127
8.4.6 Reaction progress by HPLC analysis (<i>in vitro</i> studies)	127
8.4.7 Fluorescence	127
8.4.8 Infra-Red Spectroscopy	128
8.4.9 Transmission electron microscopy (<i>in vitro</i> studies)	128
8.4.10 Preparation of the E.Coli MC-1000 stock solution	128
8.4.11 Preparation of Growth Medium	129
8.4.12 Preparation of E.Coli MC-1000 Cultures	130
8.4.13 <i>E.Coli</i> Growth Curves	130
8.4.14 Alkaline Phosphatase Activity Assay	130
8.4.15 Sample preparation for HPLC monitoring the reaction progress <i>in vivo</i>	131
8.4.15 Reaction progress <i>in vivo</i> using HPLC	131
8.4.15 Live/Dead® cell staining	132
8.4.16 Transmission electron microscopy (<i>in vivo</i> studies)	132
9.0 References	134
9.1 References	135
Appendices	146
List of abbreviations	146
List of amino acid abbreviations	148

1.0 Introduction*

* The work in this Chapter has been published, in part, to Soft Matter for publication,^{3,4} and submitted, in part, for publication in Soft Matter and Chemical Communications.

Declaration of contribution to published and submitted articles:

Any reproduced work from the aforementioned published and submitted articles, I was solely responsible for, including the written article itself, unless otherwise stated. Dr. Tell Tuttle and Pim. W.J.M. Frederix provided the molecular modelling data.

1.1 Introduction to thesis

In recent years, peptide based nanostructures have emerged as new research materials with potential applications in templating,^{5,6} cell scaffolding,^{1,7} nano-electronics^{8,9} and drug delivery.¹⁰⁻¹² By design, the peptides self-assemble *via* electrostatic interactions, hydrogen bonding and hydrophobic interactions,¹³⁻¹⁵ to mimic basic conformational protein folding units such as β -sheets¹⁶⁻²⁴ and α -helices,²⁵⁻²⁹ resulting in supramolecular structures with novel nanoscale architectures.

One class of peptide based nanostructures that show substantial morphological changes depending on the amino acid sequence are aromatic peptide amphiphiles. These are short peptide chains, generally less than five amino acids in length, chemically modified at the N-terminus with an aromatic group to aid assembly. In aqueous environments, they form supramolecular structures by π -stacking of aromatic moieties and hydrogen bonding between peptide chains, typically in a β -sheet fashion, with additional stabilisation possible from the amino acid side chains.³⁰⁻⁴⁰

In order to control the assembly process, enzymes have been employed to convert non-assembling precursors into self-assembling molecules.^{10, 41-54} In these systems, the enzymatic turnover can dictate the delivery of self-assembling molecules to the supramolecular structure,^{47, 55} typically leading to kinetically trapped, non-equilibrium structures that may be highly ordered,⁴⁷ with mechanical properties being controlled by changing enzyme concentration within the system.⁵⁶⁻⁵⁸

Complementary to these kinetically controlled systems, is a thermodynamically driven approach. Here, the isolated enzymatic reaction is thermodynamically unfavoured, however the free energy change associated with molecular self-assembly of aromatic peptide amphiphiles will favour the formation of molecular building blocks. This results in a system where self-assembly and formation of the self-assembling building blocks are coupled, in turn, systems that are fully reversible and under thermodynamic control.^{52, 59}

A variety of nanoscale architectures have become accessible, including tubes,^{16, 30, 31, 33, 60} fibres,^{1, 2} twisted ribbons,^{4, 21} tapes,^{8, 47} sheets,³ spheres⁶¹ and rings,⁶² with their morphology influenced by both the route of assembly and the amino acid sequence within the peptide chain.^{47, 63-65}

1.2 Motivation of the project

The motivation of this research was to fully characterise enzymatically triggered self-assembly of aromatic peptide amphiphiles. With a large number of morphologies becoming increasingly apparent, understanding the amino acid sequence/structure relationships, may allow rational design and tailoring of the materials for purpose.

1.3 Layout of the thesis

The thesis is split into separate Chapters. Firstly, an extensive literature review of peptide nanomaterials which becomes increasingly focused on enzymatically triggered self-assembly of aromatic peptide amphiphiles.

Each of the experimental Chapters are presented separately, each with its own introduction, results and conclusion sections. The Chapters are separated in this manner to allow readers to consult individual Chapters.

The first experimental Chapter (3.0) investigates the self-assembled structure of Fmoc-SF-OMe biocatalytically triggered by condensation of amino acid fragments using thermolysin. This particular aromatic peptide amphiphile was chosen as it was observed to be the most thermodynamically stable product from a dynamic combinatorial library study carried out by Das *et al.* in 2009.⁵² The self-assembled architecture was found to be sheet like structures which expanded in two dimensions - extremely rare as the amino acid chirality favours helical structures due to an amplification of the molecular chirality, and nucleation-growth mechanisms usually favour uni-directional growth (see Figure 1.1).³

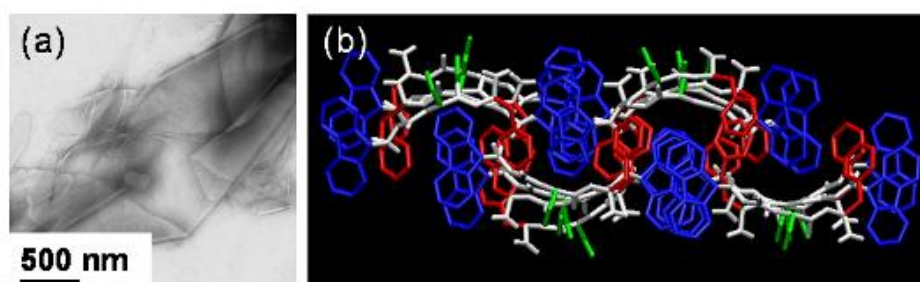


Figure 1.1 – (a) Fmoc-SF-OMe self-assembles to form sheet like structures. (b) Molecular model of the self-assembled aromatic peptide amphiphiles.

Formed under thermodynamic control using thermolysin as an enzymatic trigger for molecular self-assembly, Chapter 4.0 is a compare/contrast study of four closely related self-assembling aromatic peptide amphiphiles; Fmoc-SF-OMe, Fmoc-SL-OMe, Fmoc-TF-OMe and Fmoc-TL-OMe. As the reaction is fully reversible, and therefore self-correcting, the resulting nanostructures will be the thermodynamic minimum. This allows for direct comparison of the peptidic tail, and elucidation of amino acid sequence/structure relationships (see Figure 1.2).⁴

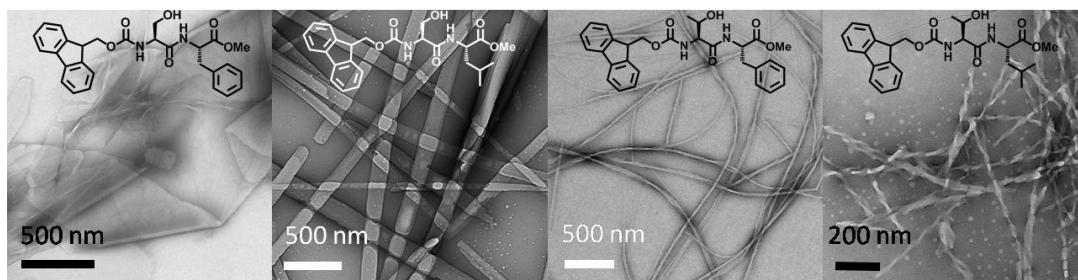


Figure 1.2 - TEM images of self-assembled Fmoc-SF-OMe, Fmoc-SL-OMe, Fmoc-TF-OMe and Fmoc-TL-OMe (from left to right). Inset, molecular structure of each aromatic peptide amphiphile.

Following on, Chapter 5.0 contains a second compare/contrast study of four closely related aromatic peptide amphiphiles; Fmoc-YT-OH, Fmoc-YS-OH, Fmoc-YN-OH and Fmoc-YQ-OH. In this Chapter it was possible to monitor the effects of interchanging the terminating amino acid residues with those of a similar chemical functionality. As these systems are triggered using subtilisin, they operate under kinetic control and therefore the study is of kinetically trapped aggregates. In order to compensate for this, repeating heat/cool cycles are introduced in order to access the thermodynamically preferred state, and the systems re-analysed to assure that the conclusions drawn were correct (see Figure 1.3).

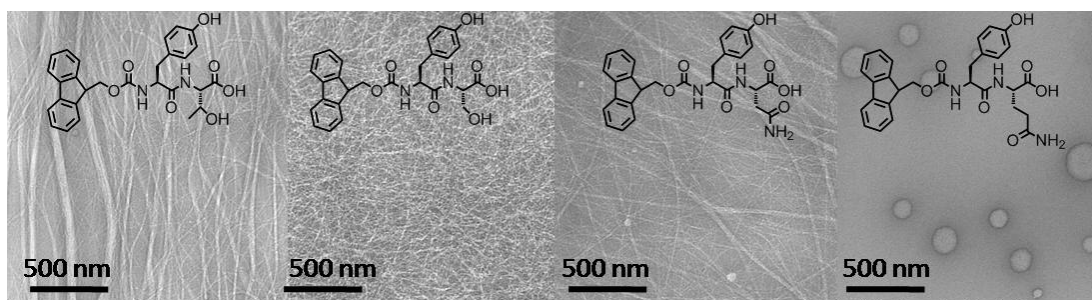


Figure 1.3 – TEM images of self-assembled Fmoc-YT-OH, Fmoc-YS-OH, Fmoc-YN-OH and Fmoc-YQ-OH (from left to right). Inset, molecular structure of the aromatic peptide amphiphile.

The final experimental Chapter, Chapter 6.0, is a study of enzymatically triggering the production of self-assembling aromatic peptide amphiphiles *in vivo*. Growth conditions of *E. Coli* cultures are manipulated to over-express alkaline phosphatase within the bacterial cells. The cultures were then treated with phosphorylated precursors of Fmoc-FY-OH, Fmoc-YT-OH, Fmoc-YS-OH, Fmoc-YN-OH and Fmoc-YQ-OH, with chemical conversion to the self-assembling aromatic peptide amphiphiles. Furthermore, cell viability was monitored after treatment with the peptide derivatives and a differential anti-microbial properties were observed for each system (see Figure 1.4).

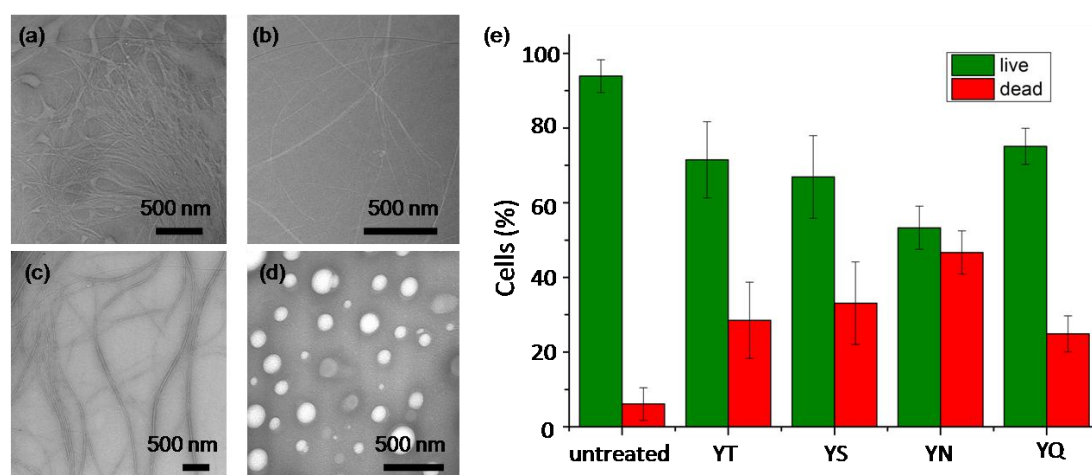


Figure 1.4 – TEM images of self assembled (a) Fmoc-YT-OH, (b) Fmoc-YS-OH, (c) Fmoc-YN-OH and (d) Fmoc-YQ-OH. (e) The differential anti-microbial properties on *E. Coli* after treatment with either Fmoc-YT-OH, Fmoc-YS-OH, Fmoc-YN-OH or Fmoc-YQ-OH.

This is followed by an overall conclusion which lists the highlights of the research within the reported work, and the final Chapter contains all the methodologies for the work contained herein.

2.0 Literature Review*

* The work in this Chapter has been published, in part, to Soft Matter for publication,^{3,4} and submitted, in part, for publication in Soft Matter and Chemical Communications.

Declaration of contribution to published and submitted articles:

Any reproduced work from the aforementioned published and submitted articles, I was solely responsible for, including the written article itself, unless otherwise stated.

2.1 Peptide Nanostructures

Polypeptides and nanostructures are key biomolecular building blocks. In their 'natural' environment, they provide a number of critical roles including structural components of cells, act as catalysts for biotransformations, and act as intra cellular messengers, to name a few. Their function is reliant on their ability to self-assemble, a process known as protein folding. Driven by the formation of intramolecular interactions, the folding process results in precisely-defined secondary, tertiary and quaternary structure, which is usually critical to their function. By utilising key protein folding signatures as a basis for their design, *de novo* designed or synthetic peptide nanostructures were pioneered in the early 1990's Ghadiri *et al.*¹⁶ and Zhang *et al.*,¹⁷ and quickly became a popular area of research. The desirability comes from their rich chemical and structural diversity that can be achieved, in combination with the possibility to effectively interface with biological systems.⁶⁶⁻⁶⁸ As a direct result, the novel nanoscale architectures generated can be applied in a wide variety of areas, such as templating,^{5, 6} nano-electronics,^{8, 9} cell scaffolding,^{1, 7} and drug delivery.¹⁰⁻¹²

2.2 Generating Nanomaterials

Traditionally, top-down approaches have been applied to the production of nanostructures. This is essentially a process of miniaturisation whereby existing pieces are removed, etched, carved or moulded from a larger bulk material.⁶⁹⁻⁷³ However, as the limits of miniaturisation are approached, with nanoscale materials at the limits of the ability to etch, there may be poor control over the nanoscale features.^{13, 70} Furthermore, there is a strong link between cost and size of the intended product due to high machine cost and complexities, contamination, physical limits, and material damage when employing top-down procedures.⁷³ Drawing inspiration from nature, the obvious solution would be to utilise bottom up approaches, whereby synthesis of nanomaterials can be controlled to intentionally tailor size, shape and surface for particular functions.⁶⁹ The route of assembly to form nanostructures may be of any means whereby discrete precursors may be linked together.⁶⁹ In the case of peptide nanostructures, a bottom up approach requires synthesis of self-assembling peptide chains, which consequently form nanostructures by supramolecular assembly of the molecular building blocks.¹³

2.3 Peptide Design

2.3.1 Creating the chain – Using amino acids as building blocks

The rich chemical diversity of peptide nanostructures is owed to the simplest of building blocks within the peptide chain – the amino acid. There are 20 gene-encoded amino acids (see Figure 2.1), with an infinite number of non-natural amino acid residues readily available.⁷⁴

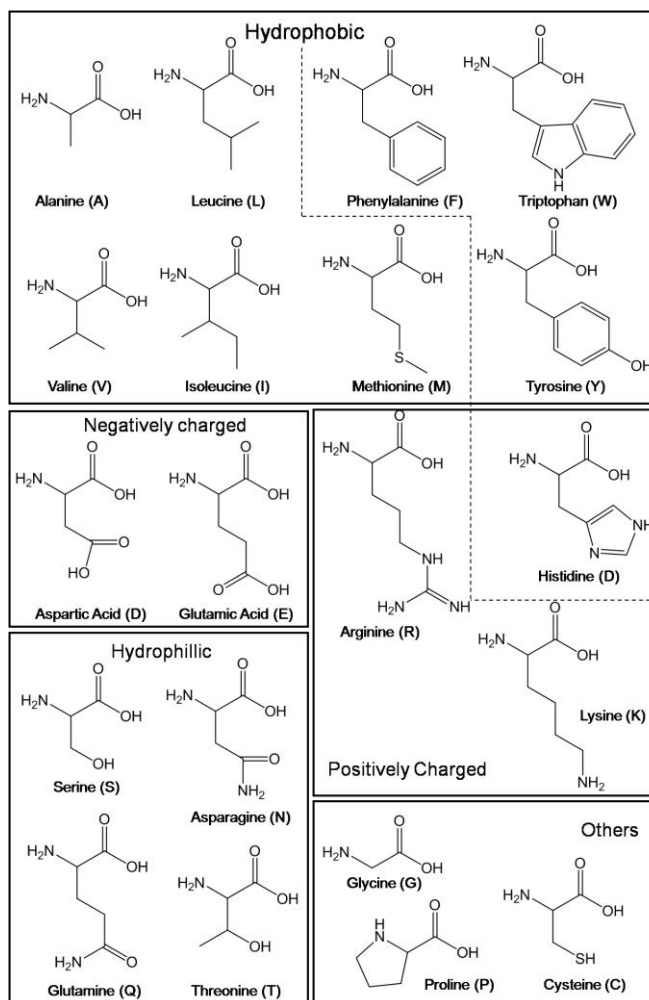


Figure 2.1 - Chemical structures of 20 gene encoded amino acids showing name and one letter abbreviations, grouped from their chemical properties.

Each of the naturally occurring amino acids, with the exception of proline, contain a carboxyl group, an amine group and a distinctive –R group, known as the side chain; and exist naturally in the L-conformation (see Figure 2.2), with the exception of glycine which is achiral.⁷⁴

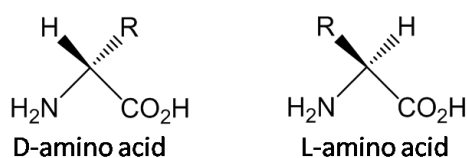


Figure 2.2 - D- and L- amino acid configurations

Peptide chains are formed by linkage between the amine group of an amino acid, with the carboxyl group of another to release water, a reaction known as condensation or dehydration, forming an amide or peptide bond (see Figure 2.3).⁷⁴ However, direct condensation of amino acid fragments does not occur spontaneously. The amino acid fragments need to be ‘activated’ by a solvent, which induces polarisation of the carboxylic acid group to create a positive dipole on the carbon, thus opening it to nucleophilic attack from the amine of another amino acid or peptide fragment. The order of amino acids within the polypeptide is known as the primary structure – the most fundamental of protein structures, and is conventionally denoted from the N to C terminus. The amine and carboxyl moieties of the peptide backbone are then available only for hydrogen bonding interactions,⁷⁴ leaving chemical nature of the peptide to be governed by the amino acid side chains.^{13, 74} Desired chemical properties can be incorporated into building blocks by simply selecting the amino acid residues with side chains that offer specific chemical functionality and structural properties. Furthermore, peptides give great potential for versatility due to the high number of amino acid combinations possible.⁷⁵

In Figure 2.1, the amino acids are grouped in terms of their chemical properties; hydrophobic, hydrophilic, and charged residues. There are also three naturally occurring amino acid residues which do not fall under any of these categories; glycine, proline and cysteine - each offering unique structural and chemical properties to the peptide chain. Glycine (G) and proline (P) offer structural modifications; glycine offering higher flexibility due to minimal steric hindrance from its –R functionality. Conversely, proline introduces structural rigidity to the peptide chain due to the fixed conformation of its side chain, and is also known to induce β -hairpin bends in the peptide chain (see Section 2.2.2). Cysteine (C) offers distinctive chemical reactivity in the terms of amino acid side chains, and is therefore often a target for chemical modification or cross-linking of peptides.

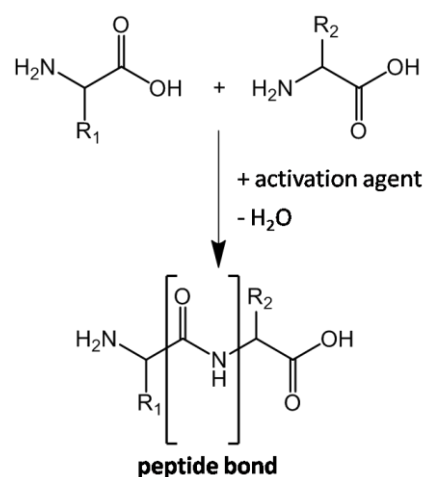


Figure 2.3 – Schematic representation of condensation of two amino acid residues resulting in a dipeptide.

2.2.2 Supramolecular Assembly

The production of peptide nanostructures is reliant on the peptides intrinsic ability to self-assemble to create supramolecular structures. Their chemical functionality comes from the presence of the amino acid side chains, however it is the availability of interactions between complementary peptide chains which allows the formation of nanostructures. The aggregation of synthesised peptides allows them to mimic the basic conformational units found in naturally occurring proteins, β -sheets and turns (hairpins), α -helices and coiled coils (see Figure 2.4).^{13, 14, 30, 76}

The conformation of naturally occurring supramolecular protein structures were derived in the early 1950s; with Pauling and Corey successfully identifying the β -sheet conformation,⁷⁷ and Pauling, Corey⁷⁸ and Crick⁷⁹ the α -helical and coiled coil structure of proteins. Supramolecular assembly of proteins is governed by weak non-covalent interactions, such as, hydrogen bonds, electrostatic interactions, hydrophobic interactions and Van der Waals interactions. The collective strength of the weak interactions allowing for supramolecular structures to be highly stable with nanoscale features.⁸⁰

Secondary protein structure is owed to the hydrogen bonding ability between carbonyl and $-\text{NH}$ groups of the peptide backbone, giving rise to highly regular substructures. Tertiary Protein structure is defined as the three-dimensional structure of a single peptide chain.

Quarternary structure arises when a folded peptide unit associates with at least one other. The functionality of the amino acid side chain allows for additional interactions necessary for further stabilising the nanostructure; the amino acid sequence is therefore critical to the self-assembly process.⁷⁴ For example, the introduction of aliphatic amino acid residues provide a hydrophobic environment necessary for hydrophobic collapse of the system in an aqueous environment, with possible aromatic groups allowing for further stabilisation due to potential π - π stacking interactions – interactions recognised as a major driving force in protein and peptide folding. Hydrophillic residues offer additional hydrogen bonding interactions may provide further stability to the self-assembled systems. Additionally, the positively and negatively charged amino acid residues can be incorporated to create complementary electrostatic interactions which may help form assemblies.

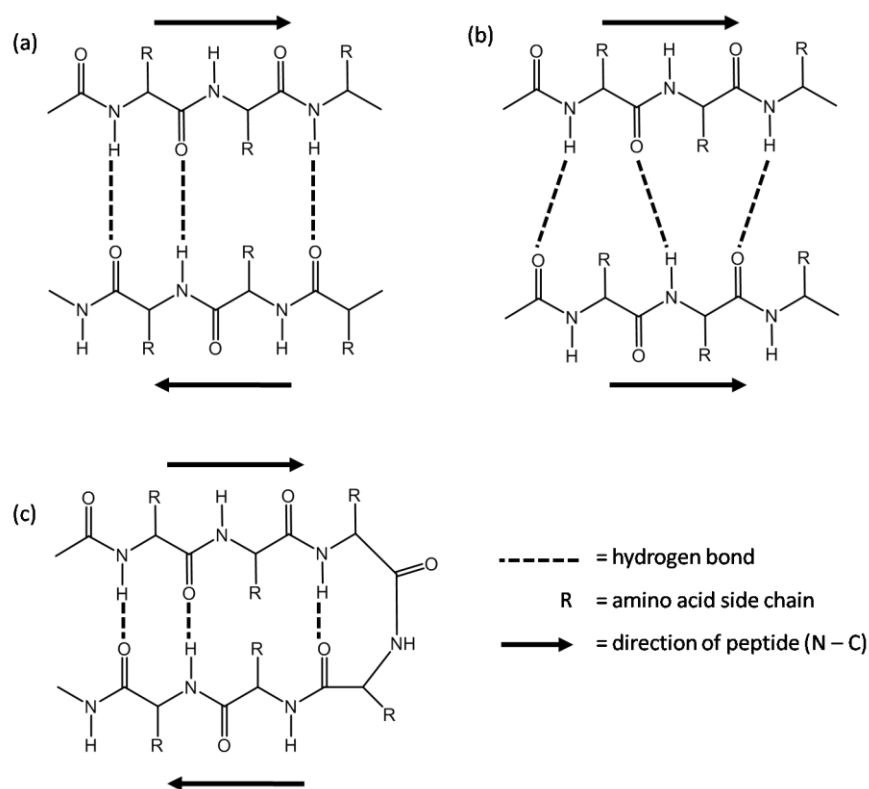


Figure 2.4- Graphical representation of (a) Anti-parallel β -sheet, (b) parallel β -sheet, and, (c) β -hairpin.

β -sheet assemblies are classed as a secondary protein structure. When the peptide backbone of different Sections of a peptide align parallel to each other, they are held in this conformation by hydrogen bonding interactions between carbonyl and NH moieties. It is classed as a β -sheet when there is an extended number of peptide fragments are aligned

and regularly hydrogen bonded in this arrangement (see Figure 2.4). The formation of a β -sheet can occur in one of two ways; the peptides can be orientated either, (1) parallel, with peptide backbones in register, the direction of every N to C peptide backbone in the same direction, or, (2) anti-parallel, where the peptide backbones are parallel however there is alternating N to C and C to N direction of the peptide chains. The parallel Vs anti-parallel configuration can have considerable effect on the hydrogen bonding orientation. β -sheet assemblies have been long known to assemble into extended fibrillar structures, such as the amyloid fibrils associated with Parkinson's and Alzheimer's disease.⁸¹ The basic amino acid motif that creates most β -sheet structures has alternating hydrophobic, hydrophilic residues, and once hydrogen bonded in conformation, the side chains will extend out to create a hydrophobic face and a hydrophilic face of the sheet – with hydrophobic faces of two β -sheets typically interacting to minimise contact with an aqueous environment.

β -hairpins induce anti-parallel β -sheet assemblies. Here, a single peptide chain is 'folded' back on itself by the inclusion of a turn sequence, i.e. an amino acid sequence which will induce the β -hairpin bend, and can immediately hydrogen bond with itself (see Figure 2.4).

The α -helical structure is also a secondary protein structure. Here, however, the peptide backbone of a single amino acid chain coils. This occurs when the peptide chain adopts repeating backbone dihedral angles of phi (ϕ) = 60° and psi (ψ) = 45° (see Figure 2.5), forming a tight right-handed helical structure. Each amino acid residue is able to hydrogen bond with the amino acid residue which is four positions further along the chain – hydrogen bonds running parallel to the helix axis, stabilising the structure, and two full rotations of the helix is equivalent a peptide sequence of seven amino acid residues in length, known as a heptad (amino acids labelled a through g).

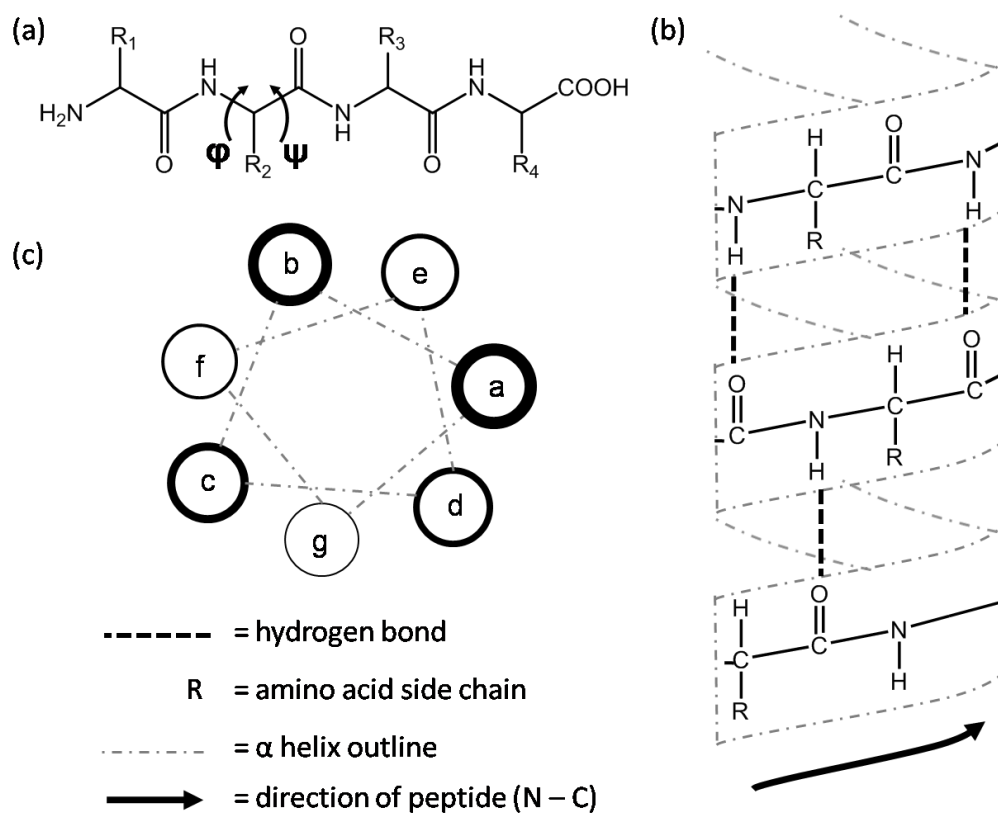


Figure 2.5 - Graphical representation of (a) a peptide chain indicating the ϕ and ψ dihedral angles, (b) α -helix structure indicating hydrogen bonding, and, (c) positions of amino acids within the heptad of an α -helix.

Coiled coils are produced when at least two of the α -helical structures interact to bury a hydrophobic face. This is achieved by spacing hydrophobic amino acid residues four positions apart (positions a and d) within the heptad, thus creating a hydrophobic strip down one side of the helix, which is then buried through interactions with another α -helix with a similar hydrophobic face. When this occurs, the helices wind around each other, and result in a supercoiled structure. Bulky amino acid residues tend not to be found in the a and d sites of the heptads, as they can disrupt the formation of coiled coils. However, it is known that by using different combinations of hydrophobic amino acids in the a and d positions, the oligomerisation to form the supercoil can be controlled (see Table 2.1).⁸²

Amino Acid Residue at Heptad Site		Number of α -helices involved in coiled coil structure
a	d	
asparagine	leucine	2
isoleucine	isoleucine	3
leucine	isoleucine	4

Table 2.1 – Combinations of amino acids present in the a and d sites of the heptad indicating the effect on the supercoiled structure. Data from reference⁸²

Additionally, the fifth and seventh amino acid (e and g) positions of neighbouring helices are close in space, thus, the heptad will commonly incorporate complementary charged amino acid residues on the corresponding helices. Further stabilisation will therefore be achieved through electrostatic attractions. In terms of designed coiled coil systems, the amino acid residues in sites e and g can be substituted which can direct the formation of supercoils with regards to relative orientations, i.e. the α -helices can align parallel or anti-parallel.

Additionally, sites b, c and f are much less restricted to which amino acid residue is used, therefore can easily be substituted for another amino acid with desirable chemical properties or offer functionalisation.

2.2.3 Chemical Modification to Aid Assembly

It is possible to make structural modifications which will increase the number of interactions and further facilitate molecular self-assembly. Chemically modified peptides are discussed in Section 2.3.

There have been a number of approaches to structural modification of peptide chains to aid assembly. For example, it has been shown that by structural modification of the N-terminus to include an aromatic group encourages molecular self-assembly due to an enhanced desire for a hydrophobic collapse in aqueous environments allowing for π -stacking interactions (discussed in Section 2.3.5). Phenyl,^{83, 84} naphthalene,^{83, 84} fluorene^{64, 85} and pyrene,⁸⁶ have all been successful N-terminus modifications (see Figure 1.6).

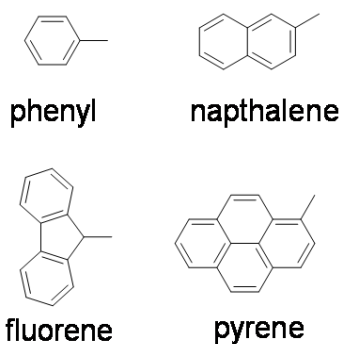


Figure 2.6 - Aromatic moieties for N-terminus modifications.

Additionally, it has also been observed that by covalently linking an alkyl chain to the peptide, thus creating an amphiphilic molecule similar to a lipid, again will encourage aggregation by the hydrophilic collapse (see Section 2.3.4).⁸⁷

2.3 Designed Peptide Nanomaterials

Since the elucidation of natural supramolecular protein structure in the early 1950s,^{77,78,79} it was understood then that the peptide sequence encoded for these supramolecular structures. However, it was half a century before these rules were exploited to design synthetic supramolecular peptide based materials.^{16,17} Their design is typically derived from naturally occurring supramolecular protein structure, such as the α -helical or β -sheet assembly (discussed in Section 2.2.2). However, they have also been based on non-natural peptide chains, where the peptides are chemically modified to induce supramolecular assembly and include specific properties, such as amphiphilic peptides or aromatic peptide derivatives.

2.3.1 β -sheet Assemblies

The first record of designer self-assembled peptide nanotubes was reported by Ghadiri *et al.* in 1993.¹⁶ Here, cyclic peptides were synthesised, eight amino acid residues in length, with alternating hydrophobic/hydrophilic residues, (AEAQ)₂, in an alternating D- and L-enantiomer configuration. The design was adopted, in order to persuade the peptide to assume a planar ring conformation with respective –R functionalities extending outward in

a radial fashion. In aqueous media, the rings stacked in a planar formation, with peptide backbones hydrogen bonding in a β -sheet fashion, resulting in tightly packed hollow tubular structures.¹⁶

In the same year, Zhang *et al.* demonstrated the assembly of 'designer' peptides to create fibrous structures and membranes from a more conventional extended β -sheet assembly in 1993.¹⁷ The peptide sequences contained a hydrophobic amino acid sequence of alanine, and alternating complementary charged amino acid residues of glutamic acid and lysine, for example, AEAKAEAEAKAK.¹⁷ Here, the peptides spontaneously assembled in aqueous solvent - with backbones hydrogen bonding to form the β -sheet assembly, with additional interactions possible between the negatively charged side chains of glutamic acid of one peptide chain with positively charged lysine amino acid residues of another, to create stable nanoscale assemblies.¹⁷

Since then, the approach of using alternating hydrophobic/hydrophilic or charged residues within the peptide chain has been adopted by a number of researchers, creating peptide nanostructures by β -sheet formation of the synthetic peptides, such as the FEFK derivatives designed by Guilbard *et al.*,¹⁸ and the (EAKA)₄ peptides developed by Zhang *et al.*¹⁹ However, by adopting the basic amino acid sequence, the alternating hydrophobic/hydrophilic sequences, to induce β -sheet formation, the same hierarchical structure is not always presented. A number of different nanoscale structures have been observed, such as tapes,²¹ ribbons, fibres,¹⁹ resulting from the packing abilities of multiple β -sheets.²⁰

An alternative to designing amino acid sequences on alternating hydrophobic/hydrophilic residues, based on the naturally occurring amyloid fibrils, hydrophobic peptide sequences have also been known to induce β -sheet assembly. Lu *et al.* designed a peptide which incorporated the central hydrophobic fragment of the Alzheimer disease related amyloid peptide, Ac-KLVFFAE-NH₂. In acidic conditions, the peptide self-assembled forming bilayers of the β -sheet arrangement, giving rise to monodispersed nanotapes.²³ Similarly, the mainly hydrophobic peptide AAKLVFF, has also been reported to form nanotubes in methanol from a β -sheet based assembly, which interestingly showed solvent induced morphological transitions between nano- tapes, fibrils and tubes by varying the water/methanol ratio.^{22, 24}

Furthermore, it has been demonstrated that peptides of as little as two amino acid residues in length have been shown to form stable β -sheet assemblies. Dipeptide sequences, such as FF, can hydrogen bond in an anti-parallel β -sheet configuration, with aromatic groups (π -stacking interactions) playing a vital role in the stabilisation of the self-assembled structures.⁶⁰

2.3.2 β -hairpins

β -sheet peptide sequences may align out of register, particularly those that contain repeating patterns of amino acid residues, leaving the terminal amino acid sequences unable to interact with another peptide, and resulting in 'defects' within the ordered supramolecular structures.¹³ However, by utilising β -hairpin bends within peptide sequences may ensure that the peptides are stacked in register, in a tightly bound anti-parallel β -sheet conformation. This is achieved by introducing a turn sequence within the peptide. Schneider and Pochan described a system such as this which included turn sequence $-V^D\text{PPT}-$ within their peptide chain – the non-natural D-configuration form of the proline residue being responsible for forcing the hairpin bend at high pH – with peptides, eight amino acids in length with a high propensity to hydrogen bond, on either side.⁸⁸ Thus giving rise to highly ordered nanoscale fibres from the peptides tightly bound in the anti-parallel β -sheet conformation.

2.3.3 α -helical and coiled coils

Complementary to the β -sheet design, the natural α -helical structure of proteins and supramolecular assembly forming coiled coils can be synthetically replicated to create self-assembling macrostructures. This has been carried out by utilising the basic heptad motifs (discussed in Section 2.2.2) - with non-covalent association of more than one α -helix to bury hydrophobic faces, leading to helical bundles and the so-called α -helical coiled coils or supercoils.

St. Pierre and Hodges were the first to design non-biological coiled coil systems in 1976 based upon amino acid sequence patterns that were observed naturally occurring fibrous

proteins such as tropomyosin.⁸⁹ Since then, de novo designed coiled coil systems have been extensively studied.

In 1995, Nautiyal *et al.* successfully designed and synthesised a trimeric coiled coil system.²⁵ Three complementary peptide sequences were synthesised which were 34 amino acid residues in length to allow for adequate stability. Isoleucine was introduced into the in the a and d sites to promote the formation of a trimeric supercoil as described by Harbury *et al.*,⁸² and complementary charged residues occupied the e and g sites to promote inter-helix electrostatic interactions and induce formation and stabilisation of the supercoils. The result, the desired heterotrimeric coiled coil which resulted in a nanoscale fibrillar network.²⁵

Potekhin *et al.* designed a system with leucine present in a and d positions of the heptad – QLAREL at cdefga, followed by (QLAREL)₄ at bcdefga. The repetitive amino acid motif was specifically included to allow for a ‘staggered’ association of the α -helices, and thus encourage longitudinal growth as a means to control result fibre width during assembly. At low pH, the designed structure formed fibrils, comprised of pentamers of the α -helical motif.²⁶ Furthermore, by substitutions of the glutamic acid residues in the g position with either Q or S, fibrils were able to form over a wider pH range (2.5 – 11), as the electrostatic repulsion experienced between α -helices at physiological pH and above, due to the deprotonation of glutamic acid residues, had been removed.⁹⁰

The Woolfson group have extensively studied synthetic α -helical and coiled coil systems. Over the last decade or so, they have developed a synthetic peptide system which adopts the α -helical motif, which self-assembles into coiled coil dimers, and results in a fibrillar network structure.²⁷⁻²⁹ The designed amino acid motifs were 28 amino acids in length, with leucine and isoleucine in the a and d sites of the peptide respectively, and complementary charged amino acids in the e and g sites of respective α -helical structures. The amino acid heptad motif of complementary chains were canonised, so to produce ‘staggered’ association of the helices, and encourage longitudinal growth of fibres.

2.3.4 Peptide Amphiphiles

Amphiphilic molecules also present a class of designed self-assembled peptides. In naturally occurring systems, the hydrophobic collapse is known to be a major driving force in molecular self-assembly and organisation, observed for amphiphilic molecules such as phospholipids.^{91, 92}

Peptide amphiphiles are classed as non-natural peptides, and consist of oligo-peptides which are chemically modified to present a distinctly hydrophilic region and a distinctly hydrophobic region, each at opposite terminating ends of the molecule (see Figure 2.7).

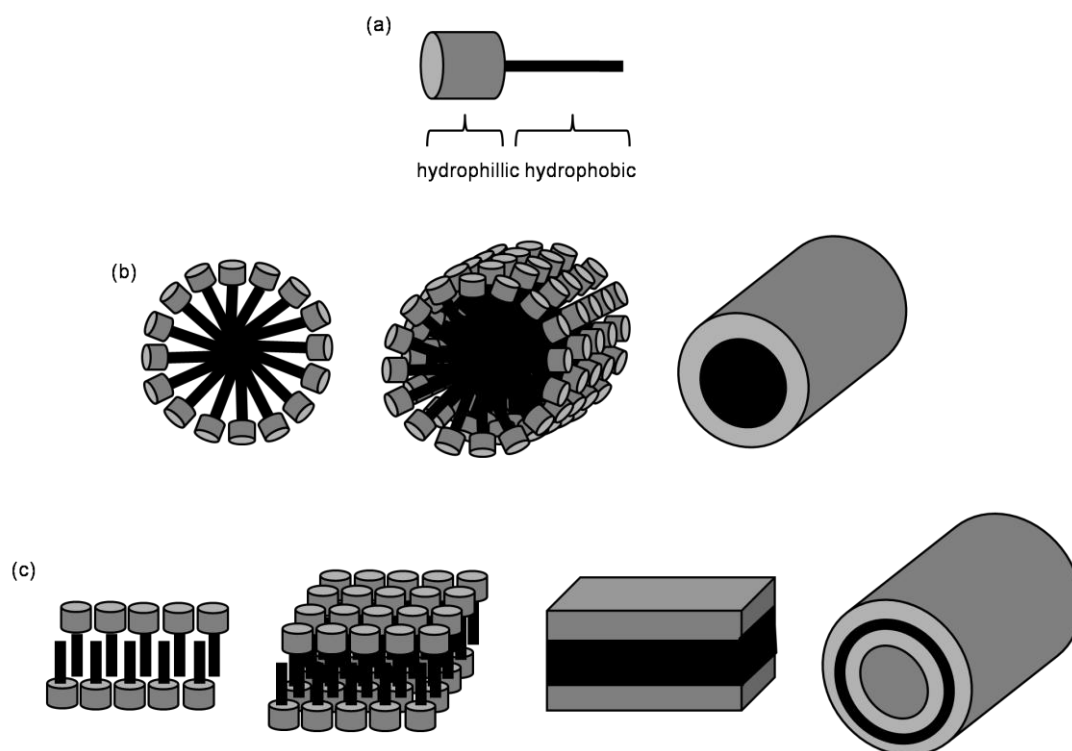


Figure 2.7 - (a) Schematic representation of a peptide amphiphile. Driven by the hydrophobic collapse, in aqueous environments peptide amphiphiles can self-assemble to form nanotubes or vesicles with either (b) a hydrophobic core, or (c) form membrane-like bilayer structures with hollow cores.

Designed amphiphilic peptides were first reported by Hartgerink *et al.* in 2001.⁸⁷ The specifically chosen peptide chain was chemically modified to include an alkyl chain on the C terminus. The alkyl tail, necessary to convey hydrophobic character, was attached to a peptide chain consisting of four cysteines, which may allow for cross-linking of peptides by

forming a disulfide bond to polymerise the self-assembled structure, three glycine residues, to provide flexibility, a phosphorylated serine, which was incorporated for interactions with calcium ions in the intended environment, and, finally amino acid sequence RGD (arginine, glycine, aspartic acid) to provide the hydrophilic head, with this specific sequence also chosen as a cell adhesion ligand.⁸⁷ In aqueous environments, driven by the hydrophobic collapse, they self-assembled into rod-like structures with a hydrophobic core, allowing for hydrogen bonding between adjacent peptides in a parallel β -sheet conformation.^{13, 87, 93-95} Subsequently, by using the design of a peptide chemically modified with an alkyl tail, it was shown that by introducing oppositely charged peptide amphiphiles to the reaction vessel, can allow for tighter packing of the molecules due to electrostatic attraction.⁹³

An alternative approach, was to chemically modify the N-terminus of a peptide consisting of a hydrophobic amino acid sequence terminated with hydrophilic residues, with a hydrophobic group, thus presenting the hydrophobic/hydrophilic design. In 2002, the Zhang group designed peptide sequences of at least four hydrophobic residues, terminated with one or two hydrophilic residues, with the N-terminus chemically modified with an acetyl group.^{96, 97} In an aqueous environment, the molecular organisation was described as a membrane-like bilayer, and resulted in hierarchical assembly to form hollow nano-tubes and vesicles.^{96, 97}

2.3.5 Aromatic Peptide Amphiphiles

Another class of non-natural peptides that have proved a successful route to producing peptide nanostructures are aromatic peptide amphiphiles. They consist of short peptide chains (generally less than five amino acids) that are typically modified with an aromatic group to drive self-assembly *via* a combination of hydrogen bonding and π -stacking, and form elongated assemblies.¹³

The concept was first derived when peptide sequence FF, the core sequence of some amyloid peptides, self-assembled to form nanotubes in aqueous environments. The mode of assembly was anti-parallel β -sheet assembly of the peptide chains – with π -stacking interactions between phenyl moieties playing a key role in stabilising the nanostructure.⁶⁰

98

Soon after, it was demonstrated that by coupling a variety of aromatic groups to the N terminus of some short peptides that supramolecular assemblies could form.⁸⁵ The mode of assembly is driven by π -stacking of the aromatic moieties, with hydrogen bonding between peptide units in an anti-parallel β -sheet fashion, although technically it is classed as quaternary protein structure as the peptide units are not connected covalently in any way (see Figure 2.8).⁸⁵

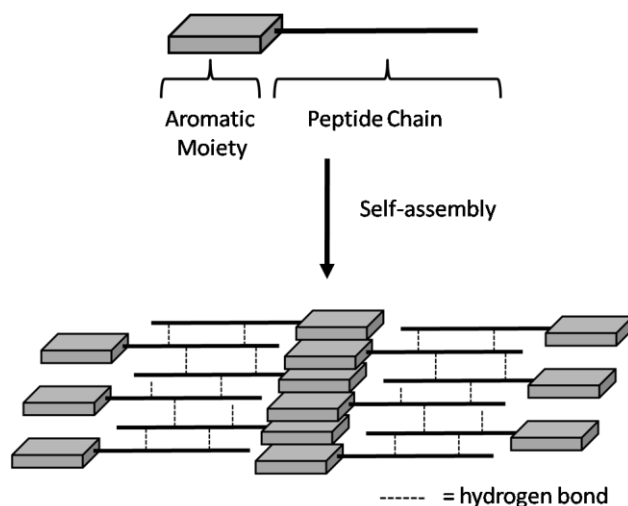


Figure 2.8 – Schematic representation of aromatic peptide amphiphile self-assembly.

This has since been demonstrated for a number of different peptides, using a number of different aromatic modifications (discussed in Section 2.2.3), with dipeptides (two amino acid residues in length) being the shortest peptides showing self-assembled supramolecular structures.

As a result of the different aromatic peptide amphiphiles designed, a number of different nanomorphological structures have been formed as a direct result of their supramolecular assembly, including tubes,³⁰ fibres,² tapes,⁴⁷ spheres⁴³ and leaf-like structures.⁴²

2.4 Self-Assembly On Cue

A major challenge in any self-assembly process is gaining control over the molecular association to produce defect-free reproducible structures. Typically, assembly is initiated as soon as the assembling components are dissolved in the reaction medium (i.e. requires no stimulus), and can often result in poorly controlled nucleation. The use of an external

stimulus to drive or direct the assembly of molecular building blocks can therefore allow for more control over the process, and provide a means to control assembly and disassembly. A number of physical and chemical means have been employed to activate the assembly process including changes in pH,^{26, 88, 99, 100} ionic strength,¹³ temperature,⁹⁹ or by exploiting enzymatic reactions (discussed in Section 2.5). Alternatively, the introduction of an external stimulus could be utilised, such as the exposure to a specific wavelength of light if the precursors are light sensitive.¹⁰¹ Synthetic self-assembling peptides can be designed to include sensitivity to any of these methods in order to control assembly and disassembly.

2.5 Biocatalytic Self-Assembly of Aromatic Peptide Amphiphiles

Enzymes have proved a powerful when attempting to control the self-assembly process of aromatic peptide derivatives. They convert non-assembling peptide precursors into self-assembling molecules, providing reproducible and homogeneous assemblies. Peptides are inherently biocompatible, so designing an enzymatically triggered system has the advantages of being useful in biological situations, and carry benefits over systems where the self-assembly is induced by an environmental trigger, such as pH switching. The use of enzymes does not require changes in the bulk conditions for the self-assembly to occur. The process will take place under constant conditions of temperature, pH, ionic strength and solvent polarity, in contrast to the chemically triggered systems where at least one of these will be altered during the course of the reaction. The use of an enzymatic trigger may also carry other advantages. The enzyme will inherently incorporate biological selectivity as substrate specificity is directly linked to each enzyme, beneficial when trying to achieve defect-free reproducible structures. It may introduce spatiotemporal control (discussed in Section 2.7), and may also allow for self-correction if the reaction is reversible. Systems can be designed with specific enzyme targets and applications in mind. Previous research has shown that enzymes can control both assembly^{41, 44, 46-50, 102} and disassembly^{44, 46, 83} of network structures; both of interest when considering their potential applications.

2.5.1 Enzyme Controlled Self-Assembly of Aromatic Peptide Amphiphiles

Enzyme controlled self-assembly is defined as the production of self-assembling molecular building blocks from non-assembling precursors *via* enzymatic catalysis. The self-assembly of peptides is reliant on the molecular packing abilities of the monomers, in combination with a delicate balance of electrostatic properties and hydrophobicity (discussed in Section 2.3). As a result the enzymatic reaction may proceed in either one of two ways; (1) by catalysing the synthesis of the self-assembling peptide chain by condensation of two amino acid or peptide fragments, or; (2) by removing a functional group associated with ‘blocking’ molecular self assembly – the ‘blocking’ group affecting molecular packing due to its steric hindrance, or by causing electrostatic repulsion between monomer units.¹³

There are a number of examples in the literature in which enzymes have been exploited to control the self-assembly of aromatic peptide amphiphiles which typically occurs in three stages; (1) the enzyme chemically converts non-assembling precursors into self-assembling components, (2) the monomers self-assemble in solution to create a supramolecular structure, and, (3) entanglement of these self-assembled structures which may result in entrapment and immobilisation of the solvent resulting in the formation of a hydrogel (see Figure 2.9).^{55, 58, 103} A number of examples have been summarised in Table 2.2.

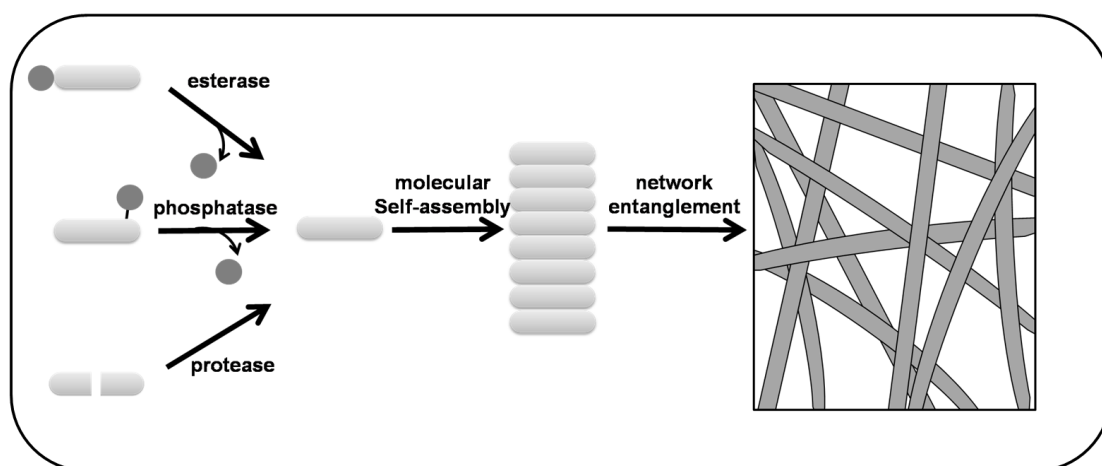


Figure 2.9 - Schematic of enzyme controlled self-assembly. The action of the enzyme on precursor molecules results in the formation of self-assembling building blocks. Building blocks then self-assemble forming supramolecular structures, followed by network entanglement.

Most commonly, phosphatases, esterases and proteases have been exploited as triggers for self-assembly of peptide derivatives.

Phosphatases catalyse the removal of a blocking (phosphate) group by bond cleavage, known as dephosphorylation.^{41-45, 56, 83, 84, 104} The electrostatic repulsion between phosphate moieties of neighbouring peptides is known to impede molecular self-assembly. However, after it has been separated from the peptide chain, molecular self-assembly is possible. As a direct result, phosphatase controlled self-assembly has produced nanoscale fibres,^{41, 44, 45, 56, 83, 84, 104} spheres,⁴³ and leaf-like structures.⁴²

Esterases may be exploited to promote ester hydrolysis of alkyl ester terminated peptides to form self-assembling peptides.^{46, 47, 102} Producing self-assembling peptide amphiphiles in this manner, has resulted in the formation of entangled network structures of hollow tubular structures⁴⁶ and fibres.^{46, 47, 102}

Proteases can either hydrolyse an amide bond to cleave a group associated with blocking¹⁰⁵ or condense two non-assembling amino acid fragments by reversed hydrolysis forming a peptide derivative with the ability to self-assemble. Again, nano-fibrillar network structures are generally formed as a direct result of molecular self-assembly.^{46, 51, 52, 59}

In the same manner as protease enzyme, thermolysin, a lipase enzyme has also been used to condense two amino acid fragments *via* reversed hydrolysis, producing nanoscale fibres from a self-assembling Fmoc-tripeptide.⁴⁸ However, in the opposite manner, Koda *et al.* have produced a hydrogelating species by hydrolysis of an amide bond, removing a fragment of the peptide chain which hinders self-assembly, a reaction catalysed by the enzyme matrix metalloproteinase-7 (MMP-7), which results in fibrillar network structures.⁴⁹ This was achieved by designing and incorporating the amino acid sequence, PLGL, within the peptide fragment, which is a known target for hydrolysis for this specific enzyme.⁴⁹

Additionally, β -lactamases have also been used to catalyse the formation of hydrogelators. Here, the precursors were designed with a specific target for β -lactamase, with the resulting cleaved molecule acting as a hydrogelator, with molecular self-assembly resulting in a nanofibrillar network structure.⁵⁰

In addition, the biocatalytic route chosen to trigger molecular self-assembly (i.e. when different enzymes can be used to generate the same self-assembling molecular building

block), can have great impact over nanostructures formed. For example, subtilisin triggered assembly of Fmoc-L₃ gives rise to hollow tubular structures,⁴⁶ where as thermolysin catalysed assembly of Fmoc-L₃ will result in fibril network structures.⁵⁹

Entry	Enzyme	Precursor	Self-Assembling Molecule	Gelation Time (min)	Yield (%)	Nanoscale Structure	Ref.
alkaline phosphatase							
1		Fmoc-Y(<i>p</i>)-OH	Fmoc-Y-OH	< 30	not specified	fibres	41
2		Fmoc-Y(<i>p</i>)-OMe	Fmoc-Y-OMe	< 10	64.3	fibres	104
3		Nap -FFGEY(<i>p</i>)-OH	Nap-FFEGY-OH	< 60	99.1	fibres	83
4		Nap -GFFY(<i>p</i>)-OMe	Nap-GFFY-OMe	17	86.4	leaf-like structures	42
5		Ada-GFFY(<i>p</i>)-OMe	Ada-GFFY-OMe	n/a	not specified	spheres	43
6		Ac-YYYY(<i>p</i>)-OMe	Ac-YYYY-OMe	3	96	fibres	44
7		Ac-FYYY(<i>p</i>)-OMe	Ac-FYYY-OMe	2.5	97.2	fibres	44
8		Ac-FFYY(<i>p</i>)-OMe	Ac-FFYY-OMe	2.5	95.8	fibres	44
9		Ac-FFFY(<i>p</i>)-OMe	Ac-FFFY-OMe	2.5	97.8	fibres	44
acid phosphatase							
10		Nap-β ³ -HPhg-β ³ -HPhg-Y(<i>p</i>)-OH	Nap-β ³ -HPhg-β ³ -HPhg-Y-OH	2	84.4	fibres	84
11		Fmoc-Y(<i>p</i>)-OH	Fmoc-Y-OH	not specified	not specified	fibres	45
12		Nap-FFY(<i>p</i>)-OH	Nap-FFY-OH	not specified	not specified	fibres	45
subtilisin							
13		Fmoc-LL-OMe	Fmoc-LL-OH	not specified	99	tubes	46
14		Fmoc-LLL-OMe	Fmoc-LLL-OH	not specified	74	tubes	46
15		Fmoc-VV-OMe	Fmoc-VV-OH	not specified	84	fibres	46
16		Fmoc-FF-OMe	Fmoc-FF-OH	not specified	40	fibres	47
17		Fmoc-FY-OMe	Fmoc-FY-OH	not specified	> 99	fibres	47
18		Fmoc-YL-OMe	Fmoc-YL-OH	not specified	> 99	fibres	47
19		Fmoc-VL-OMe	Fmoc-VL-OH	not specified	40	fibres	47
20		Fmoc-FL-OMe	Fmoc-FL-OH	not specified	> 99	fibres	47
esterase (not specified)							
21		Nap-FF-NHCH ₂ CH ₂ -O-	Nap-FF-NHCH ₂ CH ₂ OH	< 100	68	fibres	102

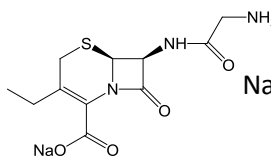
			COCH ₂ CH ₂ COOH				
	thermolysin						
22		Fmoc-T-OH + L-OMe	Fmoc-TL-OMe	< 60	91	fibres	46
				not specified	98	not specified	52
				not specified	84	not specified	47
23		Fmoc-T-OH + F-OMe	Fmoc-TF-OMe	< 60	96	fibres	46
				not specified	96	not specified	52
				not specified	96	not specified	47
24		Fmoc-S-OH + F-OMe	Fmoc-SF-OMe	not specified	98	not specified	52
25		Fmoc-S-OH + L-OMe	Fmoc-SL-OMe	not specified	85	not specified	52
26		Fmoc-A-OH + FF-OH	Fmoc-AFF-OH	not specified	27	not specified	51
27		Fmoc-V-OH + FF-OH	Fmoc-VFF-OH	not specified	64	not specified	51
28		Fmoc-F-OH + FF-OH	Fmoc-FFF-OH	not specified	54	fibres	51
29		Fmoc-L-OH + FF-OH	Fmoc-LFF-OH	not specified	51	not specified	51
30		Fmoc-F-OH + FF-OH	Fmoc-FFF-OH	60	62	fibres	59
31		Fmoc-L-OH + LL-OH	Fmoc-LLL-OH	60	< 50	fibres	59
	lipase						
32		Fmoc-F-OH + FF-OH	Fmoc-FFF-OH	not specified	30 - 33	fibres	48
	matrix metalloproteinase-7 (MMP-7)						
33		Pal-GGGHGPLGLARK-NH ₂	Pal-GGGHGPLG-OH	< 120	40	fibres	49
	β-lactamase						
34		Nap-FF-NHCH ₂ CH ₂ S	 Nap-FF-NHCH ₂ CH ₂ SH	30	49	fibres	50

Table 2.2 - Tables of examples of enzyme controlled self-assembly

2.5.2 Enzyme Controlled Disassembly of Peptide Hydrogels

Enzymatic reactions can also be exploited to control disassembly of the hydrogel network.¹³ Here, the gelating 'monomers' are converted to non-assembling molecules, and as a direct result, gel to solution phase transitions are observed due to the degradation of the network structure. This occurs in the opposite manner to enzyme-triggered assembly. The enzyme catalyses a reaction which either (1) appends a blocking group to the hydrogelating monomers, in turn, prohibiting self-assembly due to steric hindrance affecting molecular packing or causing electrostatic repulsion between monomers, or (2) ruptures a covalent bond, or (3) chemically changes functional moieties, disrupting the delicate charge balance of the species, rendering it a non-assembling molecule (see Figure 2.10). Enzyme controlled degradation of self-assembled structures may prove useful in the terms of controlled drug release,^{11, 44, 106} however, considerably less research has been done in this area when directly compared with enzyme-assisted self-assembly of aromatic peptide derivatives. A list of examples have been summarised in Table 2.3.

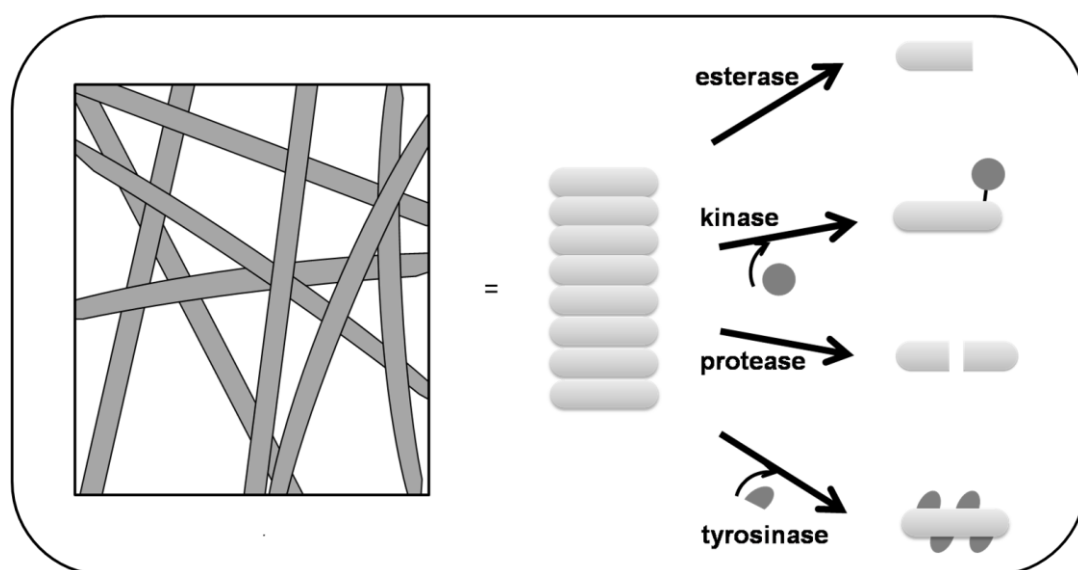


Figure 2.10 - Schematic representation of enzyme controlled disassembly. The action of the enzyme of self-assembled aromatic peptide amphiphiles renders them non-assembling molecules, resulting in a gel to solution phase transition.

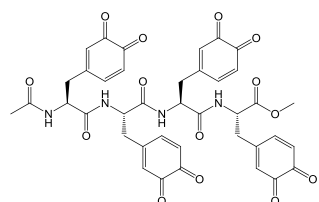
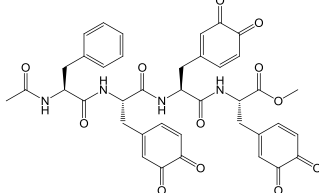
Enzyme	Self-Assembled Molecule	Non-Assembling Product	Reference
tyrosine kinase	Nap-FFEGY-OH	Nap-FFEGY(<i>p</i>)-OH	83
subtilisin	Fmoc-TL-OMe	Fmoc-TL-OH	46
tyrosinase	Ac-YYYY-OMe		44
	Ac-FYYY-OMe		44

Table 2.3 - Examples of enzyme controlled disassembly of peptide nanomaterials

It has been demonstrated that with the addition of a kinase in the presence of ATP to a hydrogel comprised of self-assembled Nap-FFGEY-OH monomers, resulted in phosphorylation of the tyrosine residue. As expected, the aromatic peptide amphiphile was no longer able to self-assemble due to electrostatic repulsion between the deprotonated phosphate groups of neighbouring peptides, and ultimately a gel to solution transition was observed.⁸³ However, by treating the resulting solution with a phosphatase, the hydrogel was restored due to the removal of the blocking group (see Section 2.5.1); allowing for a switch between solution and gel by alternating treatment with kinase/phosphatase.⁸³

Similarly, gel to solution transitions have been observed by treatment of hydrogels comprised of self-assembled Fmoc-peptide methyl esters by treatment with an esterase. In this case, the subtilisin cleaves the ester bond on the C-terminus of the peptide chain resulting in Fmoc-peptides which no longer possess the ability to self-assemble.⁴⁶ This same reaction has also been responsible for producing self-assembling aromatic peptide amphiphiles^{46, 47} (discussed in Section 2.5.1). The charge balance and possible interactions of the resulting structures will ultimately dictate their self-assembling abilities.

Most recently, Gao *et.al.* have exploited a tyrosinase enzyme to control the disassembly process in hope to exploit elevated tyrosinase activity in malignant melanoma for controlled drug release. Hydrogels assembled from aromatic tetrapeptide methyl esters,

Ac-YYYY-OMe and Ac-FYYY-OMe, were treated with the tyrosinase enzyme, which converts the tyrosine residues to quinone; the oxidation process resulting in the loss of π - π interactions between phenol rings and ultimately a gel to solution phase transition.⁴⁴

2.6 Kinetic Vs Thermodynamic Control of Enzyme Assisted Self-Assembly

Biocatalytic self-assembly may proceed under (1) kinetic control, or, (2) thermodynamic control. A combination of the two may arise.

2.6.1 Self-Assembly Under Kinetic Control

A system under kinetic control may give rise to kinetically trapped aggregates instead of the thermodynamically preferred self-assembled structure. This is possible as both the enzymatic reaction and the self-assembly process independently are thermodynamically favourable (see Figure 2.11), observed for phosphatase⁴¹ and subtilisin⁴⁷ triggered systems. The rate of catalysis determines the delivery of the self-assembling molecules. Therefore, as the reaction proceeds the system can access a variety of supramolecular structures depending on the amount of catalyst used, with fewer defects arising from a slower assembly rate.⁵⁸ Upon gelation the systems become fixed in this arrangement, a process referred to as 'kinetic locking', as it is too energetically unfavourable to reorganise the self-assembled monomers in combination with the extremely slow molecular dynamics associated with the gel phase. Consequently, the minima achieved in the free energy landscape may not represent the global thermodynamic minimum.^{47, 55} The quantity of enzyme used may allow access to a variety of local minima within the free energy landscape. Theoretically, by using a very small number of enzyme molecules to control assembly, it would be possible to access the thermodynamically favoured structure using a system which operates under kinetic control.

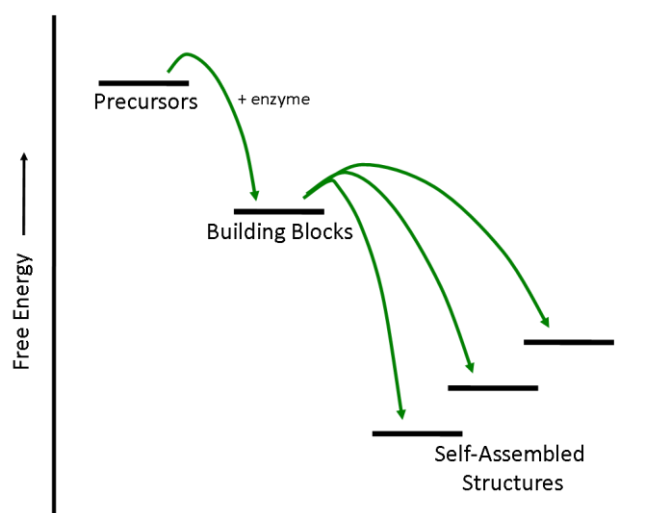


Figure 2.11 - Free energy diagram of kinetically controlled enzymatic self-assembly, where both the enzymatic reaction and the self-assembly process is thermodynamically favoured.

However, reconfiguration of a kinetically trapped system to attain a more thermodynamically stable state is possible. This is achieved by first allowing formation of the kinetically trapped aggregates and subsequently introducing heat/cool cycles. The introduction of energy (in the form of heat) will melt the gel, allowing for monomers to be freed from their 'locked' state, in turn, the monomers may reorganise on cooling.⁴⁷ Alternatively, the assembly may be reversed biocatalytically by introducing a second enzyme to trigger disassembly of the trapped aggregates^{44, 83} (see Section 2.5.2). This may give rise to either a reversible two enzyme system, such as phosphatase/kinase systems which may act as a sol-gel switch by alternating treatment of the two contradicting enzymes,⁸³ or a two enzyme system where the assembly/disassembly pathway only proceeds in solely the forward direction, such as the phosphatase/tyrosinase systems described by Gao *et al.*⁴⁴

Utilising a kinetically controlled system can in some cases be advantageous; It is possible to control properties of the resulting hydrogels and allow for tailoring of the materials. For example, it has been shown that the mechanical strength of the hydrogels has been directly linked to the enzyme concentration, with higher enzyme concentration, and thus a more rapid gel formation, producing mechanically stronger gels when directly compared equivalent systems with a lower enzyme concentration.^{56, 57}

2.6.2 Self-Assembly Under Thermodynamic Control

An enzymatically triggered system is said to operate under thermodynamic control when the enzymatic reaction producing self-assembling molecules is energetically unfavourable. However, the thermodynamic stability loss of the system as a whole associated with the unfavourable reaction is compensated by the overall free-energy change achieved by the self-assembly process (see Figure 2.12). This gives rise to dynamic and fully reversible assemblies, and in turn, allowing for defect (or self) correction and molecular reorganisation, ultimately, reproducibly achieving a homogenous assembly of the thermodynamic minimum.

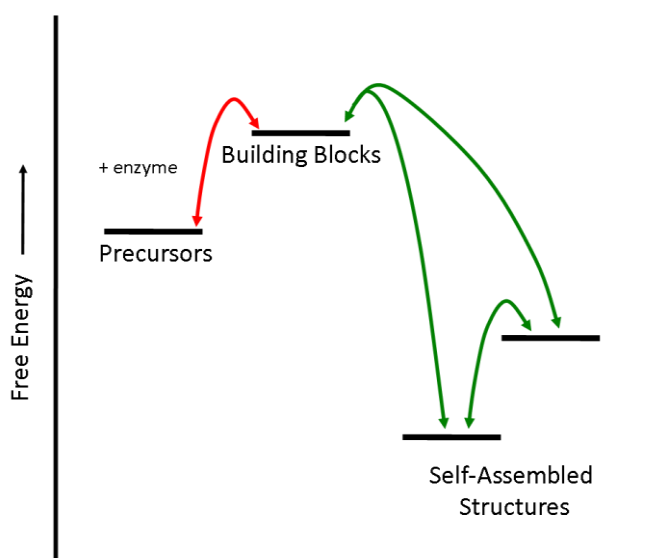


Figure 2.12 - Free energy diagram of thermodynamically controlled enzymatic self-assembly, where the enzymatic reaction to produce the self-assembling building blocks is thermodynamically unfavoured, and the self-assembly process is energetically favourable.

Additionally, utilising a thermodynamically driven system introduces a new means to directly compare the relative stabilities of each molecular building block and non-assembling precursor. This is achieved by introducing competing amino acids precursors or peptides into the system. The thermodynamic driven component selection will then allow for the dynamic interchange of units until the most thermodynamically stable structure is achieved. This type of system, where building blocks are continuously substituted until an equilibrium is reached, is known as a dynamic combinatorial library (DCL).^{107, 108}

Successful DCL's for enzymatically triggered self-assembly of aromatic peptide amphiphiles were demonstrated using protease enzyme thermolysin, which reversibly condenses amino acid fragments to form self-assembling peptide chains (see Section 2.5.1). Williams *et al.* effectively screened for dynamic peptide lengths,⁵⁹ whereas Das *et al.* used an identical enzymatic process to demonstrate relative stabilities of amino acid methyl ester precursors, and of Fmoc-dipeptide-methyl esters relative to each other.⁵²

2.7 Spatiotemporal Control Over Nucleation and Structure Growth

Enzyme assisted self-assembly also allows for controlled nucleation and structure growth, which usually remains a challenge in molecular self-assembly, allowing for structures to be formed when and where required. Self-assembling building blocks are synthesised in the direct vicinity of the enzyme, which may result in the local concentration of monomers around the enzyme to be above the critical aggregation concentration. As a direct result, the system will favour structural self-assembly and result in localised nucleation and growth. This was clearly demonstrated by Williams *et al.* where they observe the early stages of biocatalytic self-assembly and fibre growth using microscopy techniques, revealing nucleation and development of fibres occurred exclusively in the direct vicinity of the enzyme.⁵⁹ Additionally, the controlled nucleation associated with enzyme assisted self-assembly has also been demonstrated by immobilisation of protease enzymes onto surfaces; thrombin onto the surface of magnetic microbeads,¹⁰⁹ and, thermolysin onto PEGylated surfaces.⁵⁹ Again, fibril formation and development originated from the areas of immobilised enzyme, observed by phase contrast microscopy,¹⁰⁹ and congo-red staining,⁵⁹ respectively.

3.0 Biocatalytic Self-Assembly of 2D Peptide-Based Nanostructures*

* This work was published in part in Soft Matter.³

Declaration of contribution to published article:

Any reproduced work from the aforementioned published article, I was solely responsible for, including the written article itself, unless otherwise stated. Dr. Tell Tuttle, Pim W.J.M. Frederix and Daniel Cannon provided molecular modelling data.

3.1 Introduction

Fmoc-SF-OMe self-assembles to form two-dimensional sheet-like structures, which is extremely rare as nucleation and growth is generally uni-directional,¹¹⁰ and the molecular chirality is typically amplified in supramolecular structures.¹¹¹ With the recent excitement surrounding two-dimensional polymers, such as graphene, the work in this Chapter is based on the characterisation of the biocatalytic self-assembly of aromatic peptide amphiphile Fmoc-serine-phenylalanine-methyl ester (Fmoc-SF-OMe).

3.1.1 Background

It was previously demonstrated that by condensing the two non-assembling amino acid fragments of Fmoc-protected serine (Fmoc-S) and phenylalanine methyl ester (F-OMe) in the presence of protease enzyme *thermolysin*, a self-supporting suspension was formed, indicating the formation of supramolecular structure.⁵² The system was studied in a dynamic combinatorial library (discussed in Section 2.6.2). The reaction vessel simultaneously contained; thermolysin, to catalyse the condensation of amino acid fragments and therefore act as the biocatalytic trigger for molecular self assembly, and; a mixture of amino acid fragments, Fmoc-S with six different aliphatic amino acid-methyl ester residues; phenylalanine (F), leucine (L), tyrosine (Y), valine (V), glycine (G) and alanine (A). As thermolysin operates under thermodynamic control (see Section 2.6.2), theoretically, thermolysin will catalyse the coupling of Fmoc-S with the preferred amino acid methyl ester to produce the most thermodynamically stable product accessible. It was found that Fmoc-SF-OMe was produced preferentially, which indicates that it is the most thermodynamically stable product available of the possible combinations, and that it has a strong tendency for molecular self-assembly.⁵² Furthermore, as the reaction is fully reversible, it is possible for the system to reconfigure to find the most thermodynamically stable state after the introduction of new entities, that is, by introducing the amino acid fragments in sequence rather than simultaneously, the system will be able to reconfigure to find the energetic minima. The sequential addition of amino acid fragments also resulted in the preferential formation of Fmoc-SF-OMe over any other possible combinations, regardless of the order which the amino acid fragments were introduced into the system.⁵²

However, its mode of self-assembly and the resulting self-assembled nanostructure formed have not yet been elucidated.

3.1.2 Thermolysin and Reversed Hydrolysis

Thermolysin is a relatively non-specific zinc metalloprotease enzyme which typically acts by hydrolysing peptide bonds.¹¹² It contains a zinc ion, essential for catalysis,¹¹² and four calcium ions necessary for thermal stability.¹¹³ The active site consists of two rounded domains with a deep cleft creating a pocket, lined with hydrophobic amino acid residues (see Figure 3.1),¹¹⁴ and therefore shows preferential catalysis for peptide chains with hydrophobic amino acid side chains.¹¹⁵⁻¹¹⁹ By acting as a Lewis acid, the zinc ion polarises the carbonyl group of the sensitive peptide bond by attacking the carbonyl oxygen, leaving the carbonyl carbon sensitive to nucleophilic attack from a water molecule, thus initiating hydrolysis of the peptide bond.^{120, 121} The reaction mechanism of thermolysin catalysed hydrolysis of peptide bonds is detailed in Figure 3.2.

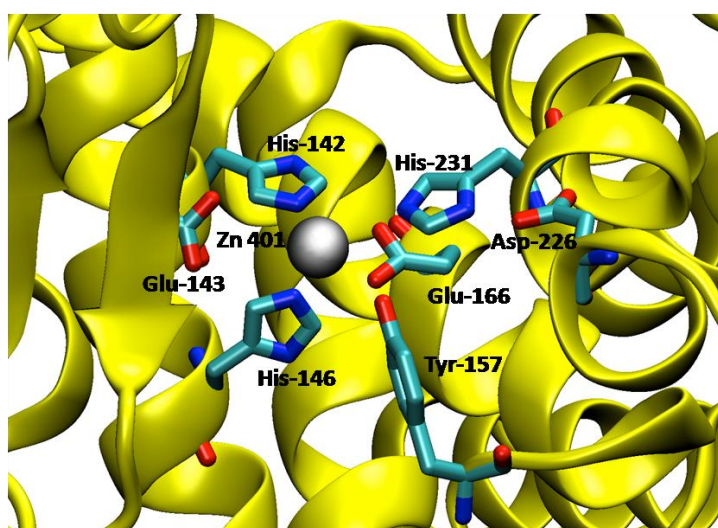


Figure 3.1 – Molecular model of thermolysin active site indicating the zinc ion and amino acid residues involved in catalysis.

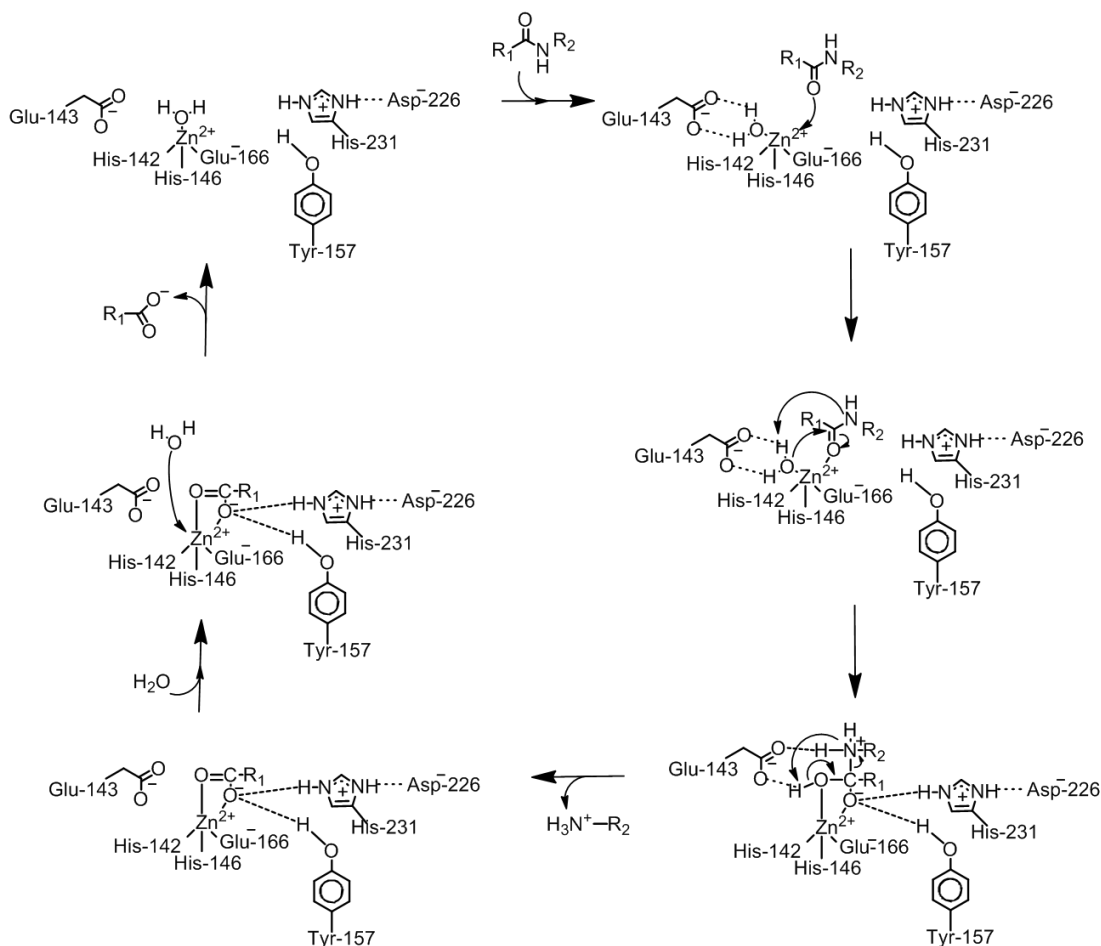


Figure 3.2 – Mechanism of thermolysin catalysed peptide bond hydrolysis.

It was demonstrated as early as 1979 that by manipulating reaction conditions, thermolysin can act in the opposite manner, catalysing condensation of amino acid fragments to synthesise peptide chains.^{120, 122, 123} The reverse reaction is known as reversed hydrolysis which is thermodynamically unfavourable in isolation. However, in terms of molecular self-assembly of aromatic peptide amphiphiles, driven by the stabilisation associated with the formation of supramolecular structures, the unfavourable equilibrium for synthesis is counteracted by the removal of the generated self-assembling peptide chains into their self-assembled state (discussed in Section 2.6.2).

A number of self-assembling di- and tri aromatic peptide amphiphiles have successfully been prepared by reversed hydrolysis of amino acid fragments using thermolysin,^{46, 47, 51, 59} including Fmoc-SF-OMe.⁵²

3.2 Results and Discussion

3.2.1 Preparation of Fmoc-SF-OMe

Self-assembling aromatic peptide amphiphile Fmoc-SF-OMe was generated by the condensation of non-assembling precursors, Fmoc-S-OH and F-OMe in a 1:4 ratio in sodium phosphate buffer pH 8, in the presence of thermolysin as previously described by Das *et al.* (see Figure 3.3).⁵²

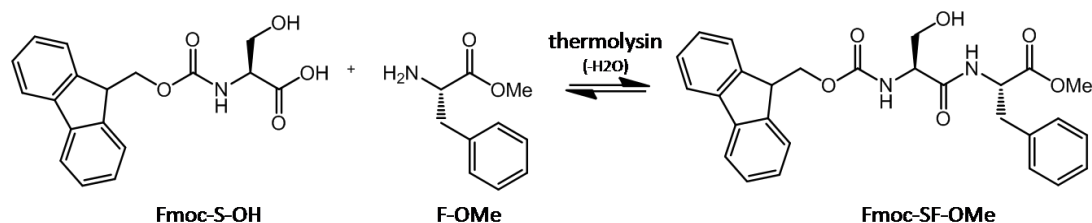


Figure 3.3 - Reaction schematic of Fmoc-S-OH reacting with F-OMe to form Fmoc-SF-OMe via reversed hydrolysis (condensation) using protease enzyme thermolysin.

The reaction progress was monitored by HPLC. The conversion of a 20:80 mM precursor mix reached a constant yield of 98 % after 24 hours (see Figure 3.4).⁵² Lower concentration mixtures were also monitored, with 10:40, 5:20, 4:16, 3:12 and 2.5:10 mM ratio of Fmoc-S-OH:F-OMe reaching yields of 92, 82, 66, 61 and 51 % respectively – exhibiting typical equilibrium behaviour, with higher yields of Fmoc-SF-OMe formed with increased concentrations of starting materials. However, rather than forming translucent self-supporting hydrogels typically observed for aromatic peptide amphiphiles,³⁰⁻³⁹ the self-assembly resulted in weak opaque suspensions, and only the 20:80 mM sample being completely self-supporting, which remained stable for a number of weeks, indicating that the self-assembled structures are large enough to scatter visible light (see Figure 3.4(c)).

The chemically synthesised compound Fmoc-SF-OMe, in a pure state, or as a 1:3 ratio mixture of compounds Fmoc-SF-OMe and F-OMe, forms amorphous precipitates in buffer with no evidence of formation of ordered nanostructures, indicating the enzyme plays a key role in stabilisation of the suspensions and in accessing the self-assembled structures.

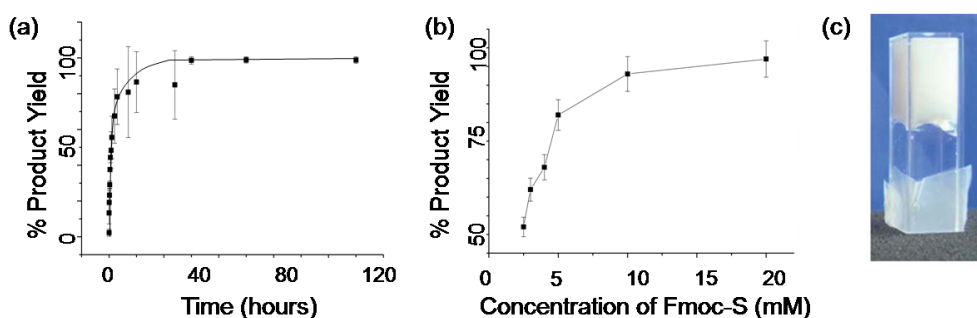


Figure 3.4 - (a) Conversion of 20:80 mM Fmoc-S + F-OMe forming Fmoc-SF-OMe followed by HPLC monitoring over time. (b) The relationship between concentration of Fmoc-S reactant used and the percentage yield of the desired aromatic peptide amphiphile Fmoc-SF-OMe; lower concentration of starting materials leads to lower product yields. Percentage yield calculated using HPLC method at 100 hours after the reaction was initiated. (c) Fmoc-SF-OMe self-assembles to form nano-sheets within a self-supporting opaque suspension at 20:80 mM concentration of starting materials.

3.2.2 Nanoscale Morphology

Initial investigation of the self-assembled structure was carried out using TEM and cryoTEM (see Figure 3.5). This revealed sheet-like structures of many microns in both X and Y dimensions, in addition to twisted nano-ribbons, which accounts for the opacity of the samples.

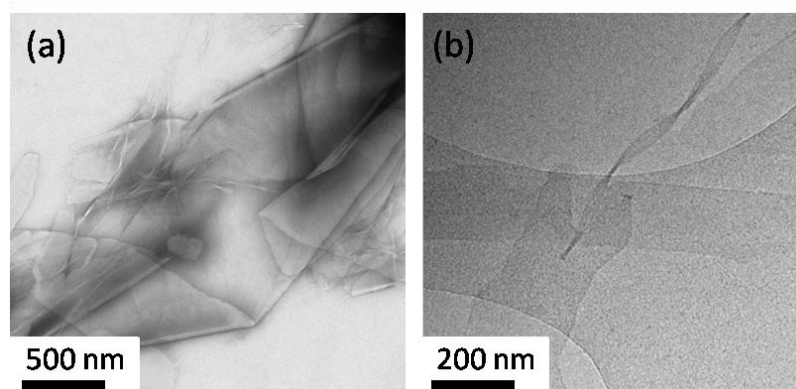


Figure 3.5 - (a) TEM and (b) Cryo-TEM images of nanostructures formed from self-assembly of Fmoc-SF-OMe obtained after 24 h.

Further investigation was carried out using TEM to monitor the development of self-assembled structures and suggest a possible mechanism for their formation. This was performed by imaging the material at key time points (see Figure 3.6). Twisted tapes were predominantly observed at the early stages (after around 1.5 hours of thermolysin addition). 24 hours after the reaction has been initiated, branching of the twisted nanoribbons and nucleation of ribbons from the edge of sheets were observed. The images suggest a progression through several phases before reaching the final sheet structures – which can be described as ‘widening’ of nano-ribbons to ultimately produce sheets. This morphological development suggests that initially the self-assembling molecules enter a kinetic state, dictated by the rate at which the enzyme delivers the molecules to the self-assembled structure. However, as the enzymatic reaction is reversible, the structural evolution can be attributed to the constant enzymatic structure correction at the edges of existing structures to find the most thermodynamically stable state.

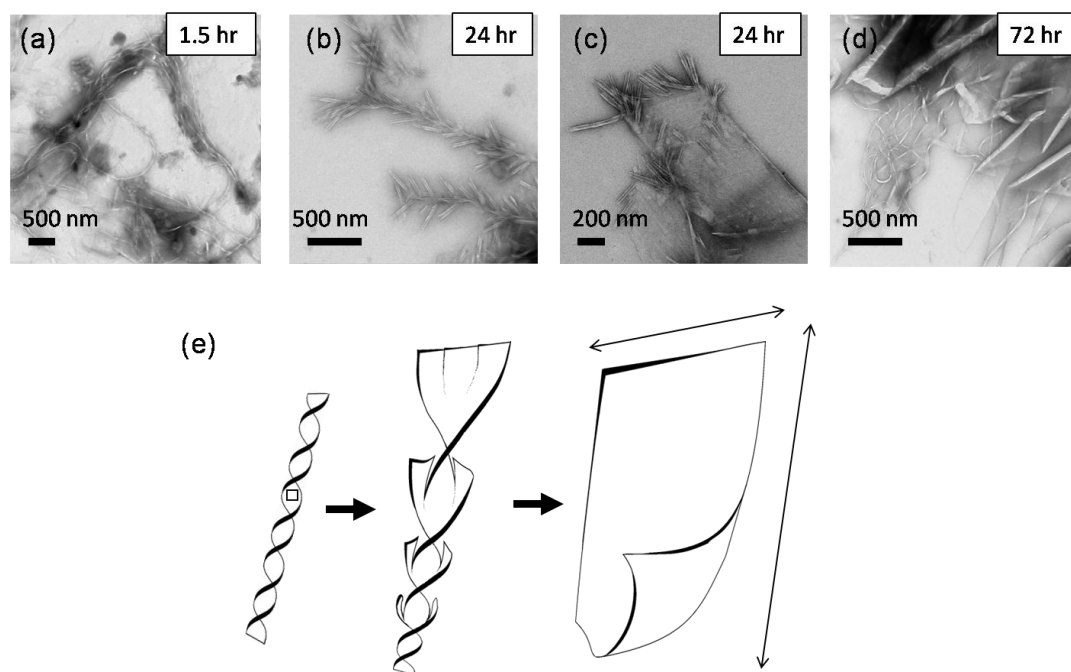


Figure 3.6 - Transmission Electron Microscopy (TEM) images of the polymorphic nanoscale structure of Fmoc-SF-OMe. Twisted ribbons, branched twisted ribbons, frayed sheets, and developed nanosheets can be observed from (a-d) respectively. (a) 1 hour, (b,c) 24 hours, (d) 72 hours. (e) Schematic representation of proposed formation of sheets.

Typically, peptide based nanostructures usually take the shape of zero- or one-dimensional chiral structures, such as micelles, tubes,^{16, 30-33, 60} fibers,^{1, 2, 124} or (twisted) ribbons,²¹ as seen

for the earlier timepoints for self-assembled Fmoc-SF-OMe. Their predisposition to adopt chiral uni-directional structures is a direct result of the combination of two factors; (1) amplification of the inherent molecular chirality in the peptide building blocks,¹¹¹ and; (2) the nucleation and growth mechanisms which generally involve formation of nuclei that have a preference to extend uni-directionally.¹¹⁰ For example, in β -hairpin assembly (discussed in Section 2.3.2), lateral growth is unfavoured because all peptides assemble in register, in which case the width is dictated by peptide length.¹²⁴ However, in cases where lateral association through formation of 'sticky ends' is possible, it remains unknown as to what causes such growth restrictions,^{8, 125} however it is most likely related to the size of initial nuclei which have a preference to grow uni-directionally, i.e. a kinetic effect. A key difference in the system described here, is that the building blocks themselves can be reversibly formed and hydrolysed, giving rise to a system which will be less prone to kinetic locking.

A number of approaches have successfully generated planar nanostructures (described as belts/tapes) from the self-assembly of peptides and peptide derivatives, overcoming their tendency to form chiral structures. However, their growth has always been restricted in one-dimension due to the preferential uni-directional growth.

In 2009, Cui *et al.* described the formation of giant peptide nanobelts from peptide amphiphiles.¹²⁵ The tetrapeptide, EVEV, was chemically modified with an alkyl tail sixteen carbon atoms in length. In aqueous environments, the peptide amphiphiles formed a bilayer similar to phospholipids (discussed in Section 3.3.4),^{91, 92} burying the hydrophobic tails from the media, and allowed for hydrogen bonding between the peptide chains, and resulting in nanobelt structures with restricted dimensions in one-dimension.¹²⁵

Shao *et al.* designed an aromatic peptide amphiphile Fmoc-dipeptide-NDI, Fmoc-KK(NDI).⁸ In aqueous media, the peptide derivatives assembled to form a β -sheet assembly interlocked by π -stacking of Fmoc groups, with the amino acid sides extending out from the β -sheet plane. This created a β -sheet with a hydrophilic face and a hydrophobic face, which dimerised in the aqueous environment to bury the hydrophobic NDI groups – the resulting nanotapes uniformly four peptide amphiphiles in width (8 nm), and resulting in solely unidirectional growth despite possible interactions evident in both directions of their molecular model.⁸

Additionally, flat belt structures have been generated by the self-assembly of more conventional peptides. Aggeli *et al.* demonstrated the production of flat β -sheet nanotapes from the self-assembly of an 11 amino acid residue peptide.¹²⁶ The peptide, CH₃CO-QQRFQWQFEQQ-NH₂, assumed an elongated β -sheet association, however the width was always restricted to one molecule width.¹²⁶ Adams *et al.* designed three surfactant-like peptides, each of 8 amino acid residues, which had the ability to form flat nanotapes with unidirectional growth by adopting the β -sheet configuration; VVVVVDD, VVVVDVD and VVVDDVV.¹²⁷ However, the nanotape structures were never exclusively observed from the self-assembly of V₆D₂, twisted ribbons and crystalline structures were also evident when examining their morphology.¹²⁷ Similarly, Matsumura *et al.* designed an amphiphilic β -sheet peptide of 10 amino acid residues in length, PKFKIIEFEP, which adopted a planar belt nanoscale morphology, again restricted to growth in one direction.¹²⁸

Zhang *et al.* produced macroscopic membrane structures in 1993 from the self-assembly of a 16 amino acid residue peptide (AEAEAKAK)₂.¹⁷ However, on closer magnification, they were not truly two-dimensional. Instead, they were comprised of a tightly woven nanofibrillar network which gave the illusion of self-assembled planar structures.¹⁷

However, in 2010 Nam *et al.* demonstrated that by using non-chiral polymers with peptide like side chains, they could successfully access crystalline two-dimensional structures.¹²⁹ However, molecularly they cannot be considered as a peptide or peptide derivative, as there are no carbonyl groups present on the molecular backbone, and so are described as peptoids throughout.¹²⁹

The biocatalytic self-assembly of Fmoc-SF-OMe using thermolysin is the first example of truly two-dimensional nanostructures from self-assembly of aromatic peptide amphiphiles, with the reversible enzymatic reaction playing a key role in accessibility of the morphology.

3.2.3 Molecular Association

Fluorescence emission spectroscopy was used to monitor changes in fluorenyl environment as the reaction proceeded (see Figure 3.7(a)). It should be noted that a substantial reduction in signal intensity was observed over time, this is, at least in part, due to the sample becoming increasingly opaque. The spectra were normalised to allow a more

accurate determination of peak formation and shifting; whilst original intensity changes of each peak of interest are shown in Figure 3.7(b). It is evident that a number of structural changes occur. The starting mixture shows two predominant features emitting at approximately 320 and 330 nm, representing monomeric and aggregated forms of Fmoc-S-OH precursors in solution. Within 10 minutes a red shift accompanied by an increase in intensity indicates a supramolecular transition producing a more intensely emitting fluorenyl species. The formation of a red-shifted peak at 365 nm accompanied by system quenching (Figure 3.7(b)) could be associated with formation of extended aggregates through π -stacked systems as previously observed, e.g. for Fmoc-LLL-OH⁹ and Fmoc-FF-OH.^{30, 32} However, it should be noted that the red-shift is much less pronounced for the system under study, suggesting that fluorenyl face to face π -stacking may not be optimal in these systems. After 24 hours, the free fluorenyl peak has nearly disappeared, suggesting that few Fmoc-S-OH or Fmoc-SF-OMe species are in the un-assembled state, which is consistent with the condensation yield observed.

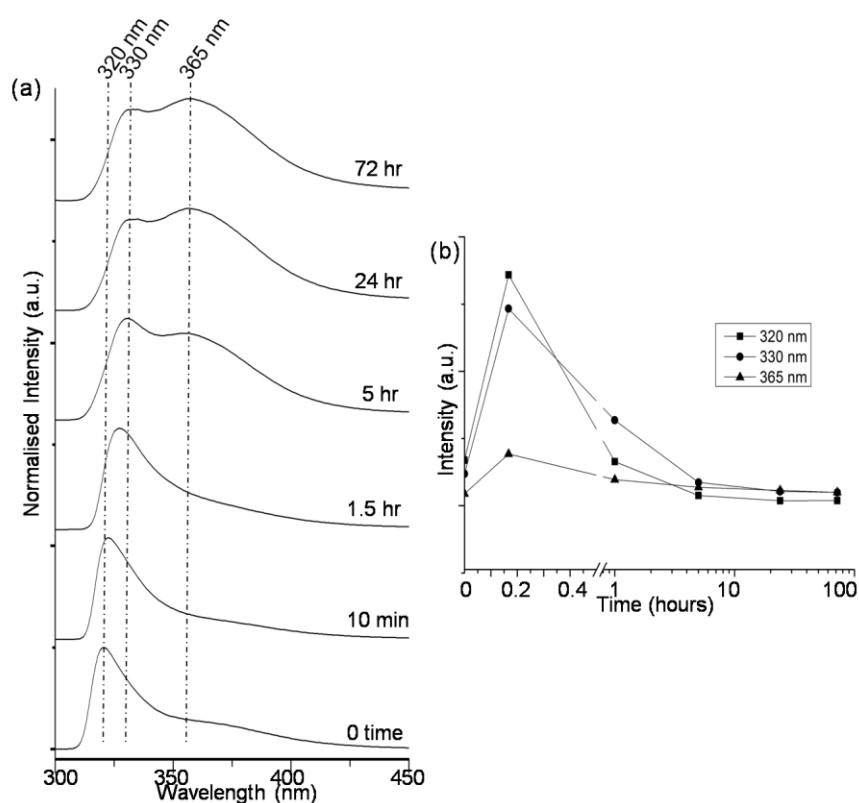


Figure 3.7 - (a) Fluorescence emission spectra monitored over 72 h. (b) Relative intensity of 320 nm, 330 nm and 365 nm peaks within fluorescence spectra monitored with time (intensity normalised).

The hydrogen bonding interactions of peptide moieties of Fmoc-SF-OMe were then monitored using FTIR spectroscopy focusing on carbonyl stretching in the amide I region. Figure 3.8(b) illustrates the time-dependent correlation peaks at 1640 cm^{-1} , 1680 cm^{-1} and 1650 cm^{-1} peak intensities. As they all appear at the same point over the reaction coordinate it can be assumed that they represent the molecular organisation of nano-structural sheets. The pair of peaks at 1640 cm^{-1} and 1680 cm^{-1} are characteristic of the formation of a β -sheet arrangement of the peptide moieties (see Figure 3.8(a)).^{9, 30-33, 130} This structure becomes evident from 5 hours and also remains in this arrangement over 72 hours. It is noticeable that the peaks gradually shift to lower frequencies during this time, consistent with hydrogen bonding strength increasing. This is accompanied by the occurrence of a peak due to the carbonyl stretch associated with the methyl ester moiety at 1728 cm^{-1} in addition to the peak at 1745 cm^{-1} attributable to the carbonyl of free F-OMe. However, a prominent peak at 1650 cm^{-1} , indicative of a random order of peptides¹³⁰ is also present, which indicates that although the structure is organised as an extended anti-parallel β -sheet arrangement, there is also a disordered component. In contrast to the similar dynamics of the FTIR peaks located at 1640 and 1680 cm^{-1} (β -sheet) and 1650 cm^{-1} (pseudo random coil), it is interesting to note the appearance of the peak at 1620 cm^{-1} , which occurs only after 24 hours. The assignment of this peak is currently unclear but the timescales are consistent with higher order structure formation of crystalline spherulitic macrostructures (as discussed in Section 3.2.4).

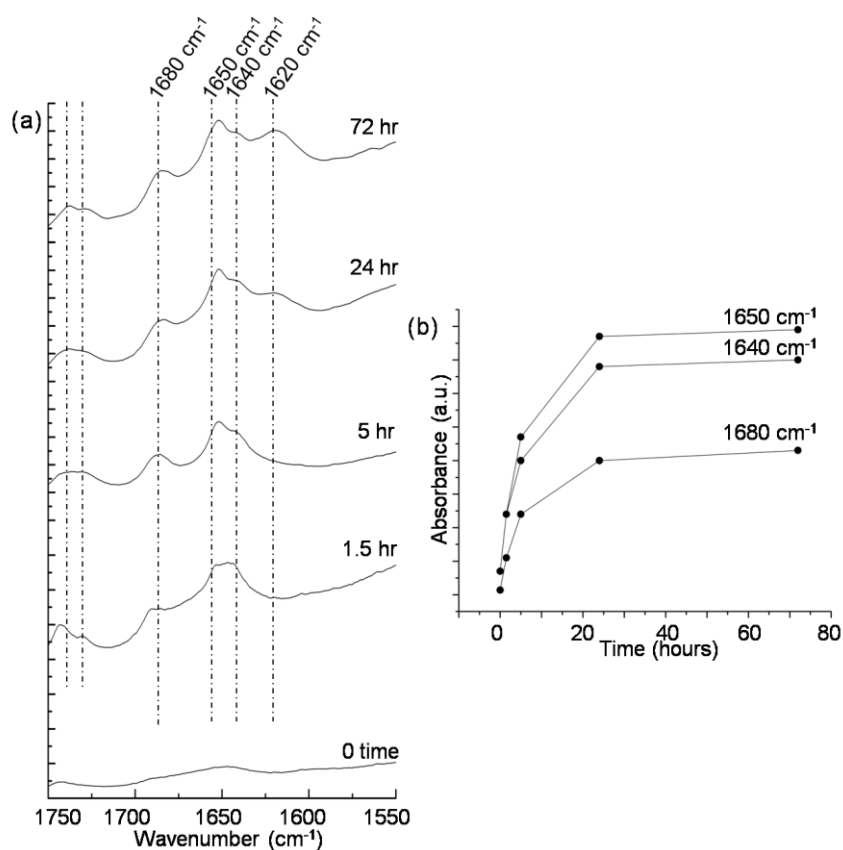


Figure 3.8 - (a) Amide I region of FTIR absorbance spectra monitored over 72 h, representing carbonyl stretching mode of amino acid residues. (b) Relative intensity of 1640 cm^{-1} , 1680 cm^{-1} and 1650 cm^{-1} bands within FTIR spectra monitored with time.

In order to confirm the proposed structure, WAXS diffraction patterns were obtained (see Figure 3.9). A prominent peak with 5 higher order reflections indicates a repeating pattern of 16 Å which we have correlated to the repeating unit along the peptide backbone, and additional peaks corresponding to 4.8 Å and 3.7 Å which relate to β -sheet spacing and π -stack spacing respectively.⁹ Typically, this type of π -interlocked β -sheet (π - β) molecular association results in fibrillar network structures,^{9,30} but has also been observed to produce belts when Fmoc-dipeptides with hydrophilic and (modified) hydrophobic residues were used.⁸

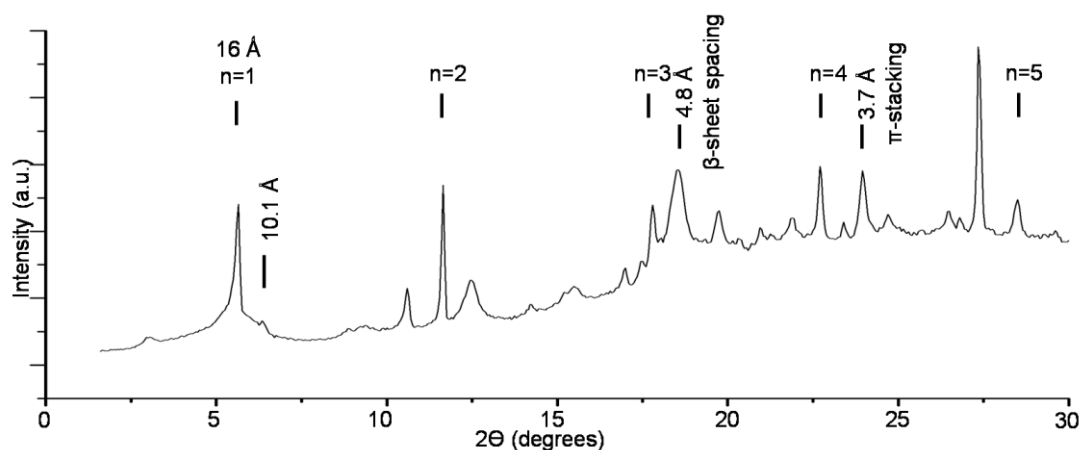


Figure 3.9 – WAXS data of Fmoc-SF-OMe (dried sample) at 24 h.

3.2.4 Molecular Modelling

A π - β molecular model of self-assembled Fmoc-SF-OMe was constructed in an attempt to demonstrate the molecular arrangement that could result in sheet formation, and determine if the molecular spacing from the WAXS data, as assigned, was feasibly assigned (see Figure 3.10). The molecular model appeared to be consistent with the observed planar sheets (see Figure 3.10). The Fmoc-groups form stacked pairs rather than a continuous π -stack proposed for Fmoc-FF.^{30, 32} In that system, the C-terminal phenyl group intercalated between the Fmoc groups to create a continuous π -stack. In the case of Fmoc-SF-OMe the methyl ester prevents the molecules assuming this configuration, which would also explain the absence of a 450 nm peak associated with J-aggregate formation observed in fluorescence by Smith *et al.*³⁰ and Xu *et al.*⁹ The phenyl moieties of phenylalanine residues can interact with those from a neighbouring array to form the π - β bilayer as illustrated in Figure 3.10(c). This molecular association also explains the formation of extended two-dimensional structures rather than one-dimensional fibres or tubes, since next to the π -stacking of fluorenyl groups and anti-parallel β -sheets there is a driving force that extends the structure in a biaxial direction, yet keeping its linearity. Overall, this assembly results in the hydrophobic phenylalanines being completely buried within the bilayer, while the hydrophilic serine residues are orientated outwards and can hydrogen bond to the aqueous environment or with serine residues of a neighbouring self-assembled bilayer system to

produce multilayers, similar to Shao *et al.*⁸ and to well-documented bilayered tapes in larger β -sheet self-assembling peptides.^{21, 131}

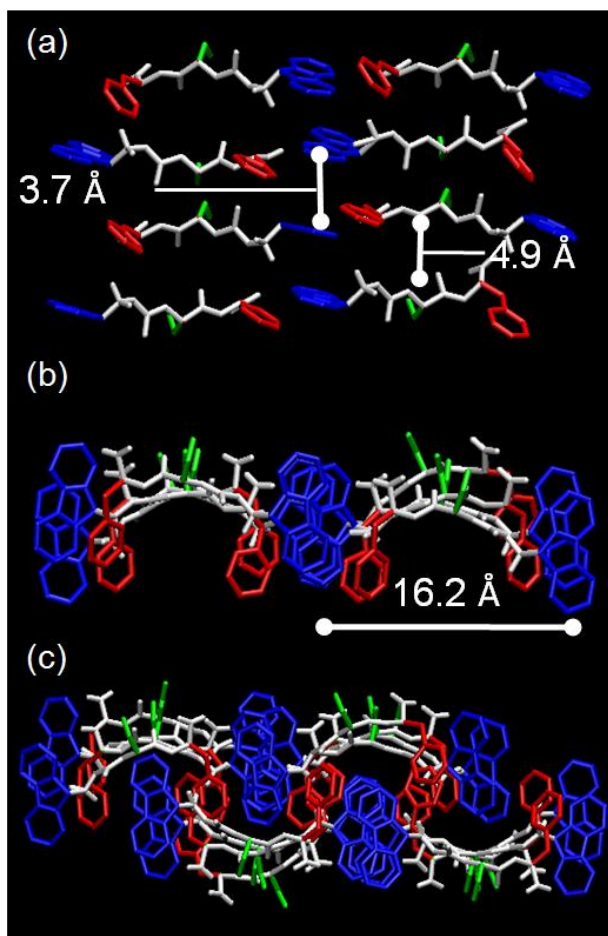


Figure 3.10 - Molecular association models. Blue: fluorenyl groups. White: peptide backbone. Red: phenylalanine side chains. Green: serine side chains. Hydrogens not shown for clarity. Spacing calculated from molecular images. (a) 8-mer anti-parallel β -sheet arrangement. (b) 8-mer side view. (c) 16-mer side view of two separate 8-mers where their hydrophobic residues interact to form a bilayer.

From the structure in Figure 3.10, a 64-mer was built of 8 x 4 x 2 molecules (see Figure 3.11). The proposed structure proved to be stable under minimization using molecular mechanics, and exhibits repeating units with average distances of 16.2 Å (Fmoc-column to Fmoc-column), 4.9 Å (peptide backbone to backbone), and 3.7 Å (Fmoc- to Fmoc- within the π -stacked columns), remaining in excellent agreement with the reflections observed in WAXS. Additionally, 10.1 Å can be observed for Fmoc-pair to Fmoc-pair in the stacking direction, which also corresponds to a peak on the WAXS data (see Figure 3.9). The

proposed model is also consistent with the other spectroscopic results such as the formation of stable β -sheets observed from FTIR. The minimized model also shows that the methyl ester may form an intramolecular hydrogen bond with the serine hydroxyl group, which may explain the observed shift in the methyl ester peak (see Figure 3.8(a)).

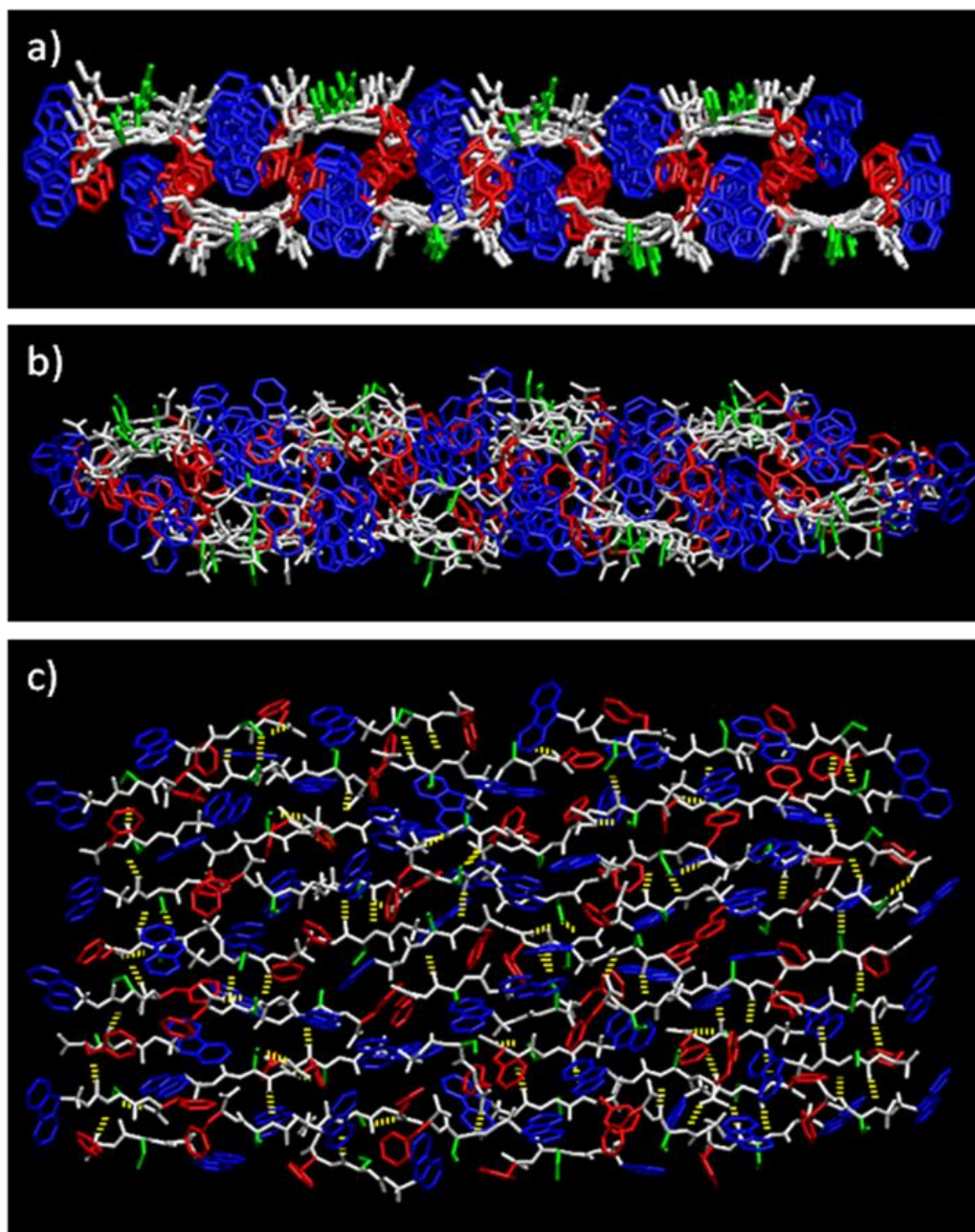


Figure 3.11 - Fmoc-SF-OMe 64 mer model: Blue: fluorenyl groups. White: peptide backbone. Red: phenylalanine side chains. Green: serine side chains. Hydrogens not shown for clarity. (a) Side view of starting structure. (b) Side view of structure minimized for 50000

steps. (c) Top view of minimized structure. Dotted yellow lines indicate hydrogen bonds with $d < 3.4 \text{ \AA}$ and donor-acceptor angle $< 25^\circ$.

3.2.5 Hierarchical Assembly

During the latter stages of self-assembly (24–72 hours), a remarkable further hierarchical self-assembly was observed which is tunable by enzyme concentration. SEM analysis reveals that macroscopic spherulitic structures are formed of several hundred microns in diameter (see Figure 3.12).

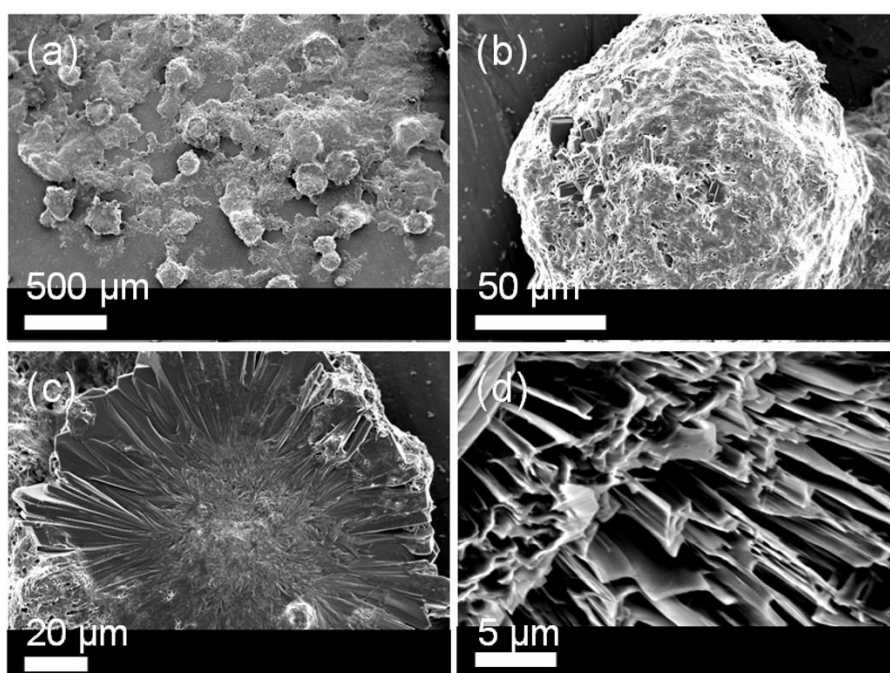


Figure 3.12 - SEM imaging of self-assembled Fmoc-SF-OMe. (a) Spherical structures and ‘halved’ spherical structures can be seen to lie on a layer of the nano-sheet material. (b) Spherical structures encased in nano-sheet material. (c) Spherical structures have crystalline spherulitic centres with no obvious nucleation point and are surrounded by a layer of sheets. (d) Lamellar structure of non-spherulitic areas.

These spherulites are surrounded by non-spherulitic areas of material being constructed of layered lamellar structures, thought to represent multilayers of the 2D sheets discussed, which could feasibly interact via hydrogen bonding of the exposed hydroxyl groups of the

serine residues. Higher magnification SEM images of the spherulitic structures shows that these structures are composed of sheets, with no obvious nucleation points at their centres. Peptide based spherulitic structures have been obtained previously by solvent induced phase transitions¹³² or by hierarchical assembly from aromatic peptide amphiphiles.¹³³

It has previously been demonstrated that self-assembly is favoured in the direct vicinity of enzymes^{43, 51, 59, 134} and therefore it is tempting to propose enzymatic control of spherulite formation. To investigate a possible link between enzyme concentration and spherulite formation, a range of enzyme concentrations (0.1, 1, 10 mg mL⁻¹) were analysed using polarising optical microscopy. The spherulitic structures displayed birefringence when viewed under cross polarisers (see Figure 3.13). Each of the samples appear as opaque suspensions at 24 hours. However, the rate at which each becomes self-supporting varies; 0.1 mg mL⁻¹ thermolysin after approximately 24 h, 1 mg mL⁻¹ within a matter of hours, and 10 mg mL⁻¹ after only a few minutes of the reaction being initiated; which is to be expected. At a low enzyme concentration of 0.1 mg mL⁻¹, no spherulitic structures form. This has been further confirmed by the formation of solely the layered lamellar structures visible using SEM. Additionally, the use of a higher enzyme concentration (10 mg mL⁻¹) displayed a dramatic increase in the number of these spherulitic structures are formed. This signifies that the enzyme plays a key role in nucleation process to form these spherulites, however it does not affect the ultimate size of the crystals (diameter of just over 100 µm).

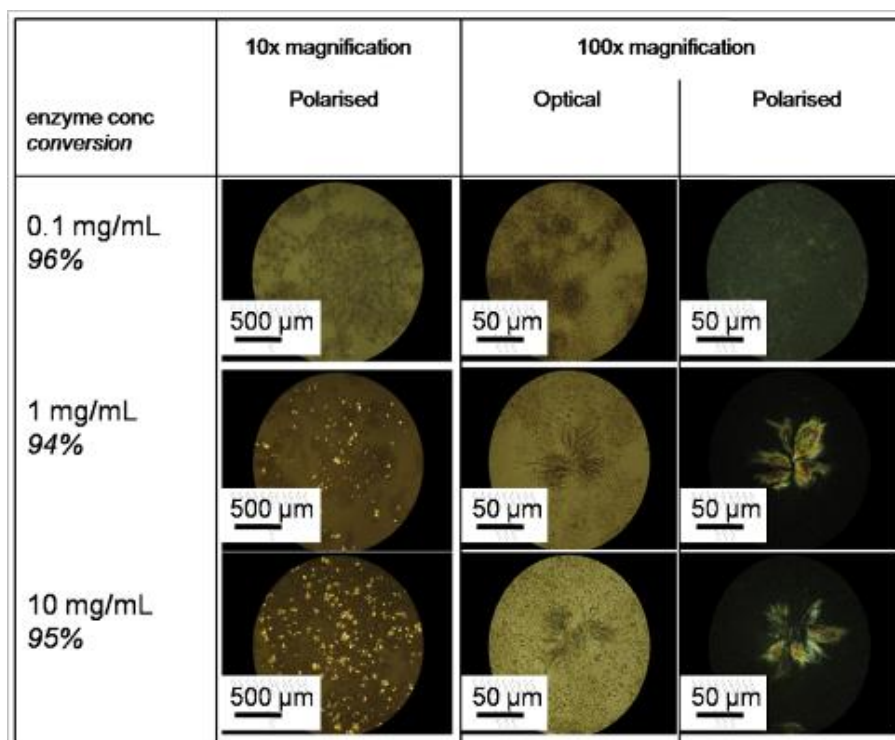


Figure 3.13 -Optical and polarised images of macrostructure. Birefringence or crystalline structure is observed when viewed under cross-polarisers. A relationship between enzyme concentration and number of spherulitic structures is observed.

3.3 Conclusions

The biocatalytic self-assembly of Fmoc-SF-OME by thermolysin has provided the first two-dimensional nanostructures from chiral peptide derivatives. The enzyme itself plays a key role in stabilisation of the suspension and nucleation of the spherulitic macrostructures, and the reversibility of the enzymatic reaction allows access to the structures by favouring the thermodynamic product (extended sheets) over the kinetically favoured one-dimensional structures. On a molecular level, the Fmoc-SF-OME molecular building blocks associate in a β -sheet fashion, which are interlocked *via* π -stacking interactions of Fmoc groups to produce extended sheet structures with a hydrophobic and a hydrophilic face. In an aqueous environment the sheets dimerise, to keep the hydrophobic faces hidden from water, with further stabilisation interactions possible *via* π -stacking of phenyl rings, and create amphiphilic bilayers.

The production of nano-sheets with well-defined chemical composition is of interest in production of surfaces with precisely presented bioactivity, and may also be used in templating,^{5, 6} and by combination with biocatalysis, dynamic template structures may be feasible.^{135, 136}

4.0 Sequence/structure relationships in aromatic dipeptide hydrogels formed under thermodynamic control by enzyme-assisted self-assembly*

* This work was published in part in Soft Matter.⁴

Declaration of contribution to published article:

Any reproduced work from the aforementioned published article, I was solely responsible for, including the written article itself, unless otherwise stated. Dr. Tell Tuttle and Pim W.J.M. Frederix provided the molecular modelling data.

4.1 Introduction

Self assembled peptide nanostructures have given rise to a variety of morphological structures, such as nano-tubes,^{16, 30-33, 59, 60} (twisted) ribbons,²¹ fibres,^{1, 2} tapes,^{8, 47} spheres,⁶¹ rings (doughnuts)⁶² and leaf-like structures.⁴² It has become increasingly clear that in addition to the chemical composition, the route of self-assembly can have a pronounced effect on the morphology and properties of the nanostructure formed,^{47, 63-65} with the self-assembled structure often reflecting a kinetically trapped state rather than the thermodynamically most favoured structure (discussed in Section 2.6). This presents a challenge when trying to elucidate the design rules for these systems as the observed structures usually emerge due to a varying combination of kinetic and thermodynamic contributions. In this Chapter, a thermodynamically controlled self-assembly is utilised, driven by enzymatic condensation of amino acid derivatives. By using thermolysin, a fully reversible system that operates under thermodynamic control (discussed in Section 3.1.2),^{52, 59} the approach can be used to elucidate sequence/structure relationships based on thermodynamic self-assembly behaviour which is not influenced by the route of assembly.

Following on from Chapter 3, the work in this Chapter is based on the characterisation of four closely related Fmoc-dipeptide-methyl esters which form the thermodynamically preferred supramolecular structures; Fmoc-serine-phenylalanine-methyl ester (Fmoc-SF-OMe), Fmoc-serine-leucine-methyl ester (Fmoc-SL-OMe), Fmoc-threonine-phenylalanine-methyl ester (Fmoc-TF-OMe) and Fmoc-threonine-leucine-methyl ester (Fmoc-TL-OMe). In particular, the influence of the additional chiral centre when interchanging the serine residue with a threonine, and the effects of the aromatic moiety of the phenylalanine residue versus leucine, in an attempt to rationalise the effect of the peptidic tail.

4.1.1 Background

It was previously demonstrated that by condensing the two non-assembling amino acid fragments in the presence of protease enzyme *thermolysin*, the product could be a self-assembling aromatic peptide amphiphile. Fmoc-SF-OMe (SF), Fmoc-SL-OMe (SL), Fmoc-TF-OMe (TF) and Fmoc-TL-OMe (TL), have all been successfully generated using thermolysin –

a fully reversible system, and given rise to supramolecular structures of the thermodynamic minimum (discussed in Section 3.1.2).^{46, 52}

Furthermore, each of these peptide derivatives have been used in a dynamic combinatorial library; a reaction vessel contained thermolysin, Fmoc-amino acid (either S or T), and six different amino acid methyl esters (F, L, Y, V, G and A). In each case, the major product was Fmoc-XF-OMe (~ 60 %), followed by Fmoc-XL-OMe (21 % and 14 % for Fmoc-S and Fmoc-T, respectively), and almost negligible amounts of any other possible product (< 3 %).⁵² As the system operates under thermodynamic control, the preferential coupling with F-OMe indicates that Fmoc-SF-OMe is the most thermodynamically stable product available, with L-OMe falling slightly behind. Das *et al.* then demonstrated that by adding the various amino acid methyl esters in sequence, the system reconfigured itself to achieve the thermodynamic composition as before, regardless of the order of addition of the amino acid methyl esters.⁵²

Furthermore, by setting Fmoc-S and Fmoc-T in direct competition to couple with F-OMe in the presence of thermolysin, a roughly 50:50 mixture of Fmoc-SF-OMe to Fmoc-TF-OMe was obtained when added simultaneously or in sequence, indicating an almost equal thermodynamic stability.⁵²

However, despite the comprehensive study on relative thermodynamic stabilities and use in DCL's, to date, the enzymatically triggered supramolecular structures of Fmoc-SL-OMe, Fmoc-TF-OMe and Fmoc-TL-OMe have not been studied, with Fmoc-SF-OMe discussed in the previous Chapter of this thesis (see Chapter 3).³ More specifically, it has not yet been established what dictates the more favourable assembly of the F containing peptides.

4.2 Results and discussion

4.2.1 Composition

The precursor solution contained a 20 : 80 mM ratio of Fmoc protected serine (Fmoc-S-OH) or threonine (Fmoc-T-OH) and the methyl ester of phenylalanine (F-OMe) or leucine (L-OMe)⁴⁶(see Figure 4.1).

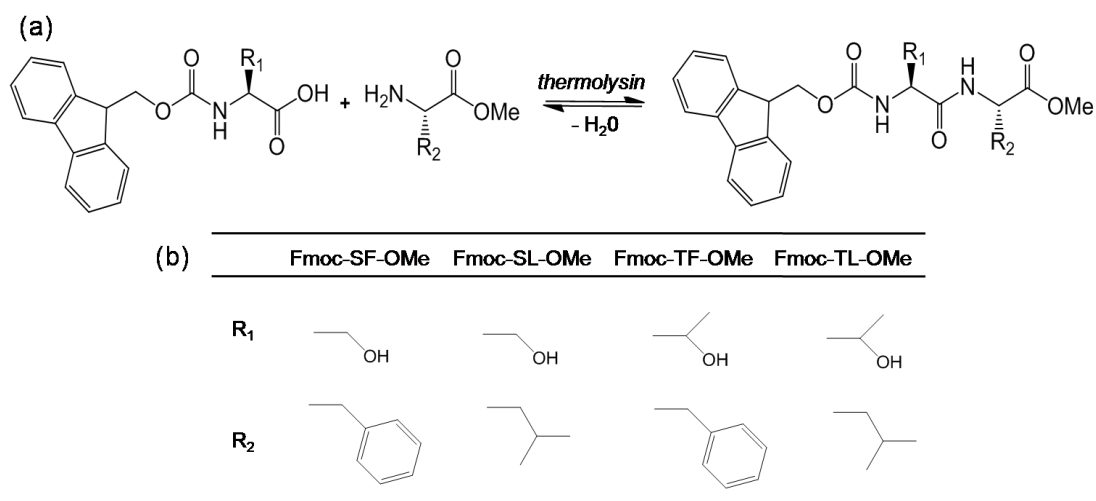


Figure 4.1 – (a) Reaction schematic of Fmoc-amino acid coupling with amino acid-methyl ester via reversed hydrolysis in the presence of thermolysin. (b) Amino acid side chains for each system under study, Fmoc-SF-OMe, Fmoc-SL-OMe, Fmoc-TF-OMe, Fmoc-TL-OMe.

The conversion from amino acid fragments to the desired self-assembling aromatic dipeptide amphiphiles via a condensation reaction catalysed by thermolysin was followed using HPLC. Each of the reaction systems had reached maximum conversion after 24 h from reaction initiation and remained relatively constant for up to 100 hours (see Figure 4.2(a)). Fmoc-SF-OMe, Fmoc-SL-OMe, Fmoc-TF-OMe and Fmoc-TL-OMe reaching yields of 98%, 79%, 94% and 75% respectively, which are in good agreement with previous studies.^{3, 52} These differences in yield reflect the relative thermodynamic stability of the self-assembling structures, with Fmoc-SF-OMe and Fmoc-TF-OMe being more thermodynamically stable than their L-OMe counterparts.⁵² For each of the four separate systems, solutions of similar opacity were transformed to a self-supporting system (see Figure 4.2 (b)-(e)), with varying degrees of turbidity; SF > TF ~ SL > TL. The variable morphology of these nanostructures appear to produce differing abilities to scatter visible light.

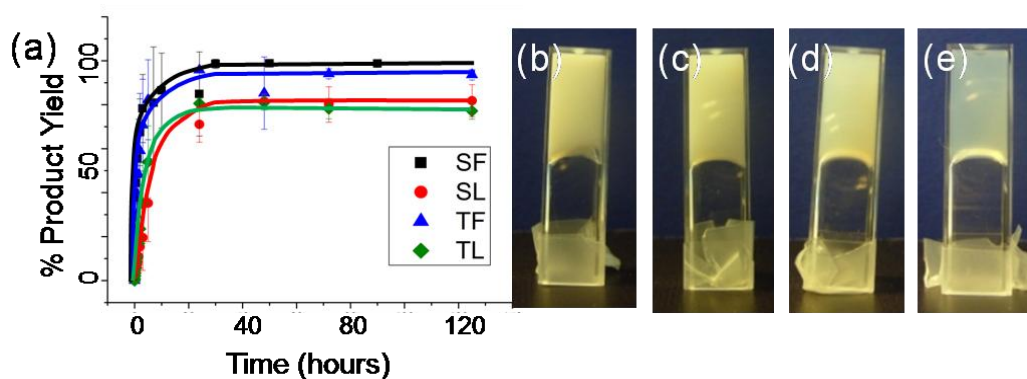


Figure 4.2 – (a) Conversion to Fmoc-dipeptide followed over time using HPLC. (b)-(e) Images of self-supporting materials taken at 24 h, Fmoc-SF-OMe, Fmoc-SL-OMe, Fmoc-TF-OMe and Fmoc-TL-OMe, respectively.

4.2.2 Nanoscale Morphology

Initial investigations into these self-assembled structures were carried out using TEM and cryoTEM (see Figure 4.3). These electron microscopy studies revealed four remarkably different nanoscale structures. As previously demonstrated, the SF system forms two-dimensional bilayer nanosheets (discussed in Section 3.2.2).³ In contrast the SL nanostructures were planar belts, TF formed an extended network of twisted fibres, while TL formed short twisted fibres. The high opacity associated with the self-assembled SF system was attributed to the size of the sheets, which span many micrometres, and hierarchical assembly into crystalline spherulitic macrostructures (discussed in Section 3.2.5);³ structures notably absent from the SL, TF, and TL systems when viewed using optical microscopy. However, we attribute the high opacity of SL, TF and TL to a dense fibre network structure.

From the data collected, it can be deduced that the presence of a serine residue in amino acid position one on the Fmoc-dipeptide appears to induce the formation of planar structures. Nano-belt structures have been described before,^{8, 125, 126, 128} however it is a rarity amongst the commonly observed chiral structures favoured due to the inherent chirality of peptides.¹¹¹ Indeed, by replacing the serine with a threonine residue (i.e. introducing an additional chiral centre to the amino acid side chain), no planar structures are observed. Instead, the familiar chiral twisted structure is restored, in the form of

twisted ribbon-like structures, most likely due to the additional hydrophobic methyl group of the threonine side chain minimising contact with the aqueous surroundings.

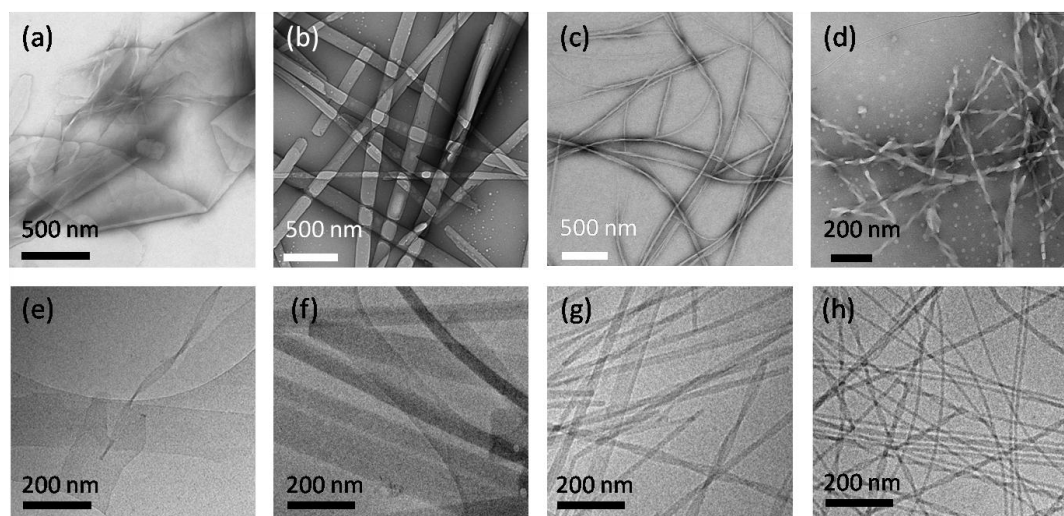


Figure 4.3 – (a)-(d)TEM images and, (e)-(h) cryoTEM images taken after 24 hours, of Fmoc–SF–OMe, Fmoc–SL–OMe, Fmoc–TF–OMe and Fmoc–TL–OMe respectively.

4.2.3 Mechanical Properties

The mechanical properties of the self-supporting samples were confirmed by rheology. By monitoring the development of the elastic (G') and viscous (G'') moduli over time (see Figure 4.4), it was observed that the elastic component of the more thermodynamically stable Fmoc–XF–OMe derivatives develop more rapidly compared to each of their corresponding Fmoc–XL–OMe peptides, where both the elastic and viscous components becoming stable within 5 hours. Furthermore, the assembly of serine containing SF and SL assemble in a two-stage process, suggesting morphological transformation from one-dimensional ribbons, followed by widening to form the observed two-dimensional nanostructures. This is consistent with the morphological evolution of these structures observed by TEM for SF (discussed in Section 3.2.2),³ and it would be rational to conclude that SL nanostructures develop in a similar manner.

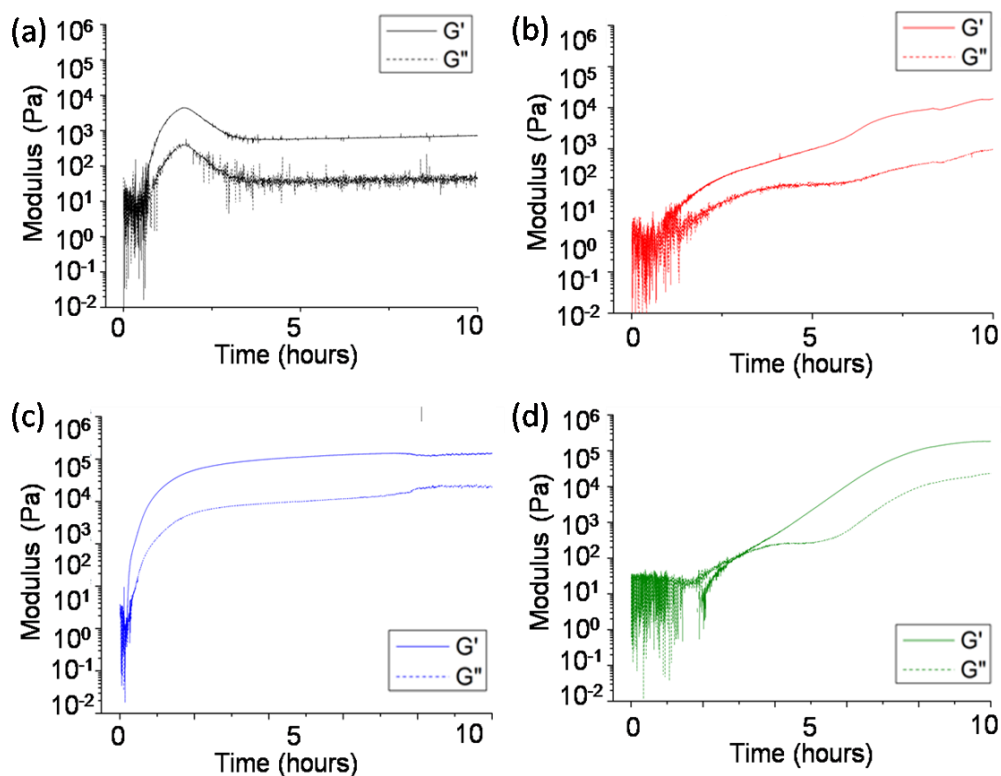


Figure 4.4 - Rheological studies of gel formation, monitoring the development of the elastic (G') and viscous (G'') modulus over 10 hours, (a) Fmoc-SF-OMe, (b) Fmoc-SL-OMe, (c) Fmoc-TF-OMe, and (d) Fmoc-TL-OMe.

Despite Fmoc-SF-OMe having a self-supporting network structure and a high elastic content, G' equilibrating around 5×10^2 Pa - an order of magnitude above its viscous modulus, it behaves as a shear thinning liquid (see Figure 4.5 (a)). The lamellar composition suggests that the two-dimensional sheets could be displaced easily and the self-supporting structure may not maintain its three-dimensional network when agitated. This effect would produce a weak structure which, in response to low shear, is able to flow as a liquid, with the deterioration of the storage modulus at shear rates of $\sim 0.012 \text{ s}^{-1}$. This is in marked contrast to SL, TF, and TL systems which produce relatively stiff peptide hydrogels (see Figure 4.5(b)). The G' values for each are in the region of 2×10^4 Pa, 1×10^5 Pa and 9×10^4 Pa respectively, with the elastic modulus (G') an order of magnitude higher than the viscous moduli (G'') in each case, and both being dependent weakly on frequency, which is characteristic of entangled polymer networks.⁴⁰ These observations are consistent with the morphological data from electron microscopy; TF producing extended twisted fibres that allow for highest degree of entanglement and therefore giving the strongest gel; TL gels

have a dense network of shorter twisted fibres that are slightly weaker; and finally SL generating flat nano-belts which are much less capable of maintaining the immobilised water compared with fibrillar networks and thus produce the weakest gel of the three.

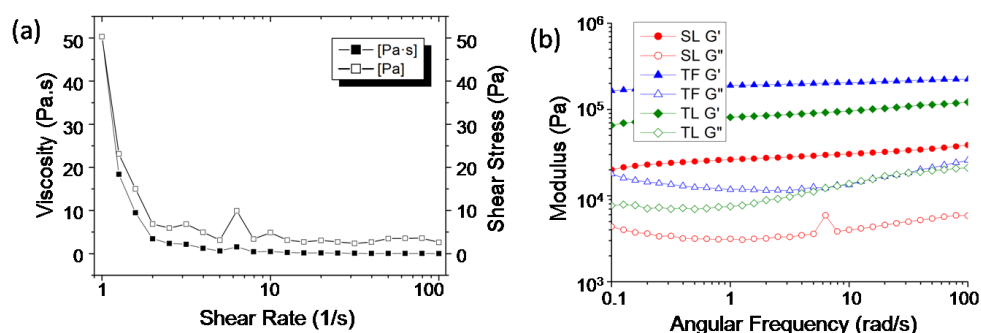


Figure 4.5 - (a) Viscosity and Flow curve of Fmoc-SF-OMe measured at 24 hours. (b) Frequency sweeps of Fmoc-SL-OMe, Fmoc-TF-OMe, and Fmoc-TL-OMe measured at 24 hours.

4.2.4 Supramolecular Structure

The driving force behind the self-assembly of aromatic peptide amphiphiles is known to be π -stacking between Fmoc- groups.⁴⁰ The fluorescence of the Fmoc-moieties was monitored over time to illustrate changes in the Fmoc environment (see Figure 4.6 (a)-(d)). These fluorescence spectra were normalised as an extensive reduction in intensity was observed over time, which was due in part to increasing opacity in each sample. For each of the four systems the starting mixture was comprised of two emitting species; the first at ~ 325 nm representing the Fmoc-amino acid monomer of the starting mixture, the second a shoulder peak at ~ 375 nm corresponding to aggregates of the precursors.³ Each system shows two distinct structural changes. Initially, a red shift of the 325 nm peak, accompanied with an increase in relative intensity. This change indicates that excimers had formed which emit at lower energy compared to Fmoc-amino acid monomers. Subsequently, the formation of a separate red-shifted peak, accompanied by a substantial decrease in relative fluorescence emission was observed. In the case of SF and TF, this red shifted peak at ~ 365 nm was evident after 5 hours. This peak represents the formation of extended π -stacked systems, and is consistent with a decrease in relative fluorescence emission. This peak is typically observed at 450 nm,^{9, 30, 32, 40} as it is with the SL and TL systems after 24 hours. However, its

presence at the shorter wavelength for the SF and TF systems could indicate that the phenyl group on the phenylalanine residue interacts with the π -stacked Fmoc columns as previously suggested,^{30, 41} and may contribute to their greater thermodynamic stability. The time scale at which each of these aggregate peaks become apparent (5 hours versus 24 hours) can further support the rheological data that systems with higher stability, SF and TF, reach their thermodynamic minima more rapidly than SL and TL. However, these results should be treated with caution due to the unquantifiable impact on emission intensity with each of the sample's increasing opacity.

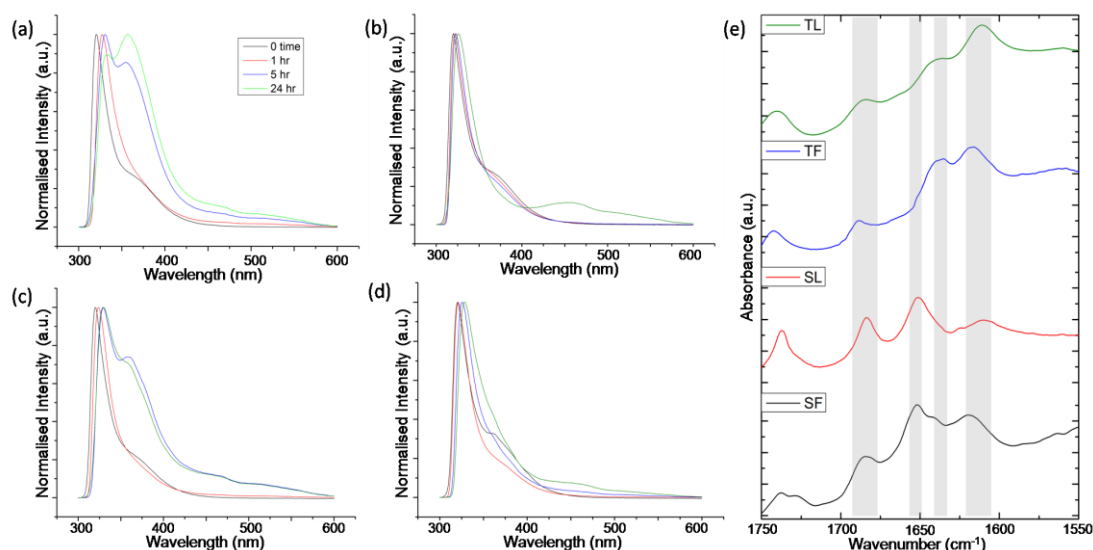


Figure 4.6 - Normalised fluorescence emission spectra of (a) Fmoc-SF-OMe, (b) Fmoc-SL-OMe, (c) Fmoc-TF-OMe, and (d) Fmoc-TL-OMe measured over 24 hours. (e) Amide I region of FTIR absorbance spectra of SF, SL, TF and TL measured at 24 hours.

The hydrogen bonding environment of the peptide chains was monitored using FTIR spectroscopy. Carbonyl stretching vibrational modes, particularly those involved in hydrogen bonding between peptide chains, can be observed in the amide I region ($\sim 1600 \text{ cm}^{-1} - 1700 \text{ cm}^{-1}$) of the spectra (see Figure 4.6(e)). There are a number of pair-wise similarities between each of the four spectra, with SF and SL spectral shapes being similar to each other, and TF and TL being closely matched. Both TF and TL spectra exhibit a peak around 1640 cm^{-1} . This, in accompaniment with a peak $\sim 1680 \text{ cm}^{-1}$, can be associated with β -sheet formation. These peaks are also observed for the SF and SL, the first as a 1680 cm^{-1} peak, and the second as a shoulder peak $\sim 1645 \text{ cm}^{-1}$. The presence of these peaks confirms an arrangement of aromatic peptide amphiphiles in a β -sheet conformation held together

by hydrogen bonding between parallel peptide backbones.¹³⁰ Typically, when studying secondary protein structure using FTIR, the 1680 cm^{-1} peak is usually less pronounced than its complementary 1640 cm^{-1} ,¹³⁰ here it is rational to assume that its amplified absorbance signal is due to differences in Fmoc-dipeptide amphiphiles rather than extended protein structures – the increased absorption is a direct result of the Fmoc carbonyl moiety hydrogen bonding into the β -sheet assembly. Additionally, in each of the serine systems, we see a prominent peak $\sim 1650\text{ cm}^{-1}$, which is noticeably absent from their threonine counterparts. Usually absorption at 1650 cm^{-1} is associated with the random coil of polypeptides,¹³⁰ but here it can be attributed to some degree of disorder in both SF and SL systems. As TF and TL adopt the natural twisted nanostructures, rather than a planar morphology, it seems reasonable that the continuous hydrogen bonding perpendicular to the peptide backbone is relatively uninterrupted along its axis and therefore does not exhibit this disordered component. Furthermore, each of the four systems, SF, SL, TF and TL, display a 1745 cm^{-1} peak arising from the carbonyl group of the free methyl ester, i.e. the excess of amino acid methyl ester present in the starting materials mixture. SF has an additional peak $\sim 1730\text{ cm}^{-1}$ indicating there is a second environment of the methyl ester carbonyl moiety which is absent from SL, TF and TL, and may be attributed to spherulitic structure formation (discussed in Section 3.2.5).³ Furthermore, a peak at 1620 cm^{-1} indicates there is hierarchical assembly and formation of a quaternary protein structure.¹³⁷ That is, molecular organisation to form β -sheet arrays in the peptide nanostructures, followed by interactions between distinct β -sheet assemblies to produce the final nanoscale structures as multilayers of β -sheets.

In order to confirm molecular association, WAXS diffraction patterns were obtained for each of the systems under study (see Figure 4.7). Any peak observed $< 5\ 2\Theta$ degrees, were discounted from analysis as they were observed in control samples containing only the enzyme. For each system, a prominent peak is observed which can be correlated to the repeating unit along the peptide backbone; SF, 15.6 \AA with five reflections, consistent with previous studies (discussed in Section 3.2.3);³ SL, 14.6 \AA with four reflections; TF, 15.8 \AA with two reflections; TL 14.6 \AA with two reflections. The difference in spacing of the repeating units of Fmoc-SF-OMe and Fmoc-TF-OMe is approximately 1 \AA larger than their leucine counterparts. This could be due to the phenyl moiety interacting with the π -stacked Fmoc-columns, increasing their stability, preventing the Fmoc-dipeptides to pack as tightly along their N-C axis. Similarly, the β -sheet spacing is also affected by the presence of the phenyl

group. For SF and TF systems, the repeating unit on the axis perpendicular to the peptide backbone is 4.7 Å, slightly larger than 4.6 Å observed for our SL and TL nanostructures, however, both lie within the typical range associated with β -sheet spacing in peptides¹³⁸ and previously observed β -sheet spacing of self assembled aromatic peptide amphiphiles.^{9, 35, 36} Additionally, SF and SL have peaks at 9.4 Å and 9.2 Å respectively, exactly double the β -sheet spacing. This may be due to either, the repeating unit of hydrogen bonded anti-parallel β -sheet units in the β -pleated sheets,^{12, 139, 140} or the 'side-chain' spacing between two interacting parallel sheets.¹⁴¹ Regardless, both explanations are in agreement with modelled bilayer structures for SF (discussed in Section 3.2.4)³ and the deduced molecular associations for the SL system. However, this peak is not visible in either of the threonine systems. As all peak intensities are shown relative to the strongest peak, a peak correlating to 7.6 Å in all cases, the intensity of which is much greater in the TF and TL systems compared with SF and SL; this may leave the relatively low intensity double β -sheet spacing peak unable to develop from the noise. This would also account for a lower number of reflections observed for the repeating unit of the Fmoc-dipeptide backbone. Nonetheless, from the FTIR studies, it is evident that associating β -sheet structures are formed in all 4 systems. Furthermore, all four systems SF, SL, TF and TL, exhibit a strong peak at 3.8 Å corresponding to distance between planar π -stacked Fmoc- groups.^{8, 12, 30, 35} The maximum peak, to which all other intensities are relative, is at 7.6 Å; exactly double the π -stacking distance and consistent with the second reflection of the Fmoc-dipeptide repeating unit. This demonstrates the high degree of periodicity associated with the Fmoc- stacked columns, which is thought to be the main driving force behind self-assembly of aromatic peptide amphiphiles.

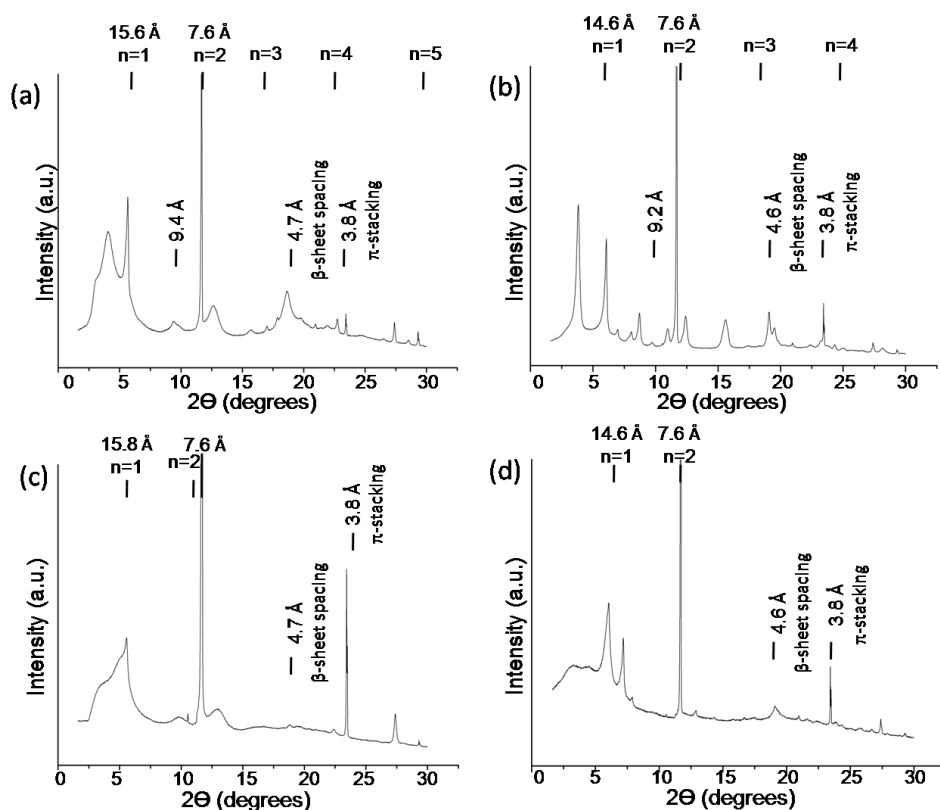


Figure 4.7 - WAXS data of dried sample measured at 24 hours; (a) Fmoc-SF-OMe, (b) Fmoc-SL-OMe, (c) Fmoc-TF-OMe, and (d) Fmoc-TL-OMe.

4.2.5 Molecular Modelling

In order to investigate the molecular arrangement and validate the proposed π - β configuration, molecular mechanic simulations were performed. For all four Fmoc-dipeptide methyl esters a sheet-like model in a π - β bilayer configuration was built of $8 \times 4 \times 2$ molecules in accordance with the previous modelling work carried out (discussed in Section 3.2.4).³ The proposed structures for SF and TF proved to be stable under energy minimization in water, while SL showed significant disruption of the initial structure. TL was mostly stable, although several molecules at the edge of the simulation box became disordered. From the minimized structures, average distances between π -stacked Fmoc-groups, hydrogen bond spacing between peptide backbones of the pleated β -sheet molecular arrangement, and laterally displaced Fmoc-columns were extracted as shown in Table 4.1.

	$\pi - \pi$		β -sheet		Fmoc - Fmoc column	
	WAXS	Model	WAXS	Model	WAXS	Model
SF	3.8	3.78 \pm 0.34	4.77	5.06 \pm 0.29	15.56	16.44 \pm 0.49
TF	3.8	3.84 \pm 0.47	4.72	5.03 \pm 0.14	15.83	16.69 \pm 0.55
SL	3.8	disordered	4.65	4.85 \pm 0.18	14.56	disordered
TL	3.8	3.97 \pm 0.42	4.65	4.87 \pm 0.19	14.6	15.67 \pm 0.54

Table 4.1 - Comparison of molecular mechanics results with WAXS. All distances are in Å

A good agreement between the distances in the model and those found from WAXS analysis, showing the π - π stacking distance of 3.80 Å, hydrogen bond spacing of approximately 4.7 Å and a lateral repeating unit along the molecular length of 15–16 Å. The model slightly overestimates the β -sheet and lateral Fmoc-stack to Fmoc-stack repeating unit distances, which may be attributed to the finite size of the simulation box. However, it accurately correlates the trend differences upon changing the amino acid residues.

4.3 Conclusions

We have investigated the self-assembly behaviour of four aromatic dipeptide amphiphile systems; Fmoc-SF-OMe, Fmoc-SL-OMe, Fmoc-TF-OMe and Fmoc-TL-OMe. From previous work, it is known that enzyme assisted self-assembly via condensation allows for access to the thermodynamic minima,³⁰ which in turn, allowed us to directly compare the effect of the peptidic tail on self-assembly. TEM imaging revealed SF, SL, TF and TL, self-assembled to produce different nanostructural morphologies. However, we can deduce that the presence of serine in amino acid position one induces the formation of planar structures, whereas the additional chiral centre in threonine induces the familiar twisted ribbon architecture commonly observed for these systems, most likely caused by minimising contact of the additional methyl group with the aqueous environment. These structures could be used to explain the mechanical properties of the hydrogels found using rheological studies. TF was the strongest gel due to the larger degree of entanglements associated with long twisted ribbons, followed by TL with shorter ribbons and therefore a lower degree of entanglement, SL with planar belts and therefore much less capable of

maintaining the immobilised water, therefore producing the weakest hydrogel, and lastly SF which behaved as a shear thinning liquid as the large two-dimensional sheets are unable to preserve their three-dimensional network structure once agitated.

Fluorescence spectroscopy revealed extended π -stacked aggregates of Fmoc-groups. In the case of SF and TF, the phenyl group of the phenylalanine residue appeared to interact with these Fmoc-columns, contributing to their greater stability. FTIR showed neighbouring peptidic tails interacted via hydrogen bonding in a β -sheet arrangement and hierarchical assembly into β -sheet multilayers. SF and SL both form planar structures rather than adopting the natural chiral twists associated with β -sheet formation, molecular frustration and the regularity of the β -sheet structure is slightly non-conventional and is therefore observed as a level of disorder. WAXS diffraction patterns confirmed that molecular association for all systems is through π -stacked Fmoc-columns and hydrogen bonded β -sheet assembly of the peptidic tail. The bulky phenyl group on the phenylalanine residues in SF and TF affected molecular packing along both hydrogen bonded and peptide backbone axis.

Therefore, of the systems under study, we can conclude that serine in amino acid position one induces planar nanostructures due to its non-conventional hydrogen bonding in the β -sheet assembly, and that greater thermodynamic stability associated with the phenylalanine residue in amino acid position two is owed to interactions between the phenyl moiety, which greatly affects molecular packing, with the π -stacked Fmoc-columns.

5.0 Differential supramolecular organisation of Fmoc-dipeptides with hydrophilic terminal amino acid residues by biocatalytic self-assembly*

* This work has been submitted for publication in part in Soft Matter

Declaration of contribution to submitted article:

Any reproduced work from the aforementioned submitted article, I was solely responsible for, including the written article itself, unless otherwise stated. Daniel Cannon provided the molecular modelling data. Dr. Louise S. Birchall and Dr. Sisir Debnath were responsible for synthesising Fmoc-Yx-OMe starting materials.

5.1 Introduction

Self-assembled peptide nanostructures have given rise to a variety of morphological structures (as discussed in Section 4.1). Following on from Chapter 4, the work in this Chapter is based on the characterisation of four closely related self-assembling Fmoc-dipeptides with terminating hydrophilic amino acid residues generated by ester hydrolysis of methylated precursors; Fmoc-tyrosine-threonine (Fmoc-YT-OH), Fmoc-tyrosine-serine (Fmoc-YS-OH), Fmoc-tyrosine-asparagine (Fmoc-YN-OH) and Fmoc-tyrosine-glutamine (Fmoc-YQ-OH). They were designed in order to introduce new chemical functionalities to peptide nanostructures, which have previously been hydrophobic in nature and/or contained a number of aromatic groups to aid assembly by π -stacking. Monitoring the influence of different amino acid residues within the peptide chain allows for the elucidation of amino acid sequence/structure relationships and providing a further step towards the fully rational design and tailoring of nanostructures.

5.1.1 Background

As the hydrophobic collapse is recognised as a major driving force in the production of peptide nanostructures, both in naturally occurring protein folding systems^{91, 92} and the assembly of aromatic peptide amphiphiles,^{44, 60, 98} typically aromatic peptide amphiphiles have been designed to be hydrophobic in nature - with the peptide component consisting mainly of hydrophobic amino acid residues or containing aromatic moieties within side chains. It has been demonstrated that in aqueous environments they form self-associating elongated assemblies. This was first demonstrated for Fmoc-Y-OH by Yang *et al.* in 2004,⁴¹ but has since been observed for a number of aromatic peptide amphiphiles, including Fmoc-FF-OH,^{30, 85} Nap-FFGEY-OH,⁸³ Fmoc-LLL-OH,⁴⁶ Ac-YYYY-OMe,⁴⁴ Nap-FFY-OH,⁴⁵ Nap-AV-OH,⁸⁶ Py-AA-OH⁸⁶ and Fmoc-AFF-OH,⁵¹ to name a few (discussed in Section 2.5.1). There are cases where hydrophilic amino acid residues have successfully been introduced into the peptide sequence to create self-assembling aromatic peptide amphiphiles. However, they are designed to be included in the centre of the molecular building blocks so the hydrophobic groups are relatively balanced throughout the molecule, such as Fmoc-SF-OMe and Fmoc-TF-OMe (discussed in Chapters 3 and 4).^{3, 4}

Adams *et al.* carried out an extensive study correlation between hydrophobicity of an Fmoc-dipeptide with gelation.¹⁴² It was found that self-assembling Fmoc-dipeptides with $\text{clog}P < 2.8$ formed unstable, weak gels, with stable gels forming when $3.4 < \text{clog}P < 5.5$ ^{37, 142} (e.g. Fmoc-FF-OH and Fmoc-VG-OH $\text{clog}P = 5.5$ and 3.6 respectively).¹⁴² Supramolecular structure formation and gelation has been observed for Fmoc-dipeptides with a low $\text{clog}P$ value, e.g. Fmoc-GG-OH $\text{clog}P = 1.22$, however has required acidic conditions for any molecular assembly to occur.⁴⁰ This is due to the protonation of carboxylic acid moieties at lower pH, thus the electrostatic repulsion between aromatic peptide amphiphiles is removed.⁴⁰

5.1.2 Subtilisin and Ester Hydrolysis

Subtilisin is a serine protease, which catalyses the hydrolysis of amides and esters.¹⁴³ The catalytic site consists of 3 amino acid residues which are essential for catalysis, Asp-32, His-64, and active Ser-221, arranged as a catalytic triad contained within a cleft on the molecule¹⁴⁴ (see Figure 5.1) – identical to the active site of chymotrypsin.¹⁴⁵

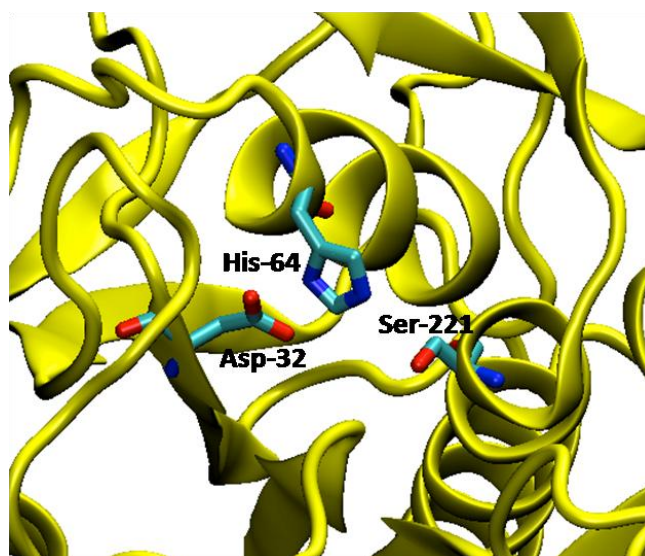


Figure 5.1 - Molecular model of subtilisin active site indicating the amino acid residues involved in catalysis.

The mechanism of action is reliant upon hydrogen bonding between the three residues which ultimately results in a charge separation on the hydroxyl moiety of the Ser-221 side chain (see Figure 5.2). This oxyanion then acts as a nucleophile of incoming substrates by

attacking the carbonyl oxygen of the susceptible bond (either peptide or ester), leaving the carbonyl carbon sensitive to nucleophilic attack from a water molecule, and thus initiating hydrolysis.^{144, 145}

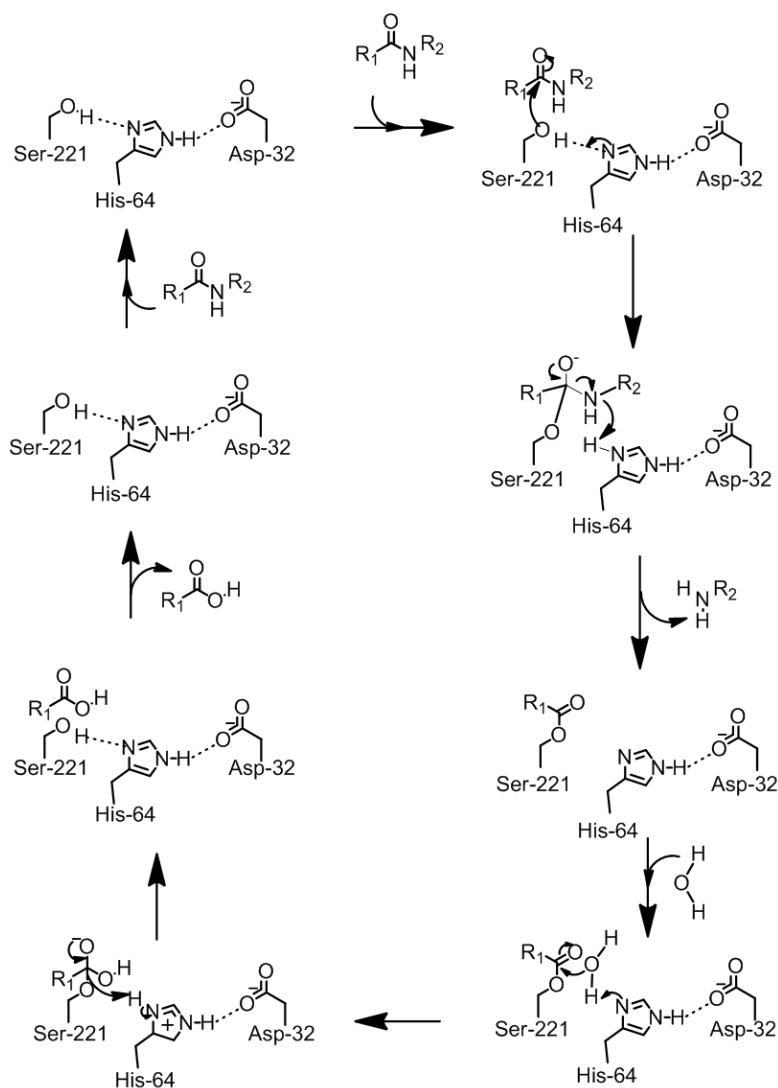


Figure 5.2 - Mechanism of subtilisin catalyzed peptide bond hydrolysis.

A number of self-assembling peptide amphiphiles have been prepared using subtilisin.^{46, 47} In each case, self-assembly has been prevented by the inclusion of a methyl ester group at the C-terminus of the peptide. Subtilisin cleaves the terminal methyl group associated with blocking molecular self-assembly *via* ester hydrolysis and thereafter the aromatic peptide amphiphiles can form supramolecular assemblies.^{46, 47}

5.2 Results and Discussion

5.2.1 Composition

The precursor suspension contained 10 mM of the starting material, either Fmoc-tyrosine-threonine-methyl ester (Fmoc-YT-OMe), Fmoc-tyrosine-serine-methyl ester (Fmoc-YS-OMe), Fmoc-tyrosine-asparagine-methyl ester (Fmoc-YN-OMe) or Fmoc-tyrosine-glutamine-methyl ester (Fmoc-YQ-OMe), in pH 8 phosphate buffer. The insoluble starting materials were then converted to self-assembling peptide amphiphiles by treatment with subtilisin from *Bacillus licheniformis*, heated to 55 °C converting the Fmoc-dipeptide-methyl esters to their respective free acids, and cooled to 20 °C over 3.5 hours (see Figure 5.3).

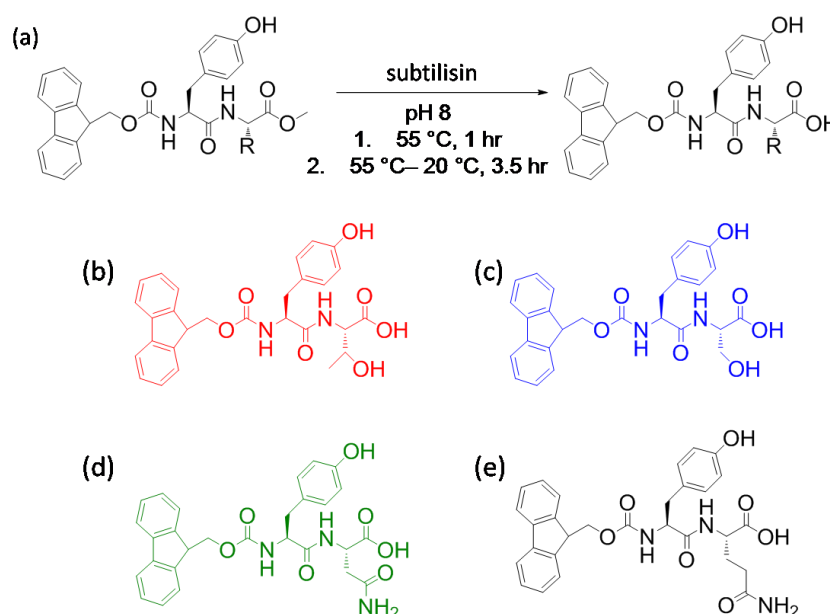


Figure 5.3 - (a) Reaction schematic of subtilisin triggered ester hydrolysis of Fmoc-dipeptide methyl esters. (b) - (e) Chemical structures of Fmoc-dipeptides after treatment with subtilisin, Fmoc-YT-OH, Fmoc-YS-OH, Fmoc-YN-OH and Fmoc-YQ-OH, respectively.

The biocatalytic transformation was followed using HPLC by aliquoting each sample and dissolving in a solution of 50 % ACN, 0.1 % TFA before injecting onto a reversed-phase HPLC column. After 24 hours there was no trace of starting materials within any of the reaction vessels; Fmoc-YT-OMe, Fmoc-YS-OMe, Fmoc-YN-OMe and Fmoc-YQ-OMe yielding 97 %, 91 %, 97% and 93 % of their desired free acids Fmoc-YT-OH (YT) , Fmoc-YS-OH (YS), Fmoc-YN-OH (YN) and Fmoc-YQ-OH (YQ) respectively (see Table 5.1), with the remaining fraction, being attributed to the generation of Fmoc-tyrosine (Fmoc-Y-OH) due to non-specific

hydrolysis of the amide bond by the enzyme. The hydrophilicity of the molecular products increased from YT, being the most hydrophobic of the systems under study, $YS < YN < YQ$. After 24 hours of treatment with the enzyme, each of the four systems had been transformed from their suspensions to; YT, a clear viscous liquid; YS, a clear self-supporting gel; YN, a slightly turbid self-supporting gel, and; YQ, a translucent solution; indicating molecular self-assembly of the Fmoc- dipeptide amphiphiles had occurred (see Figure 5.4), with all samples remaining stable over a number of weeks. It should be noted that the methyl ester precursors of YT, YS, YN and YQ do not self-assemble in the absence of subtilisin, and precipitate in the aqueous environment without heating step to dissolve the precursors.

Compound	cLogP	Composition (%)	Appearance
YT	3.2814	Fmoc-YT-OH = 97 Fmoc-Y-OH = 3	Viscous Solution
YS	2.9724	Fmoc-YS-OH = 91 Fmoc-Y-OH = 9	Gel
YN	2.7134	Fmoc-YN-OH = 97 Fmoc-Y-OH = 3	Gel
YQ	2.2336	Fmoc-YQ-OH = 93 Fmoc-Y-OH = 7	Solution

Table 5.1 – Table summary of compounds YT, YS, YN and YQ at 10 mM concentration. cLogP values calculated using ChemBioDraw Ultra 12.0, composition 24 hours after treatment with subtilisin, and hydrogelation ability assessed via inversion of the reaction vials after 24 hours.

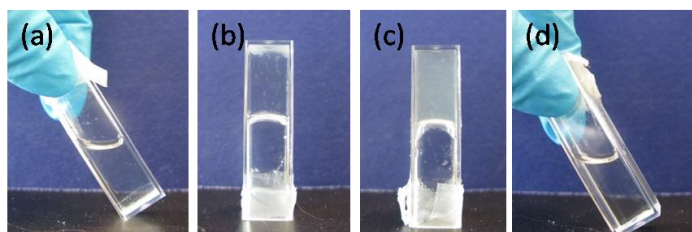


Figure 5.4 – (a) – (d) Hydrogelation of samples YT, YS, YN and YQ respectively tested by vial inversion after 24 hours of enzyme addition.

5.2.2 Supramolecular structure

π -stacking is known to be the driving force behind self-assembly of aromatic dipeptide amphiphiles.^{40, 44, 60, 98, 146} By monitoring the environment of Fmoc-moieties using fluorescence, we can interpret any structural changes (see Figure 5.5). For each of the four systems, the starting materials contained a single emitting species which represents the fluorenyl of Fmoc-YX-OMe; ~ 325 nm for Fmoc-YT-OMe, Fmoc-YS-OMe and Fmoc-YN-OMe, and a longer wavelength of ~ 345 nm for Fmoc-YQ-OMe. The longer wavelength observed for Fmoc-YQ-OMe is an indication of increased stability of the fluorenyl interactions in the aqueous environment when directly compared to the other systems under study. This could be owed to its higher hydrophilicity accompanied by an increased flexibility in the amino acid side chain allowing to maximise interactions with the aqueous environment. After 24 hours, YT, YS and YN display a red-shifted Fmoc peak accompanied with the formation of a J-aggregate peak ~ 450 nm, indicating the formation of an extended Fmoc stacks, stabilised by π -stacking interactions. Additionally, the J-aggregate peak of YN, is much more pronounced than that of YT or YS, indicating that the Fmoc stacking are more greatly extended. YQ displays a blue shifted Fmoc peak after 24 hours of subtilisin addition, which indicates a destabilisation of the Fmoc environment. Although the self-assembly is driven by the hydrophobic collapse, π -stacking interactions between neighbouring Fmoc groups are not apparent. Most likely, their relative orientation within the self-assembled structure does not allow for stabilising π -interactions between the aromatic moieties, *i.e.* the aromatic groups are not aligned parallel or in close enough proximity for these interactions to occur. Being the least hydrophobic Fmoc-dipeptide studied, the destabilisation of Fmoc environments is compensated by the hydrogen bonding interactions of the peptidic tail with with aqueous environment.

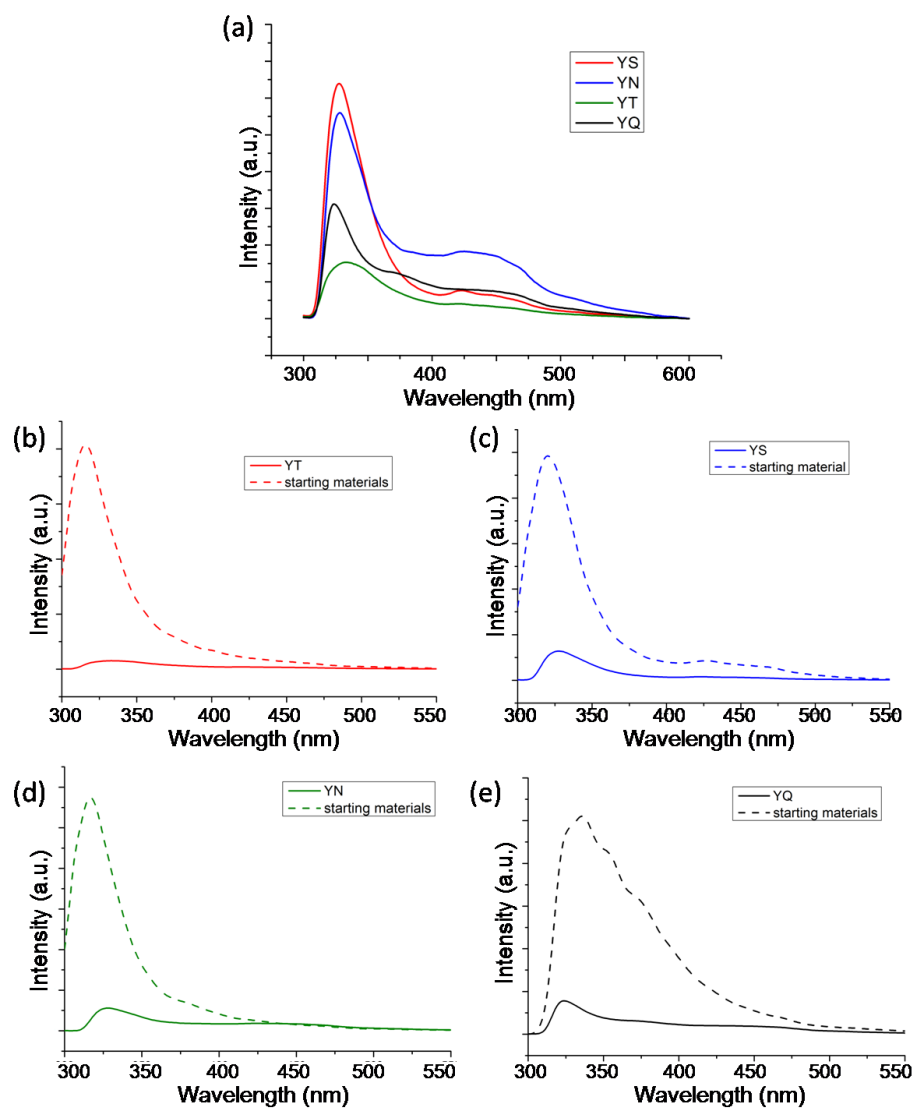


Figure 5.5 – (a) Fluorescence emission spectra of YT, YS, YN and YQ measured at 24 hours. (b) – (e) Fluorescence emission spectra of YT, YS, YN and YQ respectively measured at 24 hours overlaid with emission of starting materials.

The 304 nm absorbance peak in the CD spectra (see Figure 5.6(a)) can determine the supramolecular chirality of the Fmoc stacks formed. The chirality originates from the preferred handedness, or chiral orientation, of the supramolecular assembly, as the monomeric Fmoc¹⁴⁷ and subtilisin themselves display no CD signal at this concentration. YT, YS and YN all display the same handedness of chirality associated with the Fmoc stacks; YN forming the most extended aggregates with the highest order of chirality, and YS lowest chirality indicating that the Fmoc-stack is not as regularly ordered. YQ displays no supramolecular chirality at this wavelength.

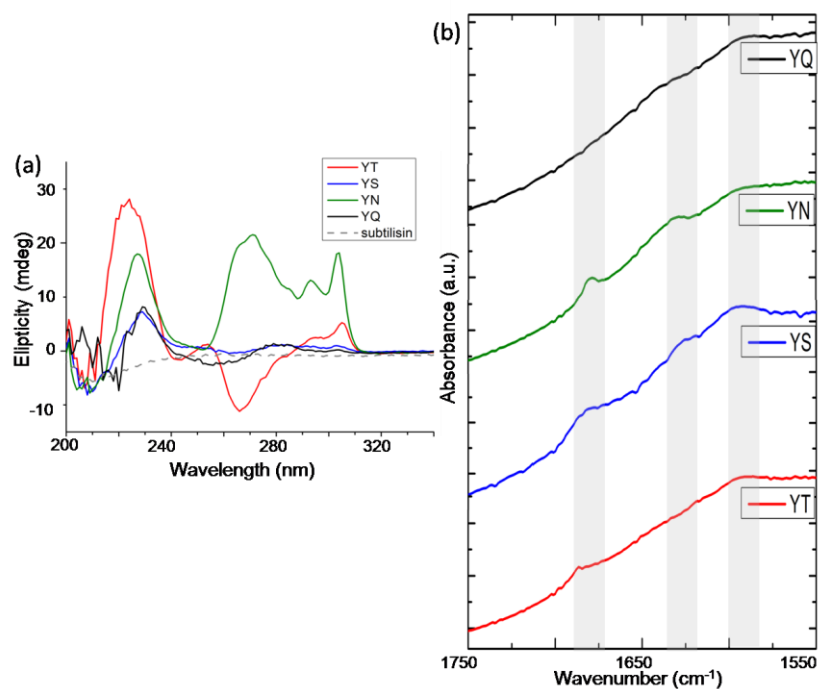


Figure 5.6 – (a) CD spectra, and (b) Amide I region of FTIR absorbance spectra of YT, YS, YN and YQ measured after 24 hours.

By monitoring the amide I region of the FTIR absorbance spectra ($1600\text{ cm}^{-1} - 1700\text{ cm}^{-1}$), the hydrogen bonded environment of the peptide chains can be deduced. More specifically, the amide I region illustrates stretching of carbonyl moieties which are involved in the hydrogen bonding of self-assembled peptides (see Figure 5.6 (b)). After 24 hours, YT, YS and YN display peaks associated with β -sheet formation. YS and YN display a combination of peaks $\sim 1680\text{ cm}^{-1}$ and $\sim 1640\text{ cm}^{-1}$, with the 1680 cm^{-1} peak being more pronounced than that of its 1640 cm^{-1} counterpart – consistent with previous studies of similar self-assembling Fmoc-dipeptides,^{3, 4, 9, 32, 47} and the reverse of that observed when studying secondary protein structure, where the 1640 cm^{-1} peak is usually more prominent.¹³⁰ YT exhibits only the 1680 cm^{-1} band as its intensity is amplified in the study of Fmoc-peptide amphiphiles,⁴ with complementary 1640 cm^{-1} band assumed to be lost to background. YN displays slightly stronger β -sheet absorption bands than that of YS, which we attribute to the increased hydrogen bonding capability of amino acid residue N compared with S. The asparagine side chain of YN, is known to have a high propensity to hydrogen bond, as it can donate two and accept two hydrogen bonds (see Figure 5.7). In contrast, the serine –R functionality can only donate one and accept one hydrogen bond, hence weaker β -sheet absorption bands are observed for YS. Lastly, no β -sheet bands are observed for YQ. YQ

does not adopt the same β -sheet structure as any of the other systems due to the steric effects of the glutamine side chain.

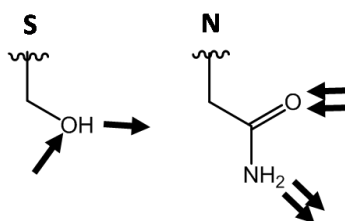


Figure 5.7 - Chemical structures of amino side chains of serine (S) and asparagine (N). Arrows indicate hydrogen bonding donating and accepting abilities of functional moieties.

5.2.3 Nanoscale Morphology

Investigation into their nanoscale architecture was carried out using TEM and cryoTEM (see Figure 5.8). The starting materials in aqueous solution showed no discernable structure when using these microscopy techniques. However, after the addition of subtilisin and heating to dissolve, and cooling to room temperature, YT, YS and YN formed fibril network structures; YT having variable fibre diameter, and, YS and YN forming dense networks of relatively homogenous fibres. However, YQ behaves in an entirely different manner, self-assembling to form spheres in the aqueous environment. DLS measurements of these spherical aggregates confirm the average hydrodynamic radius to be ~ 700 nm – 900 nm when measured at different scattering angles (see Figure 5.9), however these measurements have large errors associated with them due to their highly variable dimensions which can be observed in the TEM images.

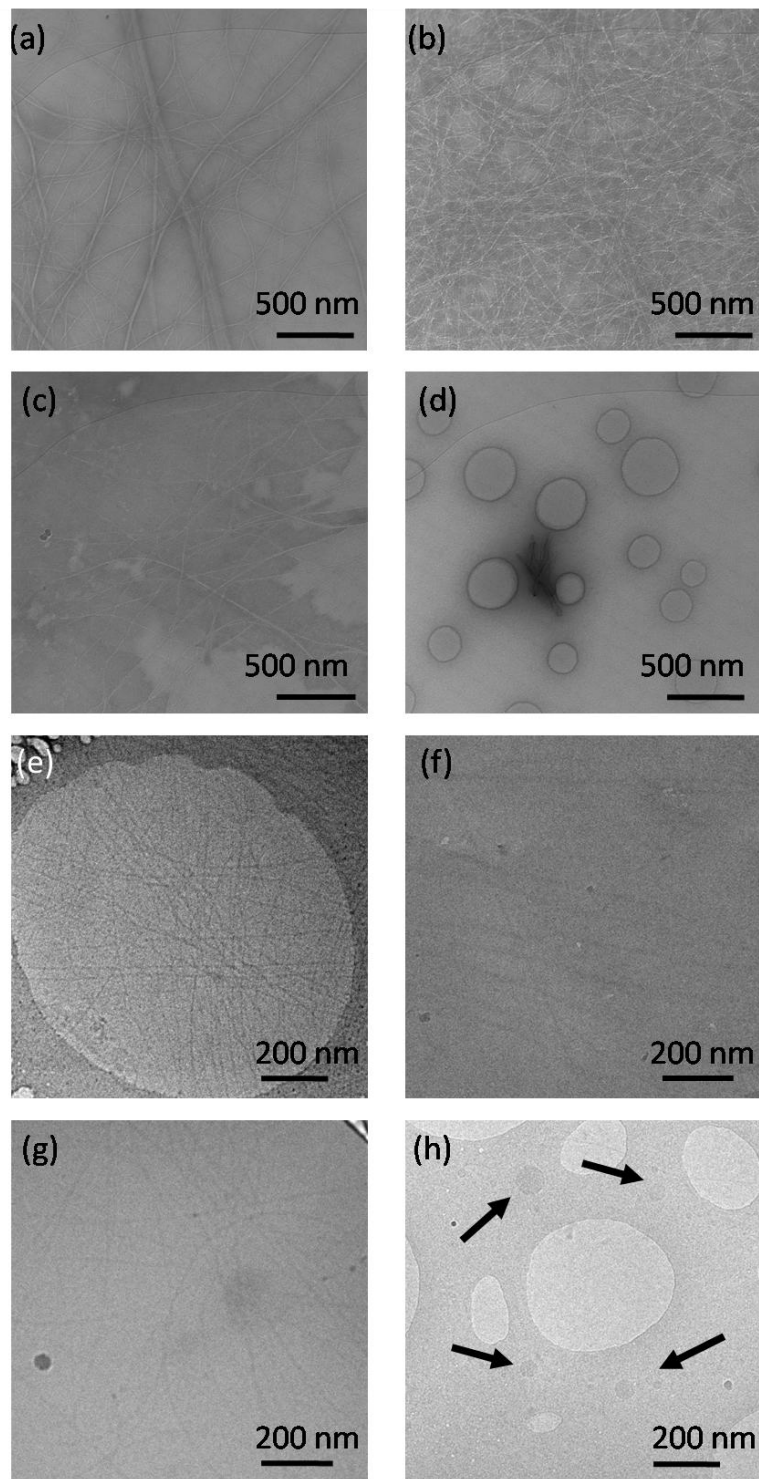


Figure 5.8 - (a) – (d) TEM images of self-assembled structures of YT, YS, YN and YQ respectively, after 24 hours from enzyme addition. (e) – (h) cryoTEM images of self-assembled structures of YT, YS, YN and YQ respectively, after 24 hours from enzyme addition. Arrows indicate the spherical aggregates which were present only on the cryoTEM grids.

Given that the side chain of asparagine and glutamine have the same chemical functionality (-CONH₂), from these results, it can be deduced that the steric effects of the additional CH₂ within the glutamine side chain has a substantial influence on the molecular packing and prohibits the formation of fibre network structures. As a direct result, Fmoc-YQ-OH will form spherical structures most likely due to minimising contact of the hydrophobic N-terminus of the Fmoc-dipeptide amphiphiles with the aqueous environment, but is unable to form the typical fibril nanostructures associated with self-assembly of aromatic dipeptide amphiphiles.

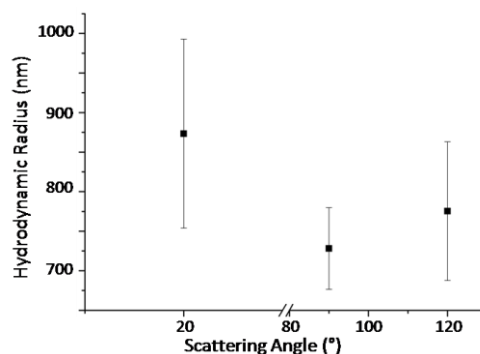


Figure 5.9 - DLS data of Fmoc-YQ-OH, measured after 24 hours.

5.2.4 Mechanical Properties

The mechanical properties of the samples were confirmed by rheology (see Figure 5.10). Although YT self-assembles to form fibril network structures, its elastic component (G') is never more prominent than its viscous component (G''), thus is unable to completely immobilise the water molecules, and so behaves as a shear thinning liquid. As shear rates are increased, it causes degeneration of the three-dimensional network, consequently, we observe a decrease in viscosity as the solution is allowed to flow progressively more freely. YS forms a typically mechanical hydrogel, with an elastic modulus (G') of $\sim 3.40 \times 10^3$ Pa, an order of magnitude higher than its viscous component (G''), and both moduli being weakly dependant on frequency – which is characteristic of entangled polymer network structures.⁴⁰ YN also forms a gel, however, in comparison with YS, it is a much weaker. Again, both elastic (G') and viscous (G'') moduli are dependent on frequency, but the difference in magnitude is limited; $G' \sim 3.01 \times 10^3$ Pa and $G'' \sim 9.49 \times 10^2$ Pa. The high liquid component within the system having great influence over the mechanical strength, with

the resulting hydrogel of YN being much weaker compared with the Fmoc-YS-OH system. Additionally, both YS and YN exhibit an upturn in moduli at high frequency possibly due to a thickening instability, previously observed by Cheng *et al.* for self-assembled Fmoc-tripeptides.³⁸ Previous studies of self-assembling Fmoc-dipeptide-methyl esters which directly compared the effects of amino acid residues threonine versus serine, analogous to YT versus YS, found peptide sequence TL (Fmoc-TL-OMe) to have a stronger network strength than that of SL (Fmoc-SL-OMe).⁴ However, in this study, YS formed stronger networks structures than that of YT, indicating that the order in which amino acid residues appear in the peptide sequence can dictate the mechanical properties. The increased gel strength of YS compared with YN, can be directly linked to the intermolecular interactions associated with the amino acid residue in position two, with serine allowing for stronger non-covalent interactions than those associated with asparagine, despite having a lower hydrogen bonding capability. Additionally, it was already deduced that the length of the side chain of the amino acid in position two directly affects the molecular packing from studying their nanoscale morphology. The amino acid side chain residue of asparagine in YN is one CH₂ longer than the serine side chain, which may also influence gel strength; with the longer side chain disrupting the tight molecular packing of the fibres, but not to the extent of prohibiting the fibre formation, as seen with YQ. Furthermore, YQ behaves as an ideally viscous solution, with constant viscosity and increasing shear stress with increasing shear rate. The formation of nanospheres allows for the solvent to flow freely – the spherical design allows for the supramolecular structures to flow past/over each other with ease, creating no friction or tension, and thus behaves as a newtonian fluid.

Previously studies found that self-assembling Fmoc-dipeptides with $\text{clog}P < 2.8$ formed unstable, weak gels, with stable gels forming when $3.4 < \text{clog}P < 5.5$ ^{37, 142} (discussed in Section 5.1.1). Supramolecular structure formation and gelation has been observed for Fmoc-dipeptides with a low $\text{clog}P$ value, e.g. Fmoc-GG-OH $\text{clog}P = 1.22$, however has required acidic conditions for any molecular assembly to occur.⁴⁰ However, here, it has been demonstrated that it is possible to form stable gels from self-assembling aromatic peptide amphiphiles at neutral pH when $\text{clog}P < 3$.

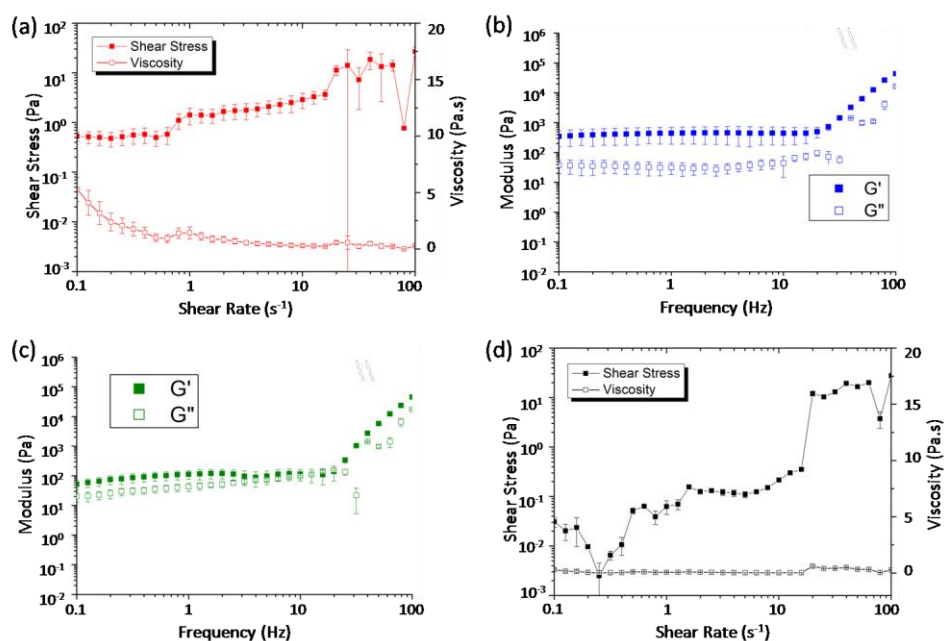


Figure 5.10 - Rheological data of materials measured after 24 hours. (a) Viscosity and flow curves of YT. (b) Frequency sweep of YS. (c) Frequency sweep of YN. (d) Viscosity and flow curves of YQ.

5.2.5 Characterisation of the thermodynamically favoured state

The subtilisin triggered self-assembly of aromatic peptide amphiphiles gives rise to kinetically trapped states, as shown previously for Fmoc-YL-OH.⁴⁷ Although these systems are stable, representing an energetic minima that cannot be overcome by thermal fluctuations, they may not represent the global thermodynamic minima – which would be the most appropriate route to determine conclusive design rules in terms of molecular bonding (as discussed in Chapter 4).⁴ In order to ensure the understanding and conclusions drawn for this comparative study are correct, it was therefore important to also investigate the thermodynamically preferred state. This was achieved by introducing heat/cool cycles, heated to 55 °C for 1 hour to free molecules from their kinetically trapped state, then cooled to 20 °C over 3.5 hours to allow molecular reorganisation. The supramolecular organisation was monitored using fluorescence (see Figure 5.11). With each heat/cool cycle, YT, YS and YQ demonstrated an increasing J-aggregate peak indicating that the Fmoc-stacks were becoming increasingly extended after every heat/cool cycle. The systems were assumed to have reached the thermodynamic state when the ratio of 450 nm J-aggregate

peak to the 320 nm peak arising from the monomeric Fmoc-YX-OH had reached a constant value, observed after the fourth heat/cool cycle for all systems.

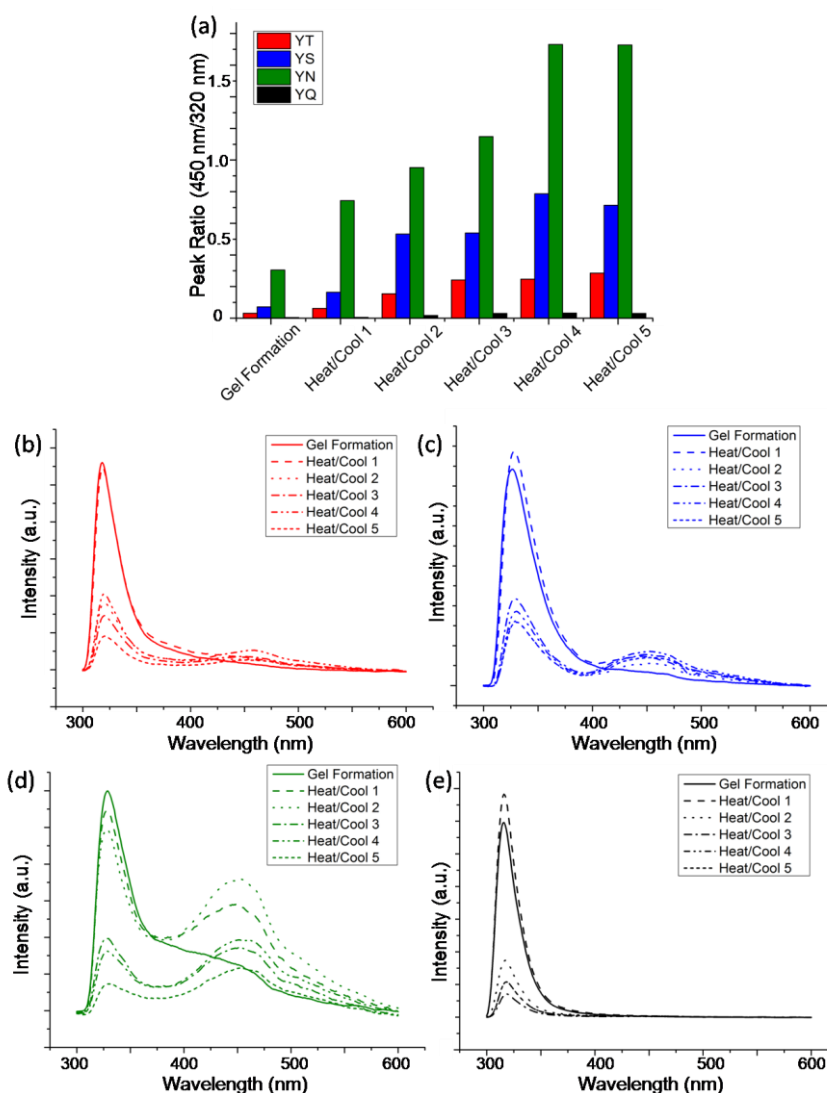


Figure 5.11 - (a) Peak Ratios of J-aggregate:Fmoc monomer calculated from fluorescence emission spectra data after each heat/cool cycle. (b)-(e) Fluorescence emission spectra of YT, YS, YN and YQ respectively obtained 24 hours after each heat cool cycle.

In contrast, YQ only exhibited a change in emission intensity, and therefore it can be assumed that on cooling, Fmoc-YQ-OH reassembles itself in the same manner during each heat/cool cycle, which indicates that YQ originally accessed its thermodynamic state. It should be noted at this point that without the introduction of energy in the form of heat into the systems, no structural reconfigurations were observed by monitoring over time.

The chirality of the Fmoc-stack (304 nm peak) remains unchanged; YT, YS and YN showing positive chirality. However, in the thermodynamically preferred state, YT and YS display a higher order chirality, and YN a slightly lower order of chirality around the Fmoc-stacks. YQ again showing no chirality as the Fmoc stacks do not assemble (see Figure 5.12 (a)).

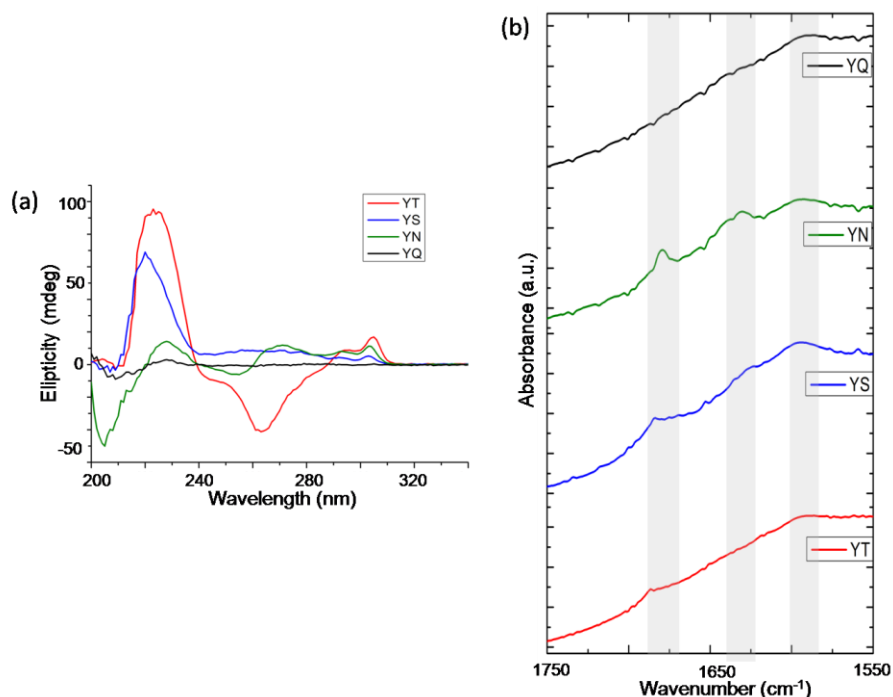


Figure 5.12 - (a) CD spectra of the thermodynamically preferred states of YT, YS, YN and YQ. (b) Amide I region of FTIR absorbance spectra of YT, YS, YN and YQ of thermodynamically preferred state.

Furthermore, by monitoring the amide I region of the FTIR spectra, all four remain unchanged, YT, YS and YN displaying β -sheet configuration, with YQ being rather featureless (see Figure 5.12 (b)). The only notable difference being in the absorbance spectra of YN, where the β -sheet absorbance bands are of higher intensity indicating that the self-assembled structure has higher order within the β -sheet regime. However, despite slight molecular reorganisation after each heat/cool cycle, visually the samples remained unchanged - YT remains as a liquid, YS and YN as self-supporting gels, and YQ as a clear solution which is supported by rheological data, where the gel strengths of YS and YN are unaffected by the formation of greatly extended aggregates formed in the thermodynamic state with the elastic component measuring at 4.72×10^3 Pa and 3.03×10^3 Pa respectively (see Figure 5.13).

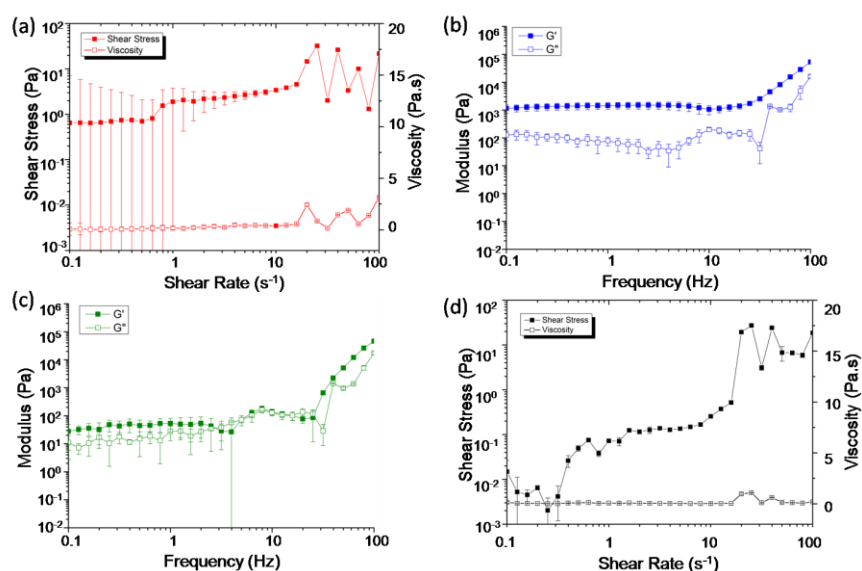


Figure 5.13 - Rheological data of materials in thermodynamically preferred state. (a) Viscosity and flow curves of YT. (b) Frequency sweep of YS. (c) Frequency sweep of YN. (d) Viscosity and flow curves of YQ.

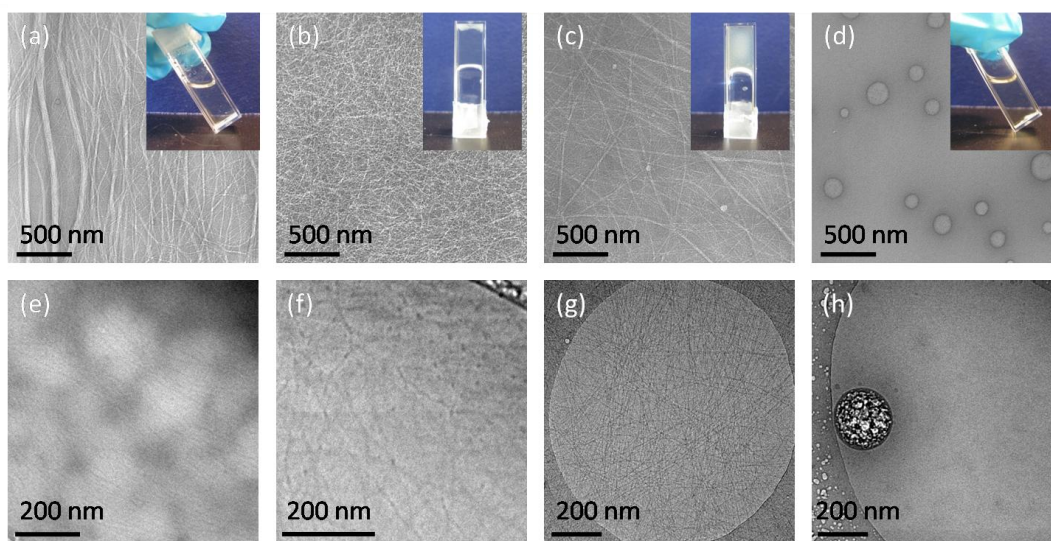


Figure 5.14 – (a) – (d) TEM images of self-assembled structures YT, YS, YN and YQ respectively in their thermodynamically preferred state. Inset; Images of hydrogelation tested by vial inversion. (e) – (h) CryoTEM images of self-assembled structures YT, YS, YN and YQ respectively in their thermodynamically preferred state.

Additionally, their nanoscale morphology also remains unchanged, with TEM and cryoTEM investigation into their self-assembled morphologies illustrates YT, YS and YN remain as

fibrous network structures, and YQ forming spherical structures of variable diameters (see Figure 5.14).

5.3 Conclusions

The production of nanomaterials from self-assembling Fmoc-dipeptides with terminating hydrophilic amino acid residues was demonstrated. YT, YS and YN self assemble via π - β interactions to give fibrous self-assembled structures, with YS and YN fibrillar networks able to completely immobilise water molecules within the reaction vessel resulting in a self-supporting gel. YQ, on the other hand, aggregates due to the hydrophobic collapse in the aqueous environment. However, the supramolecular assemblies are stabilised by hydrogen bonding interactions of the peptide chain with the media, rather than π -stacking of the Fmoc groups and β -sheet formation, as typically observed for self-assembling Fmoc-dipeptides.^{4, 30, 35, 40, 46} The molecular association resulting in spherical nanostructures, and behaved as a Newtonian fluid. As the chemical functionality of YQ compared with YN is identical, the difference only of an additional CH₂ on the amino acid side chain, we can conclude that length of the side chain in amino acid position two can affect the formation of π - β assemblies, in the case of glutamine, it completely prohibits the formation hence the typically fibrillar network structure is not observed. The higher gel strength of YS compared with YN, can be attributed to a combination of the strength of intermolecular interactions and the molecular packing, with serine forming stronger hydrogen bonds than that of asparagine and its side chain containing one less carbon, which we have already deduced can greatly affect the molecular packing abilities of the Fmoc-dipeptides. However, as asparagine has the ability to form a double the number of hydrogen bonds than that of serine, the FTIR absorbance spectra of YN compared with YS has stronger β -sheet absorption bands. Additionally, we can conclude that the order in which amino acid residues appear in the peptide chain, can also affect the mechanical properties of the materials.

After characterisation of the systems in their thermodynamically preferred state, it was observed that there were only minor structural reconfigurations on a molecular level when compared to the initial studies of the kinetically trapped aggregates. YT, YS and YN remained in π - β assemblies with the thermodynamically preferred state having more

extended aggregates than the initial structure formation, and YQ re-entering the same structural assembly as initially formed. Subsequently, there was no change to mechanical properties or morphology, and therefore we can assume our original conclusions drawn from the kinetically trapped aggregates are assumed to be correct.

In brief, a new chemical functionality of self-assembled Fmoc-dipeptide nanostructures has been introduced by successfully incorporating hydrophilic amino acid residues into the peptide chains to give stable nanostructures, and deduced that the side chain functionality of the amino acid residue in position two can greatly influence gel strength and molecular packing abilities of the self-assembling molecules.

6.0 Differential antimicrobial properties of enzymatically triggered self-assembling aromatic peptide amphiphiles *in vivo**

*The work in this Chapter has been submitted, in part, for publication in Chemical Communications.

Declaration of contribution to submitted article:

Any reproduced work from the aforementioned submitted article, I was solely responsible for, including the written article itself, unless otherwise stated. Daniel Cannon provided the molecular modelling data. Dr. Sisir Debnath was responsible for synthesis and characterisation of phosphorylated precursors of Fmoc-YX-OH, as well as their *in vitro* fluorescence and *in vitro* HPLC yield studies.

6.1 Introduction

There have been a number of enzymes utilised in biocatalytic self-assembly and disassembly from aromatic peptide amphiphiles, most commonly phosphatases, esterases and proteases (discussed in Section 2.5.1 and 2.5.2). As they are naturally occurring in mammalian and bacterial cells, it is therefore rational to conclude that the self-assembly or dis-assembly of aromatic peptide amphiphiles may be biocatalytically triggered *in vivo*. A number biocatalytically triggered self-assembly or disassembly of aromatic peptide amphiphiles have been designed with specific enzymatic targets for *in vivo* applications.

In 2007 Yang *et al.* designed a phosphatase responsive system for biomedical applications. The self-assembling monomer was a β -amino acid derivative, Nap- β^3 -HPhg- β^3 -HPhg-Y-OH, as it was demonstrated to have a longer biostability than that of its analogous α -peptide.¹⁴⁸ The phosphorylated precursor was converted to the self assembling building block by treatment with acid phosphatase, and resulted in hydrogelation of blood samples.¹⁴⁸

In the same year, Yang *et al.* demonstrated that it was possible enzymatically triggered self-assembly of Fmoc-FFY-OH within *E. coli* bacterial cells and inhibit cell growth, deeming the bacteria inactive.¹⁴⁹ The self-assembling precursor, Fmoc-FFYp, was converted to the self-assembling aromatic peptide amphiphile within the cells by enzymatic dephosphorylation by the *E. coli*'s alkaline phosphatase.¹⁴⁹ The production of self-assembling building blocks initiated self-assembly within the cells and resulted in cell inactivity, commonly referred to as cell 'death'.¹⁴⁹ Similarly, Yang *et al.* also designed a system where the self-assembly of aromatic peptide amphiphiles within HeLa cells resulted in cell depletion.¹⁰² The self-assembly of Nap-FF-OH was triggered by ester hydrolysis of the capped precursor, Nap-FF-NHCH₂CH₂COOH, using the cells own esterase enzyme, and ultimately resulted in cell death.¹⁰²

In 2011, Gao *et al.* demonstrated the self-assembly of Ac-YYYY-OMe, triggered using alkaline phosphatase to dephosphorylate the non-assembling precursor Ac-YYYYp-OMe, resulting in a fibrillar network structure. After exposure to tyrosinase, an enzyme known to be over-expressed in malignant melanoma, the network structure was degraded. The work hypothesized that the system could be used as an anti-cancer treatment for controlled drug released *in vivo*.⁴⁴

The work in this Chapter is based on biocatalytically triggering self-assembly of aromatic peptide amphiphiles in bacterial cells, using systems known to be responsive to alkaline phosphatase. It was hypothesised that the treatment of *E. Coli* with different aromatic peptide amphiphiles would result in differential anti-microbial properties.

6.1.1 Background

Alkaline phosphatase has been shown to biocatalytically trigger self-assembly of aromatic peptide amphiphiles (discussed in Section 2.5.1). Phosphorylated precursors are unable to self-assemble due to electrostatic repulsion between the negatively charged phosphate moieties. The enzymatic action cleaves the 'blocking' group and initiates molecular self-assembly generally resulting in nanoscale fibres, however, nanospheres and leaf-like structures have also been observed.

Alkaline phosphatase is present in a number of biological systems including mammalian and bacterial cells. Alkaline phosphatase from *E. Coli* is found in the periplasmic space of the bacterial cell, *i.e.* the space between the cytoplasmic membrane and the outer membrane, and has been extensively studied over the last four decades including characterisation of binding properties, catalytic mechanism (discussed in Section 6.1.2), specificity and kinetics. It has also been demonstrated that by altering media composition the alkaline phosphatase may be over-expressed in the bacterial cells, which was conclusively determined by purification of the enzyme from the bacterial culture.

In 1997, Yang *et al.* demonstrated that it was possible to introduce alkaline phosphatase responsive precursors of self-assembling aromatic peptide amphiphiles into *E. coli* cells, and initiate self-assembly *in vivo* (discussed in Section 6.1).

6.1.2 Alkaline Phosphatase

Alkaline phosphatase is a relatively non-specific phosphomonoesterase, *i.e.* removes phosphate groups by hydrolysis, and displays optimum activity in alkaline pH.¹⁵⁰ The active enzyme is comprised of two identical subunits, and therefore has two active sites – although only one is active at any one time.^{151, 152} Each active site contains three metal ions

essential for catalysis, two of which contain zinc ions and one magnesium ion, arranged as a catalytic triad within a shallow pocket (see Figure 6.1).¹⁵³

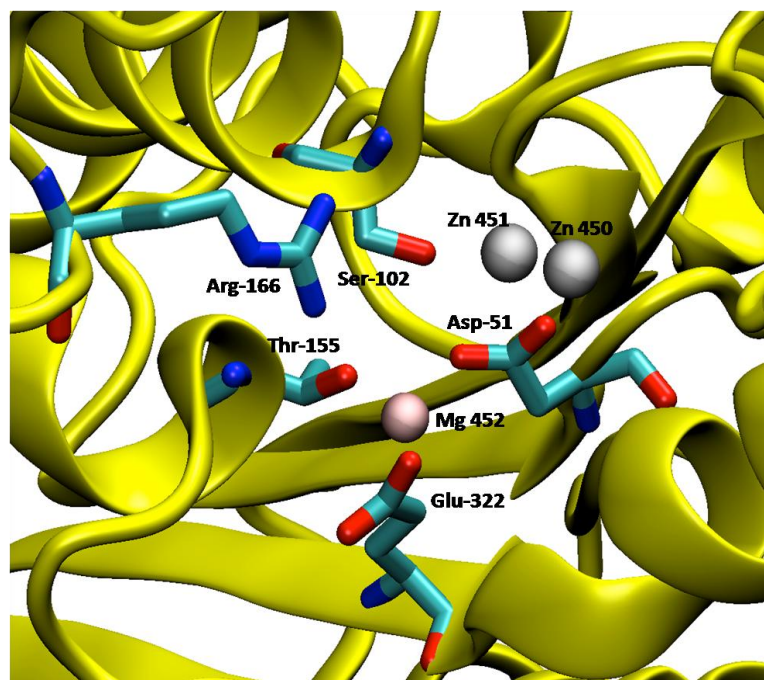


Figure 6.1 - Molecular model of alkaline phosphatase active site indicating the metal ions and amino acid residues involved in catalysis.

As the substrate approaches the active site, the phosphate group becomes coordinated to each of the zinc metal centres. One of these zinc centres can also coordinate to the hydroxyl group of Ser-102 of the enzyme, thus activating the oxygen for nucleophilic attack on the phosphate monoester centre, and cleaving the bound phosphate group. The remaining zinc facilitates the alcohol leaving group, and activates a water molecule for nucleophilic attack on the Ser-102-phosphate covalent bond (see Figure 6.2).¹⁵³

A number of self-assembling aromatic peptide amphiphiles have successfully been prepared by desphosphorylation using alkaline phosphatase,^{41-44, 83, 104} including Fmoc-FY-OH.¹⁵⁴

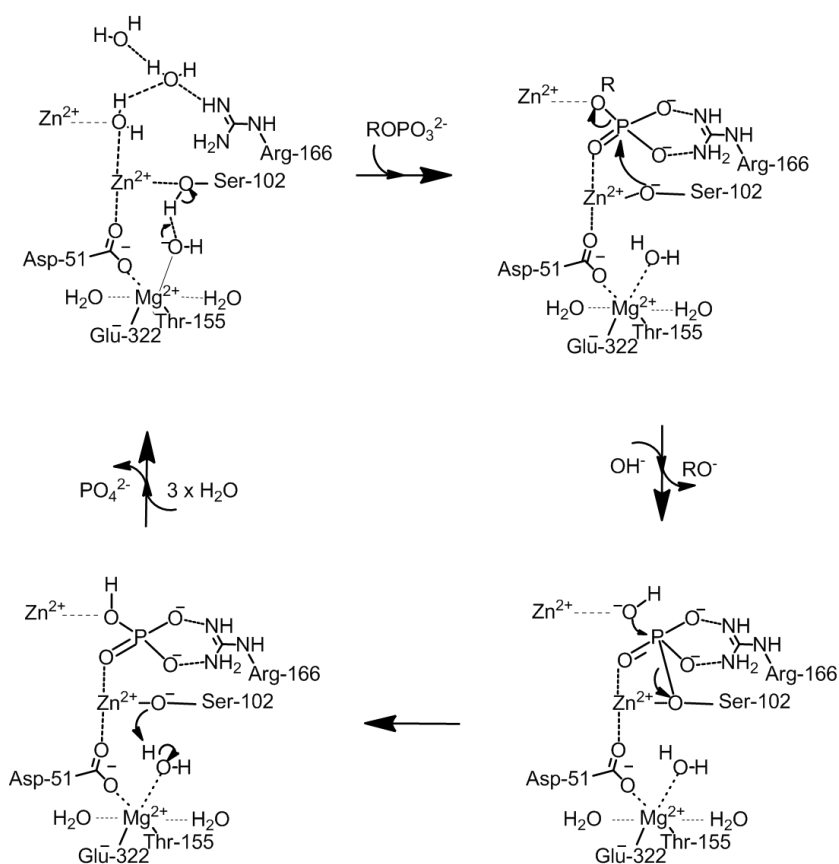


Figure 6.2 - Mechanism of alkaline phosphatase catalysed dephosphorylation.

6.2 Results and Discussion

6.2.1 *In vitro* self-assembly studies of alkaline phosphatase triggered self-assembly of Fmoc-FY-OH

The self-assembly of aromatic peptide amphiphile Fmoc-FY-OH was biocatalytically triggered by enzymatic dephosphorylation of precursor Fmoc-FY p -OH at a 10 mM concentration in 0.6 M sodium phosphate buffer pH 8, as previously described by Sadownik *et al.*¹⁵⁴ (see Figure 6.3).

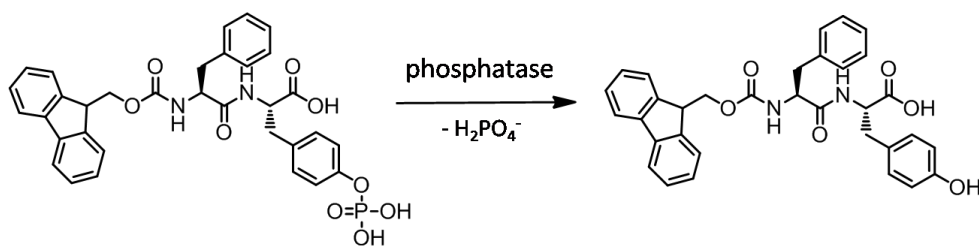


Figure 6.3 – Reaction schematic of enzymatic dephosphorylation of Fmoc-FYp-OH forming Fmoc-FY-OH.

The conversion of precursors to the desired Fmoc-FY-OH dipeptide was monitored using HPLC, which reached 96 % conversion after 24 hours. The clear solution formed a self-supporting translucent hydrogel within 3 hours of treatment with alkaline phosphatase enzyme (see Figure 6.4(c) inset), indicating the molecular self-assembly of the generated Fmoc-FY-OH species.

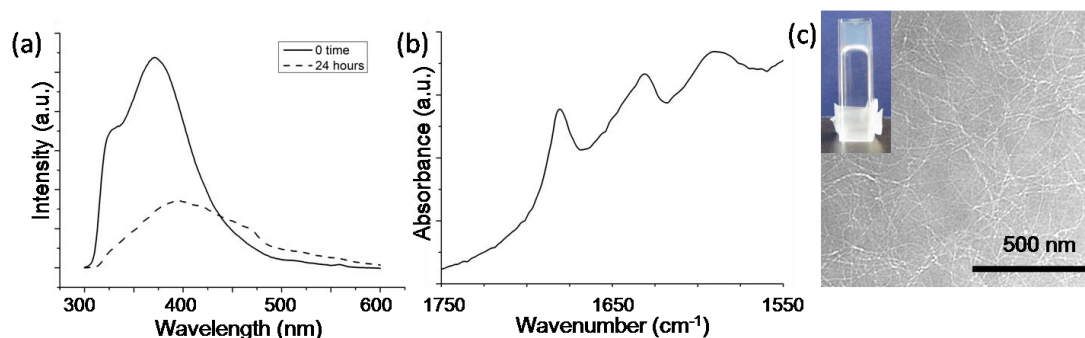


Figure 6.4 – (a) Fluorescence emission spectra of Fmoc-FYp-OH measured before enzyme addition (0 time), and after 24 hours of the addition alkaline phosphatase (24 hours). (b) Amide I region of FTIR absorption spectra of Fmoc-FYp-OH measured after 24 hours of enzyme addition. (c) TEM image of supramolecular structure imaged at 24 hours. Inset, hydrogelation of sample tested by vial inversion at 24 hours.

Fluorescence emission spectroscopy was used to monitor changes in the fluorenyl environment (see Figure 6.4(a)). The starting mixture displayed a peak ~ 320 nm, representative of the monomeric Fmoc-FYp-OH, and a peak ~ 375 nm representing micellar aggregates of Fmoc-FYp-OH in solution which is consistent with previous studies.¹⁵⁴ After 24 hours of treatment with alkaline phosphatase, a peak ~ 395 nm, accompanied by system quenching, is indicative of J-aggregate formation, where the Fmoc moieties stack parallel in ‘columns’. At this point in the supramolecular assembly, both the monomeric and micellar

peaks have completely disappeared, indicating that all the Fmoc groups are assembled within the extended J-aggregate structure.

The hydrogen bonding environment of peptide components was monitored using FTIR absorbance spectroscopy. Carbonyl moieties within the peptide chain involved in hydrogen bonding can be monitored using the amide I region of the spectra (see Figure 6.4 (b)).¹³⁰ After 24 hours of enzyme addition, three absorbance bands are evident. One band $\sim 1590\text{ cm}^{-1}$ corresponds to carbonyl stretching of the carboxylic acid carbonyl moiety at the N-terminus of the aromatic peptide amphiphile. The combination of two bands, $\sim 1630\text{ cm}^{-1}$ and $\sim 1680\text{ cm}^{-1}$, represents the carbonyls of the peptide backbone hydrogen bonded in a β -sheet arrangement,¹³⁰ with the Fmoc carbonyl moiety contributing to the 1680 cm^{-1} peak (as discussed in Section 4.2.3).

The π -stacked Fmoc groups and β -sheet supramolecular assembly (π - β assembly) resulted in nanoscale fibres as observed using TEM (see Figure 6.4 (c)), consistent with previous studies of the self-assembly of this system.¹⁵⁴

6.2.2 *In vivo* alkaline phosphatase triggered self-assembly of Fmoc-FY-OH using *E. Coli*

Two formulations of bacterial growth media were prepared, discussed as Medium A and Medium B (see Table 6.1). The basic formulation of each Media was identical based on the recipes described by Csopek *et al.* where inclusion of inosine in the growth medium has been shown to promote the expression of alkaline phosphatase in Medium B.¹⁵⁰

	Medium A	Medium B
tris	0.12 M	0.12 M
KCl	0.08 M	0.08 M
NaCl	0.02 M	0.02 M
KCl	0.02 M	0.02 M
NH ₄ Cl	0.003 M	0.003 M
Na ₂ SO ₄	0.001 M	0.001 M
MgCl ₂	2.0×10^{-4} M	2.0×10^{-4} M
ZnCl ₂	2.0×10^{-5} M	2.0×10^{-5} M
Glucose	0.50%	0.50%
Difco Bactopectone	0.50%	0.50%
Inosine	-	1.0×10^{-5} M

Table 6.1 - Concentration of ingredients for Growth Medium A and B.

MC-1000 *E. Coli* was inoculated from a stock solution into each of the media, and bacterial growth monitored using fluorescence over 24 hours (see Figure 6.5). It was observed that both bacterial cultures remained in the lag phase for ~ 6 hours, with the rate of growth being unaffected by the media.

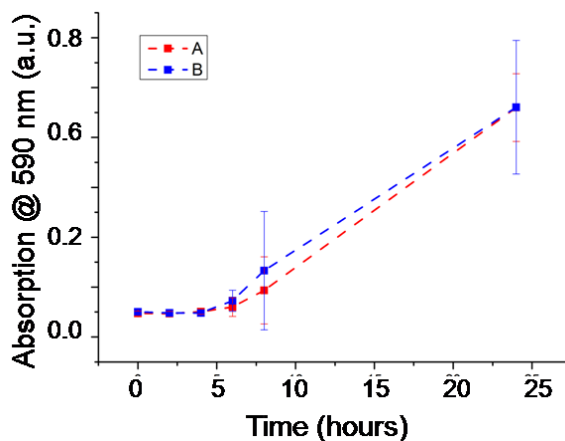


Figure 6.5 - *E. coli* growth curves in media A and media B monitored over 24 hours using fluorescence.

The activity of alkaline phosphatase within each of the cultures was then monitored using an assay method modified from the Worthington Enzyme Manual,¹⁵⁵ using p-nitrophenyl phosphate (PNP) as a substrate, and monitoring the production of p-nitrophenol over 10 minutes using fluorescence. The rate of production of p-nitrophenol in media A and B were $0.128 \text{ a.u. min}^{-1}\text{mL}^{-1}$ and $0.245 \text{ a.u. min}^{-1}\text{mL}^{-1}$ respectively. The rate of production in of p-nitrophenol in media B was double than that in media A, proving that the alkaline phosphatase in the media was active in both cultures, and assumed to be over-expressed in the media B culture due to the inclusion of the inosine.

After 24 hours of growing each of the cultures media A or media B, they were then treated with 13.0 mg of Fmoc-FY ρ -OH and incubated at 37 °C for 24 hours. 13.0 mg of precursor was chosen as the characterisation *in vitro* was carried out at 10 mM concentration (13.0 mg in 2 mL), and deemed a sufficient concentration for gelation within cells. The bacterial cells were separated from the media by centrifugation, the cells lysed in acetonitrile to dissolve the organic matter. Both media and cell samples were syringe filtered to make them suitable for HPLC analysis to monitor the conversion of Fmoc-FY ρ -OH to Fmoc-FY-OH *in vivo*. Each of the samples with active bacterial cultures displayed a conversion to the

desired self-assembling aromatic peptide amphiphile, media A and B with an 84.2 % and 99.5 % conversion respectively (see Table 6.2), confirming successful enzymatic conversion to the desired product, with a 0 % conversion observed in the absence of bacterial cells.

Media	Conversion to Fmoc-FY-OH (%)
A	84.2
B	99.5

Table 6.2 – Percentage conversion to Fmoc-FY-OH *in vivo* of *E. Coli* bacterial cells grown in media A and media B monitored using HPLC.

Furthermore, as the cells and the media samples were analysed separately, it could be assessed where both the precursor and Fmoc-FY-OH was located within the samples (see Figure 6.6). The Fmoc-FYp-OH precursor remained in the media, with the predominant portion of Fmoc-FY-OH reaction product found within the cell samples, confirming the accumulation of the product within the cells suggesting that self-assembly may occur within the cells. The accumulation of the product within cells can be directly linked to the hydrophobicity of the analytes. As Fmoc-FY-OH is more hydrophobic than Fmoc-FYp-OH ($cLogP = 5.45$ and 4.12 respectively), the product had a tendency to stay inside the cells in which it was formed rather than migrate to the aqueous media, which is consistent with previous studies by Yang *et al.* whilst monitoring the self-assembly of aromatic peptide amphiphiles within bacterial cells using HPLC techniques.¹⁴⁹

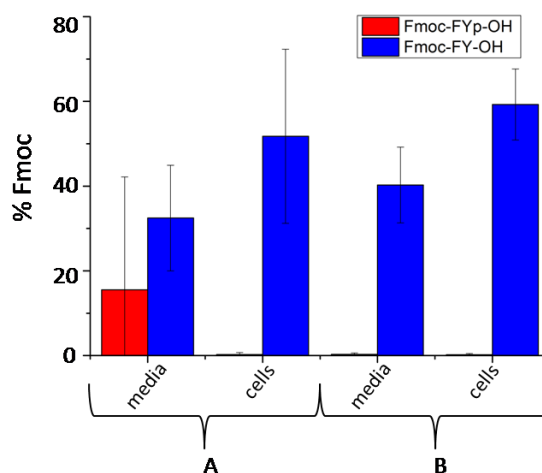


Figure 6.6 – Conversion to Fmoc-FY-OH *in vivo* of *E. Coli* bacterial cells grown in media A and media B illustrating the location of precursors and aromatic peptide amphiphiles monitored using HPLC.

In an attempt to confirm molecular self-assembly occurred within the *E. coli* bacteria cells TEM imaging was carried out. Bacterial cultures, both treated and untreated with Fmoc-FYp-OH, were imaged. However, the fibrous network structure could not be distinguished within the bacterial cell.

Furthermore, the cells were concentrated and re-suspended in 2 mL of 0.6 M sodium phosphate buffer pH 8 to confirm the occurrence of molecular self-assembly of Fmoc-FY-OH. However, attempts to lyse the cells, and therefore manipulate the self-assembling Fmoc-FY-OH to migrate to the aqueous environment and result in hydrogelation, proved unsuccessful. This was carried out in two different ways; (1) by sonication of the samples for 5 minutes, and; (2) by the addition of 1 mg of lysozymes (Sigma-Aldrich). In each case, the samples remained as solutions, with the bacterial culture settling at the base of the reaction vessel.

After confirming that the conversion to self-assembling aromatic peptide amphiphiles had indeed taken place and product located within the cells, the bacterial cell viability was monitored using Live/Dead[®] cell staining. Each of the bacterial samples were grown in either media A or B and treated with the self-assembling aromatic peptide amphiphile precursors, Fmoc-FYp-OH. After 24 hours, the cells were treated with a solution of 1.67 μ M SYTO 9 dye and 9.99 μ M propidium iodide in DMSO to monitor cell viability, SYTO 9 staining live cells and propidium iodide staining inactive cells. The samples were viewed using a fluorescent microscope. The bacterial samples that were treated with the peptide displayed a higher percentage of dead cells when compared to their untreated counterparts (see Table 6.3).

Media	Treatment with Fmoc-FYp-OH	% Live	% Dead
A	-	93.5	6.5
A	✓	84.6	15.4
B	-	84.9	15.1
B	✓	65.1	34.9

Table 6.3 – Table summary of percentage live and dead cells of *E. Coli* samples grown in media A and B, and treated with self-assmebly precursor.

The cell cultures in media A displayed 6.5 % of the cells were inactive (dead). After treatment with Fmoc-FYp-OH, the percentage of inactive cells rose to 15.4 %, a 9.9 % increase. However, the cells cultured in media B displayed 15.1 % of the cells were inactive,

which increased by 19.8 % to 34.9 % when treated with Fmoc-FYp-OH. The higher cell mortality in media B is most likely due to the higher conversion to self-assembling precursors within the cells, and can conclude that the anti-microbial properties of aromatic peptide amphiphiles may be more conveniently studied for *E. Coli* cells cultured in Media B.

6.2.3 *In vitro* self-assembly studies of alkaline phosphatase triggered self-assembly of Fmoc-YX-OH

Analogous to the systems studied in Chapter 5, four alkaline phosphatase responsive aromatic peptide amphiphiles were designed and synthesised, Fmoc-YpT-OH, Fmoc-YpS-OH, Fmoc-YpN-OH and Fmoc-YpQ-OH. The self-assembly of the aromatic peptide amphiphiles Fmoc-YX-OH were biocatalytically triggered by enzymatic dephosphorylation of Fmoc-YpX-OH precursor using alkaline phosphatase at a 10 mM concentration in 0.6 M sodium phosphate buffer pH 8, giving rise to four self-assembling aromatic amphiphiles, Fmoc-YT-OMe, Fmoc-YS-OMe, Fmoc-YN-OMe and Fmoc-YQ-OMe (see Figure 6.4).

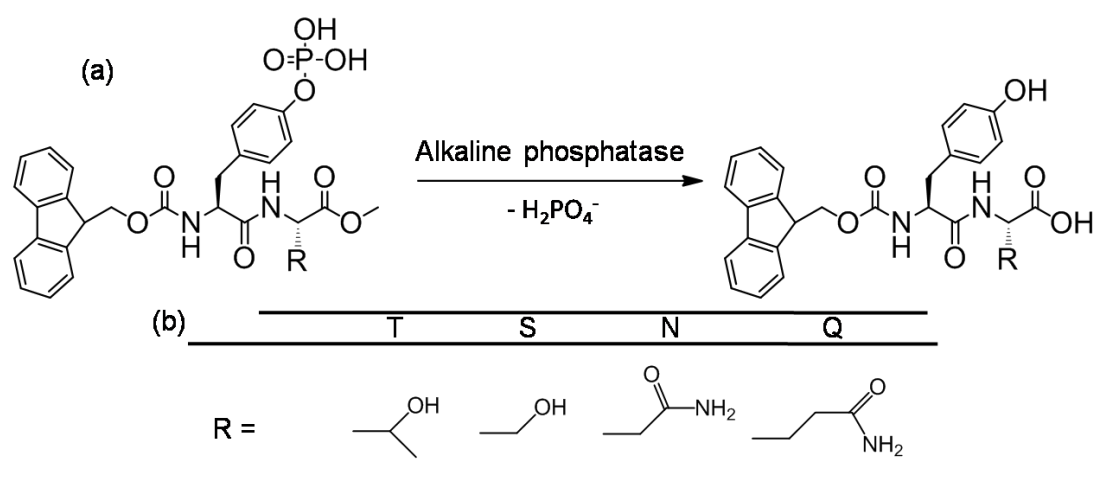


Figure 6.7 – (a) Reaction schematic of alkaline phosphatase triggered dephosphorylation of phosphorylated Fmoc-dipeptides to produce self-assembling aromatic peptide amphiphiles.

(b) Table of amino acid side chains of T, S, N and Q.

The conversion of precursors to the desired Fmoc-YX-OH dipeptide was monitored using HPLC, with Fmoc-YT-OH (YT), Fmoc-YS-OH (YS), Fmoc-YN-OH (YN) and Fmoc-YQ-OH (YQ) yielding 97.1 %, 95.0 %, 99.9 % and 99.9 % respectively after 24 hours of enzyme addition. At this time, each of the four suspensions had been transformed to; YT, a clear viscous

liquid; YS, a clear self-supporting gel; YN, a translucent self-supporting gel, and; YQ, a clear solution; indicating that molecular self-assembly had occurred (see Figure 6.8).

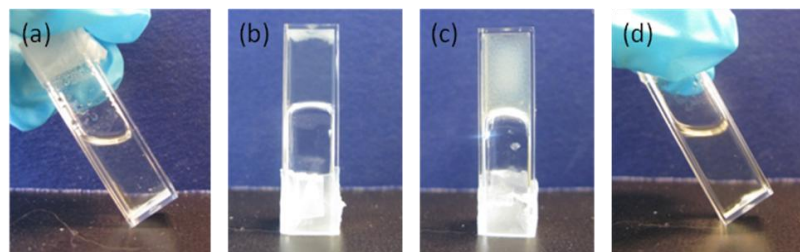


Figure 6.8 – Hydrogelation of samples YT, YS, YN and YQ respectively tested by vial inversion after 24 hours of enzyme addition.

Fluorescence emission spectroscopy was used to monitor changes in the fluorenyl environment (see Figure 6.9 (a)-(d)). The starting mixtures containing the phosphorylated precursors of YT, YS, YN and YQ displayed a peak ~ 320 nm, representative of the monomeric Fmoc-YpX-OH, and a shoulder peak ~ 375 nm representing aggregates of the precursors in solution, most like spherical aggregates similar to those reported for Fmoc-FYp-OH.¹⁵⁴ After 24 hours of treatment with alkaline phosphatase, the 320 nm peak of YT, YS and YN had been sufficiently quenched, indicating π -stacking of Fmoc groups in close proximity. In the case of YQ (Figure 6.9 (d)), the system quenching was accompanied with a blue shift indicating a destabilisation in the Fmoc environment, consistent with the self-assembly of subtilisin responsive self-assembly of Fmoc-YQ-OH (discussed in Section 5.2.2). The blue shift indicates that although molecular self-assembly is driven by the hydrophobic collapse, stabilising π -interactions between neighbouring Fmoc-groups is not possible due to their relative orientation within the self-assembled supramolecular structure.

By monitoring the amide I region of the FTIR absorbance spectra ($1600\text{ cm}^{-1} - 1700\text{ cm}^{-1}$), the hydrogen bonded environment of the peptide chains can be deduced. More specifically, the amide I region illustrates stretching of carbonyl moieties which are involved in the hydrogen bonding of self-assembled peptides (see Figure 6.9 (e)). The FTIR absorbance spectra obtained are almost identical to those obtained for subtilisin triggered self-assembly of YT, YS, YN and YQ (discussed in Section 5.2.2). After 24 hours, YT, YS and YN display peaks associated with β -sheet formation - a combination of peaks $\sim 1680\text{ cm}^{-1}$ and $\sim 1640\text{ cm}^{-1}$, with the 1680 cm^{-1} peak being more pronounced than that of its 1640 cm^{-1} counterpart due to a contribution from the Fmoc carbonyl group which also hydrogen

bonds into the β sheet arrangement (discussed in Section 4.2.4), which is consistent with previous studies of similar self-assembling Fmoc-dipeptides,^{3, 4, 9, 32, 47} and the reverse of that observed when studying secondary protein structure, where the 1640 cm^{-1} peak is usually more prominent.¹³⁰ YN displays slightly stronger β -sheet absorption bands than that of YT and YS, which we attribute to the increased hydrogen bonding capability of amino acid residue N compared with S (discussed in Section 5.2.2). Lastly, no β -sheet bands are observed for YQ. YQ does not adopt the same β -sheet structure as any of the other systems due to the steric effects of the glutamine side chain prohibiting molecular packing in this arrangement, consisted with subtilisin triggered self-assembly of Fmoc-YQ-OH (discussed in Section 5.2.2).

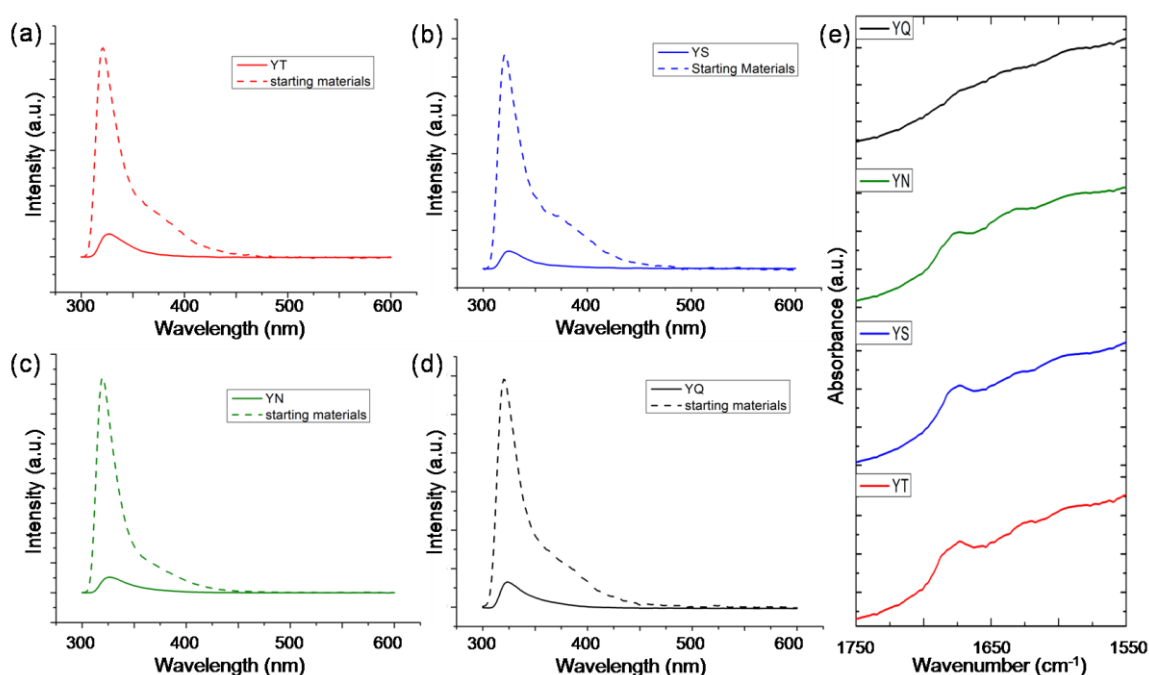


Figure 6.9 – (a) – (d) Fluorescence emission spectra of YT, YS, YN and YQ respectively at 24 hours overlaid with emission of precursor solution. (e) Amide I region of FTIR absorbance spectra of YT, YS, YN and YQ measured after 24 hours of enzyme addition.

Investigation into their supramolecular structure was carried out using TEM (see Figure 6.10). YT, YS, and YN formed fibril network structures, with YT also displaying spherical and globular structures. YQ self-assembled to form spheres in the aqueous environment due to the steric effects of the additional CH_2 on the glutamine side chain (discussed in Section 5.2.3).

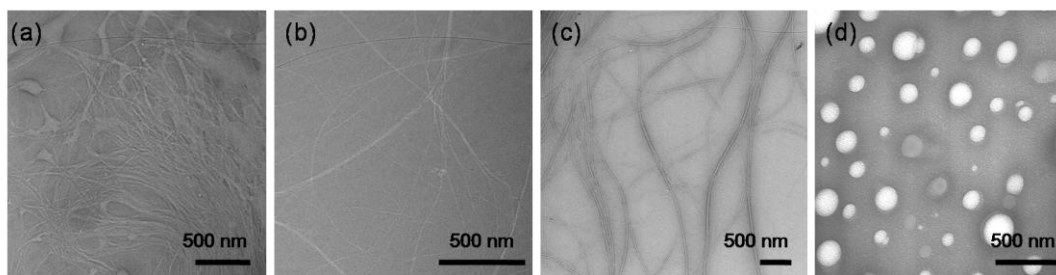


Figure 6.10 – (a) – (d) TEM images of self-assembled structures of YT, YS, YN and YQ respectively, after 24 hours of enzyme addition.

Overall, the alkaline phosphatase triggered self-assembly of YT, YS, YN and YQ, are similar to the self-assembled structures observed for the subtilisin triggered systems discussed in Chapter 5.

6.2.4 Monitoring differential anti-microbial response *In vivo* of alkaline phosphatase triggered self-assembly of Fmoc-YX-OH using *E. Coli*

MC-1000 *E. Coli* was inoculated from a stock solution media B, and incubated for 24 hours at 37 °C. The cultures were then treated with 2×10^{-5} mols of the phosphorylated precursor (approximately 13 mg) of YT, YS, YN or YQ and incubated at 37 °C for 24 hours. As before, the bacteria were separated from the media by centrifugation, the cells lysed in acetonitrile to dissolve the organic matter. Both media and cell samples were syringe filtered to make them suitable for HPLC analysis to monitor the conversion of precursors to the desired self-assembling aromatic peptide amphiphile *in vivo*. Each of the four systems were successfully converted by the bacterial alkaline phosphatase with YT, YS, YN and YQ yielding 31.4 %, 49.5 %, 60.7 % and 87.9 % respectively. However, both the precursors and products are predominantly found within the media with only a small concentration found within the cell samples (see Figure 6.11). This is in contrast to the Fmoc-FY-OH system discussed in Section 6.2.2, where the product was found to remain predominantly within the cells. However it can be linked to the hydrophilicity of the generated aromatic peptide amphiphiles. As Fmoc-YT-OH, Fmoc-YS-OH, Fmoc-YN-OH and Fmoc-YQ-OH have terminating hydrophilic amino acid residues, they are much less hydrophobic than Fmoc-FY-OH ($\log P$ values discussed in Section 5.2.1). Therefore, they have a much higher affinity to migrate to the

aqueous media, rather than be retained within the more hydrophobic environment of the cells.

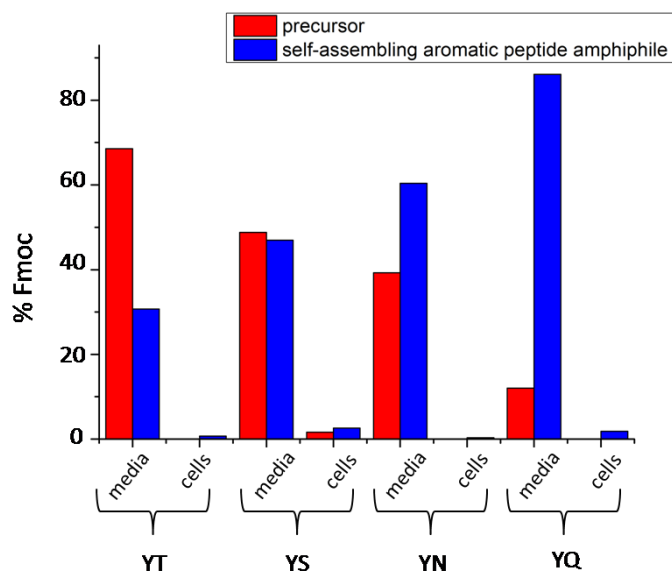


Figure 6.11 - Conversion to self-assembling aromatic peptide amphiphile either YT, YS, YN or YQ *in vivo* of *E. Coli* bacterial cells grown in media B illustrating the monitored using HPLC.

Live/Dead[®] cell staining of each bacteria sample treated with the precursors of either YT, YS, YN or YQ (as in Section 6.2.2), to monitor cell viability and give an indication of differential bacterial response (see Figure 6.12). Bacterial samples that were treated with the peptide displayed a higher percentage of dead cells when compared to the untreated cultures which demonstrated only 6.1 % of cells were inactive. The highest percentage of inactive cells were present in samples which were treated with either YS or YN, with 33.1 % and 46.7 % of cells found to be inactive respectively. YT and YQ displayed a lower anti-microbial effect with 28.5 % and 24.9 % respectively.

Overall aromatic peptide amphiphiles which had the ability to form hydrogels displayed the highest cell mortality; Fmoc-YS-OH , 33.1 %; Fmoc-YN-OH, 46.7 %, and; Fmoc-FY-OH, 34.9 % (discussed in Section 6.2.2). Aromatic peptide amphiphiles which formed supramolecular structures, but were unable to immobilise the solvent molecules, demonstrated less efficient anti-microbial properties, Fmoc-YT-OH and Fmoc-YQ-OH resulting in 28.5 % and 24.9 % respectively, of *E. Coli* found to be inactive.

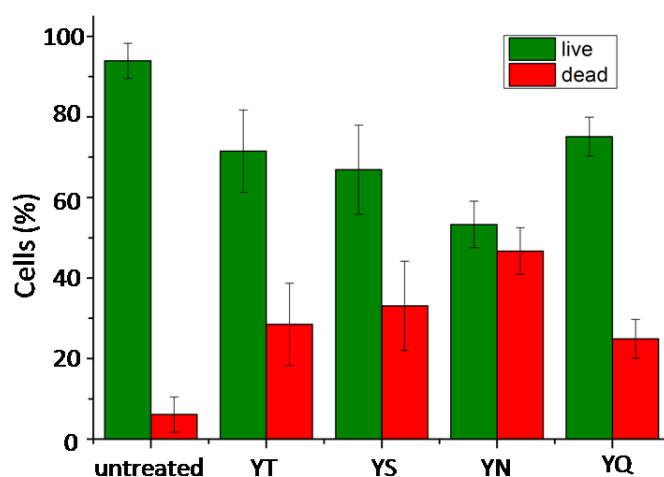


Figure 6.12 – Percentage of active (live) and inactive (dead) cells in bacterial cultures after no treatment, or treatment with the phosphorylated precursors of self-assembling aromatic peptide amphiphiles YT, YS, YN or YQ.

6.3 Conclusions

The production of peptide nanostructures has been demonstrated using alkaline phosphatase as an enzymatic trigger for the self-assembly for Fmoc-FY-OH, Fmoc-YT-OMe, Fmoc-YS-OH, Fmoc-YN-OH, and Fmoc-YQ-OMe. FY, YT, YS and YN self-assemble via π - β interactions to form nano fibrillar structures, with FY, YS and YN able to completely immobilise water molecules resulting in translucent hydrogels - consistent with previous studies carried out by Sadownik *et al.*¹⁵⁴ and those discussed in Chapter 5.0. YQ forms spherical structures via hydrophobic interactions as the steric effects of the longer glutamine side chain prohibits π - β assembly.

It has been demonstrated that by the inclusion of inosine within the culture media results in an over-expression of alkaline phosphatase when culturing *E. Coli*. The non-assembling precursors can be converted to self-assembling aromatic peptide amphiphiles *in vivo*, with the location of the products being directly linked to the hydrophobicity of the products - the more hydrophobic Fmoc-FY-OH products accumulating within the cells and the hydrophilic Fmoc-Yx-OH peptides migrating to the media.

Furthermore, the presence of the aromatic peptide amphiphiles within the cultured *E. Coli* demonstrates differential anti-microbial response. Aromatic peptide amphiphiles with the

ability to form hydrogels *in vitro* (FY, YS and YN) displayed a higher anti-microbial effect *in vivo*.

7.0 Conclusions and Future Work

7.1 Conclusions

By utilising thermodynamically driven enzymatic self-assembly, it is possible to reproducibly access the most thermodynamically stable structures representing the folded structures with minimal free energy. The self-assembly of Fmoc-SF-OMe triggered using protease enzyme thermolysin, gave rise to the first truly two-dimensional supramolecular structures from chiral peptide building blocks. The enzyme playing a key role in stabilising the suspension to allow for molecular self-assembly, and the reversibility of the reaction allows for 'self-correction' and access to the thermodynamically preferred sheet structures over kinetically trapped one-dimensional aggregates.

Furthermore, by utilising thermodynamically driven enzymatic systems it is possible to directly compare the effect of the peptidic tail of four closely related self-assembling aromatic peptide amphiphiles; Fmoc-SF-OMe, Fmoc-SL-OMe, Fmoc-TF-OMe and Fmoc-TL-OMe. The presence of a serine residue in amino acid position one induces planar structures, with the additional chiral centre on their threonine counterparts presenting the familiar chiral nanostructures. The presence of a phenylalanine residue in amino acid position two provides more thermodynamically favoured structures than their leucine counterparts. This is due to an interaction of the phenyl moiety with the π -stacked Fmoc columns, providing extra stability to the system.

In Chapter 5, the production of peptide nanostructures from aromatic peptide amphiphiles containing terminating hydrophilic amino acid residues was demonstrated; and therefore the successful introduction of a new chemical functionality into the supramolecular structures. The four systems under study, subtilisin triggered self-assembly of Fmoc-YT-OH, Fmoc-YS-OH, Fmoc-YN-OH and Fmoc-YQ-OH, could then be directly compared to monitor the influence of each terminating amino acid residue. It was deduced that the addition CH_2 on the glutamine side chain prohibited tight molecular packing in π - β configuration, and resulted in the formation of micellar structures rather than fibrillar structures as observed for YT, YS and YN. Additionally the hydrogen bonding ability of the amino acid side chain of the residue in the second position can have an influence over the mechanical properties.

Finally, it was demonstrated that non-assembling phosphorylated precursors could be converted to self-assembling aromatic peptide amphiphiles *in vivo* by alkaline phosphatase present within *E. Coli* cells. By treatment with different precursors, the bacterial cultures

demonstrated a differential anti-microbial response, with higher cell inactivity, or death, caused by treatment of peptides with the ability to form hydrogels *in vitro*.

Overall, the work in this thesis has demonstrated successful characterisation of enzymatically triggered self-assembly of aromatic peptide amphiphiles, allowed for successful elucidation of amino acid sequence/nanostructure relationships, and demonstrated that aromatic dipeptide amphiphiles have anti-microbial effects when self-assembly is triggered *in vivo*.

7.2 Future Work

The most obvious future work resulting from this thesis as a whole would be to analyse further combinations of the dipeptide sequence, to elucidate further amino acid sequence/structure relationships, as well as monitor the effects of interchanging the Fmoc-group with other aromatic moieties. As peptide nanostructures are relatively new materials, a complete set of design rules to predict the behaviour of self-assembly would be beneficial for future tailoring and design.

It would also be interesting to include charged amino acid residues into Fmoc-dipeptide amphiphiles. We would generally expect the formation of micellar structures in solution due to electrostatic repulsion between monomers. However, by the introduction of an oppositely charged species may allow for a two-component system with novel nanoscale architecture.

Following on from Chapters 3 and 4, where the thermolysin driven reaction allowed access to the most thermodynamically favoured supramolecular structures, it would be interesting to have the synthesised molecular building blocks self-assemble without the enzymatic trigger. Fmoc-SF-OMe demonstrated insolubility in aqueous environment, and we assume SL, TF and TL to be the same, however, by utilising pH switching the monomers may be dissolved in the aqueous environment.

The micellar structures observed in Chapters 5 and 6, may have potential as a hydrophobic drug carrier. Furthermore, they may be useful in terms of controlled drug release, by the introduction of a second enzyme which can trigger disassembly of the nanostructures.

Finally, the anti-microbial studies of aromatic peptide amphiles on *E. Coli* is far from complete (Chapter 6). The molecular assembly of the peptide derivatives remains unconfirmed. Congo Red staining may allow for visualisation of self-assembly within the bacterial cells. Furthermore, by testing a range of alkaline responsive aromatic peptide amphiphiles on cell viability may allow for a correlation to be made between peptide sequence and anti-microbial effect.

8.0 Materials and Methods

8.1 Methods and Materials associated with the study of Fmoc-SF-OMe (discussed in Chapter 3.0)

8.1.1 Thermolysin catalysed condensation of amino acid residues to form Fmoc-SF-OMe

Fmoc-S-OH (Bachem, UK) and F-OMe (Sigma-Aldrich, UK) were weighed as a 20:80 mM ratio in a glass vial. The powder mixture was dissolved in 2 mL of 0.1 M pH 8 potassium phosphate buffer with the addition of the 1mg/ml lyophilised *thermolysin* powder (*bacillus Thermoproteolyticus rokko* from Sigma-Aldrich, UK) unless otherwise stated. The solution was vortexed and sonicated to ensure dissolution. Samples were incubated at room temperature.

8.1.2 Monitoring the conversion of Fmoc-S-OH to Fmoc-SF-OMe using HPLC

A Dionex P680 system operating with a Macherey-Nagel 250 Å, 4.6 x 250 mm, C18 column was used for reversed phase HPLC. 10 µL of sample was injected. The mobile phase was comprised of water and acetonitrile ramped from 20-80 % over 35 minutes at a flow rate of 1 mL min⁻¹. Detection of the peptide amphiphiles was carried out using a UVD170U UV-Vis detector at a 300 nm wavelength.

8.1.3 Fluorescence

Fluorescence emission spectra were measured on a Jasco FP-6500 spectrofluorometer with light measured orthogonally to the excitation light with a scanning speed of 200 nm min⁻¹. Excitation light at 280 nm and emission data range between 300 nm and 600 nm. The emission spectra were measured with a bandwidth of 3 nm with a medium response and a 1 nm data pitch. Spectra were normalised to maximum intensity.

8.1.4 Infra-red spectroscopy

FTIR spectra were acquired in a Bruker Vertex spectrometer with a spectral resolution of 2 cm⁻¹. The spectra were obtained by averaging 64 interferograms for each sample. Measurements were performed in a standard IR cuvette (Harrick Scientific), in which the

sample was contained between two CaF₂ windows (thickness, 2 mm) separated by a 25-mm PTFE spacer. All sample manipulations were performed in a glove box to minimize interference from carbon dioxide and water vapour; D₂O was used as the solvent for all the IR measurements.

8.1.5 WAXS

WAXS analysis were performed using a Philips X'Pert diffractometer with a wavelength of 1.5406 Å. Fmoc-SF-OMe gel and buffer solution were spread on two separate silica substrates as film and allowed to air dry prior to data collection.

8.1.6 TEM

Carbon-coated copper grids (200 mesh) were glow discharged in air for 30 seconds. A 10 µL volume of gel was transferred onto the support film and blotted down using filter paper. 20 µl of negative stain (1% aqueous methylamine vanadate obtained from Nanovan; Nanoprobes) was applied and the mixture blotted again using filter paper to remove excess. The dried specimens were then imaged using a LEO 912 energy filtering transmission electron microscope operating at 120kV fitted with 14bit/2K Proscan CCD camera. TEM imaging was carried out at the University of Glasgow.

8.1.7 CryoTEM

Gel samples were blotted onto a thin film grid of 100-200 nm. The grid was then plunged into liquid ethane (temperatures below -170 °C) and transferred to a GATAN 626 cryoholder and imaged using a JEOL 2100 transmission electron microscope fitted with a GATAN 4K Ultrascan camera. The cryoTEM analysis was carried out at Unilever, Bedford.

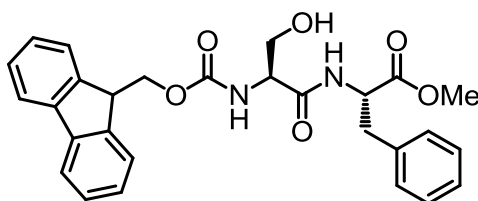
8.1.8 Optical Microscopy

10 µL of sample was transferred onto a glass slide and covered with a cover slip. The samples were then examined using a Zeiss Axio Imager A1 optical microscope equipped

with polarising lenses at 0° using a bright lens and transmitted light. Homogeneity was ensured by repeating in triplicate.

8.1.9 Synthesis of Fmoc-SF-OMe

Fmoc-S-OH (1 g, 2.8 mM), F-OMe (0.72g, 3.4 mM) and HBTU (1.26g, 3.4 mM) were dissolved in 10 mL of DMF. 1.041 mL (5.6 mM) of DIPEA was added and solution stirred for 24 hours. The solvent was removed by evaporation *in vacuo*. The resulting solid was dissolved in ethyl acetate, washed in duplicate with equal volumes of 1M sodium bicarbonate, brine and 1M HCl. The organic layer dried using sodium sulphate and filtered. Solvent removed by evaporation *in vacuo*. The white solid then purified over a silica column using 2.5 % - 7.5 % methanol in chloroform. Aliquots evaporated at room temperature and pressure and white solid combined (21 % yield, 98 % purity).



δ_{H} (DMSO, 500 MHz): 8.24 (1H, d, $J = 7.6$ Hz, NH), 7.98 (2H, d, $J = 7.5$ Hz, fluorenyl Ar CH), 7.73 – 7.71 (2H, m, fluorenyl Ar CH), 7.42 – 7.17 (10H, m, four fluorenyl Ar CH, five Phe Ar CH, NH), 4.84 (1H, t, $J = 5.6$ Hz, Ser C_{α} H), 4.48 (1H, q, $J = 7.2$ Hz, one Ser CH), 4.26 (2H, d, $J = 6.9$ Hz, fluorenyl CH_2), 4.22 – 4.19 (1H, m, Phe C_{α} H), 4.11 – 4.07 (1H, m, fluorenyl CH), 4.56 (4H, s, CH_3 , one Ser CH), 3.50 – 3.45 (1H, m, OH), 3.03 – 2.99 (1H, m, one Phe CH), 2.96 – 2.92 (1H, m, one Phe CH). δ_{C} (DMSO, 125 MHz): 172.1 (Phe C=O), 170.6 (Ser C=O), 156.3 (fluorenyl C=O), 144.2 (fluorenyl C_{q}), 141.1 (fluorenyl C_{q}), 137.4 (Phe C_{q}), 129.5 (Phe Ar CH), 128.6 (Phe Ar CH), 128.1 (fluorenyl Ar CH), 127.5 (fluorenyl Ar CH), 127.0 (Phe Ar CH), 125.7 (fluorenyl Ar CH), 120.5 (fluorenyl Ar CH), 66.2 (fluorenyl CH_2), 62.1 (Ser CH_2), 57.5 (Ser C_{α}), 54.0 (Phe C_{α}), 52.2 (CH_3), 47.1 (fluorenyl CH), 37.1 (Phe CH_2). MS (ES+); m/z 488.93 $[\text{M} + \text{H}]^+$. Elemental analysis for $\text{C}_{28}\text{H}_{28}\text{N}_2\text{O}_6$: expected C: 68.8 %, H: 5.8 %, N: 5.7 %; found C: 67.3 %, H: 5.8 %, N: 6.4 %.

8.1.10 Computer Modelling

All structures were constructed in Avogadro¹⁵⁶ and subsequently energy-minimized in vacuum using the conjugate gradient method as implemented in NAMD.¹⁵⁷ The minimization procedure was carried out for 10,000 steps, at which point the fluctuations in the energy were $< 10^{-4}$ kcal/mol and the structure was considered to be converged. The CHARMM c36a3 force field¹⁵⁸ was used to minimize the structure. VMD¹⁵⁹ was used to visualize the results.

8.2 Methods and Materials associated with the comparative study of thermolysin catalysed self-assembly of Fmoc-SF-OMe, Fmoc-SL-OMe, Fmoc-TF-OMe and Fmoc-TL-OMe (discussed in Chapter 4.0)

8.2.1 Thermolysin catalysed condensation of amino acid fragments

The Fmoc-amino acid (Fmoc-S-OH from Sigma-Aldrich, Fmoc-T-OH from Bachem) and amino acid-methyl ester (F-OMe and L-OMe as hydrochloride salts from Sigma-Aldrich) were mixed at a 20:80 mM ratio in a glass vial. The mixture was suspended in 2.0 mL of 0.1 M pH 8 sodium phosphate buffer with the addition of the 1 mg ml⁻¹ lyophilised *thermolysin* powder (*bacillus Thermoproteolyticus rokko* from Sigma-Aldrich, batch 079K1706, mol wt 34.6 kDa by amino acid sequence). The mixture was vortex mixed for 10 seconds and sonicated for 1 minute to ensure dissolution. Samples were incubated at room temperature for 24 hours before analysis unless otherwise stated.

8.2.2 Monitoring the conversion of amino acid fragments to Fmoc-dipeptide using HPLC

Aliquots of each sample (25 μ L) were diluted to 500 μ L with 50 % acetonitrile (Sigma-Aldrich) solution in water containing 0.1 % trifluoroacetic acid (Sigma-Aldrich). Then, an aliquot (10 μ L) of sample was injected on a Dionex P680 system operating with a Macherey-Nagel 250 Å, 4.6 \times 250 mm, C18 column was used for reversed phase HPLC. The mobile phase was comprised of water and acetonitrile ramped from 20 – 80 % over 35 minutes at a flow rate of 1 mL min⁻¹. Detection of the Fmoc- peptide amphiphiles was carried out using a UVD170U UV-Vis detector at a 300 nm wavelength.

8.2.3 Fluorescence Spectroscopy

2 mL samples were prepared in a 1 cm² quartz cuvette. Fluorescence emission spectra were measured on a Jasco FP-6500 spectrofluorometer at a scanning speed of 200 nm min⁻¹. The emission spectra were recorded between 300 and 600 nm resulting from excitation at 280 nm, using a bandwidth of 3 nm with a medium response and a 1 nm data pitch. Spectra were normalised to maximum intensity.

8.2.4 FTIR Spectroscopy

FTIR spectra were acquired using a Bruker Vertex spectrometer with a spectral resolution of 2 cm⁻¹. The spectra were obtained by averaging 64 interferograms for each sample. Measurements were performed in a standard IR cuvette (Harrick Scientific), in which the sample was contained between two CaF₂ windows (thickness, 2 mm) separated by a 10 μm PTFE spacer. All sample manipulations were performed in a glove box to minimize interference from atmospheric water vapour; D₂O (Sigma-Aldrich) was used as the solvent for all the infrared spectral measurements.

8.2.5 TEM

Carbon-coated copper grids (200 mesh) were glow discharged in air for 30 seconds. The support film was touched onto the gel surface for 3 seconds and blotted down using filter paper. Negative stain (20 μL, 1 % aqueous methylamine vanadate obtained from Nanovan; Nanoprobes) was applied and the mixture blotted again using filter paper to remove excess. The dried specimens were then imaged using a LEO 912 energy filtering transmission electron microscope operating at 120kV fitted with 14 bit/2 K Proscan CCD camera.

8.2.6 CryoTEM

Gel samples were blotted onto a thin film grid of 100 – 200 nm. The grid was then plunged into liquid ethane (temperatures below -170 °C) and transferred to a GATAN 626

cryoholder and imaged using a JEOL 2100 transmission electron microscope fitted with a GATAN 4 K Ultrascan camera.

8.2.7 WAXS

WAXS analyses were performed on a PANalytical X'Pert Pro X-ray powder diffractometer, equipped with a copper K α source (wavelength 1.54 Å). Measurements were performed in reflection mode on an Al plate, revolving at 1 Hz, applying scans from Bragg angles of 1.5° - 30°. An aliquot (500 μ L) of wet sample was spread on an aluminium plate as a film and allowed to air dry prior to data collection.

8.2.8 Rheometry

Rheological properties were assessed using an Anton Paar Physica MCR 101 rheometer with temperature controlled at 20 °C using a 10 mm vane geometry. Gel formation was monitored by measuring G' and G'' at constant 1 rad s⁻¹ frequency and 0.1 % strain every 0.1 minutes over 10 hours. Viscometry measurements were taken by monitoring the viscosity and shear stress over controlled shear rates from 1 - 100 s⁻¹. The dynamic moduli of the hydrogel were measured as a function of frequency in the range of 0.1 – 100 rad s⁻¹ with constant strain value. To ensure the measurements were made in the linear viscoelastic regime, amplitude sweeps were performed at constant frequency of 1 rad s⁻¹, from shear strain 0.01 – 100 %, where no variation in G' or G'' was observed up to a strain of 0.2 % for Fmoc-SL-OMe, and 0.4 % for Fmoc-TF-OMe and Fmoc-TL-OMe.

8.2.9 Computer modeling

All structures were constructed in ArgusLab.¹⁵⁶ VMD¹⁵⁹ was used to visualize the results and to solvate the stack in a rectangular TIP3P water box with a 9 Å water layer on all sides. The structure was subsequently energy-minimized using the conjugate gradient method as implemented in NAMD.¹⁵⁷ The minimization procedure was carried out for 10,000 steps, at which point the fluctuations in the energy were <10⁻⁴ kcal mol⁻¹ and the structure was

considered to be converged. The CHARMM c36a3 force field¹⁵⁸ was used to minimize the structure.

8.3 Methods and Materials associated with the comparative study of subtilisin catalysed self-assembly of Fmoc-YT-OH, Fmoc-YS-OH, Fmoc-YN-OH and Fmoc-YQ-OH (discussed in Chapter 5.0)

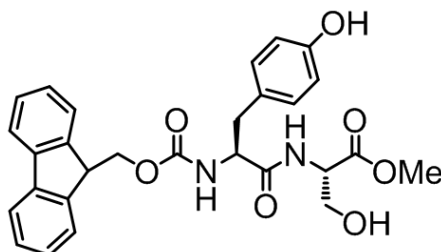
8.3.1 General reagents and analytical methods used in the synthesis of non-assembling precursors

All commercial reagents were used as supplied. Thin layer chromatography (TLC) was performed on aluminium sheets coated with 60 F₂₅₄ silica. Sheets were visualised using a UV light source (254 nm). Low resolution mass spectra (LRMS, *m/z*) were recorded on a Finnigan LCQ duo using electrospray (ES) detection. High resolution mass spectra (HRMS) were recorded on a Thermo Electron Exactive. ¹H and ¹³C nuclear magnetic resonance (NMR) spectra were recorded on Bruker AV500 spectrometer (¹H: 500 MHz and ¹³C: 125 MHz) in the deuterated solvent stated and interpreted with the aid of COSY spectra. ¹³C multiplicities were assigned using a DEPT sequence. All chemical shifts (δ) are quoted in ppm and coupling constants (*J*) given in Hz. Residual signals from the solvents were used as an internal reference. Elemental analysis (CHN) was performed on a Perkin Elmer 2400 Series 2 CHNS analyser. HPLC was carried out by injecting an aliquot (10 μ L) of sample on a Dionex P680 system operating with a Macherey-Nagel 250 Å, 4.6 \times 250 mm, C18 column for reversed phase HPLC. The mobile phase was comprised of water and acetonitrile ramped from 20 – 80 % ACN over 35 minutes at a flow rate of 1 mL min⁻¹. Detection of the Fmoc- peptide amphiphiles was carried out using a UVD170U UV-Vis detector at a 300 nm wavelength.

8.3.2 Synthesis of Fmoc-YS-OMe

Fmoc-Y-OH (1 g, 2.48 mmol), S-OMe hydrochloride salt (0.463 g, 2.98 mmol), HBTU (0.941 g, 2.98 mmol) and DIPEA (1.08 mL, 6.2 mmol) were dissolved in anhydrous dimethylformamide (15 mL) and left to stir overnight. The dimethylformamide was removed by evaporation *in vacuo*. The resulting oil was dissolved in ethyl acetate (70 mL)

and washed with equal volumes of saturated sodium bicarbonate, brine, hydrochloric acid (1 M) and brine. The organic layer was then dried with magnesium sulphate. The ethyl acetate was then removed by evaporation *in vacuo*. The resulting solid was washed with diethyl ether to gain the product as a white powder (1.25 g, 89.7 %).

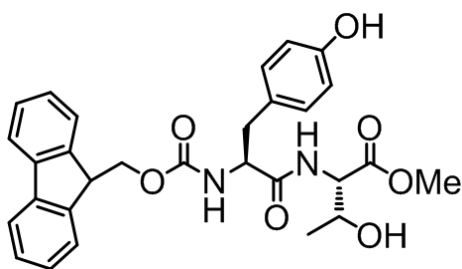


δ_{H} (DMSO, 500 MHz): 8.35 (1H, d, $J = 8.4$ Hz, Tyr NH), 7.86 (2H, d, $J = 7.6$ Hz, fluorenyl Ar CH), 7.65 – 7.61 (2H, m, fluorenyl Ar CH), 7.52 (1H, d, $J = 8.9$ Hz, Ser NH), 7.41 – 7.26 (2H, m, fluorenyl Ar CH), 7.32 – 7.26 (2H, m, fluorenyl Ar CH), 7.12 (2H, d, $J = 8.4$ Hz, Tyr Ar CH), 6.64 (2H, d, $J = 8.4$ Hz, Tyr Ar CH), 5.08 (1H, t, $J = 5.5$ Hz, Tyr OH), 4.39 – 4.36 (1H, m, Tyr C α H), 4.30 – 4.25 (1H, m, one Ser CH), 4.18 – 4.09 (4H, m, fluorenyl CH $_2$, fluorenyl CH, one Ser CH), 3.76 – 3.72 (1H, m, Ser C α H), 3.65 (1H, t, $J = 5.0$ Hz, Ser OH), 3.62 (3H, s, CH $_3$), 2.94 – 2.90 (1H, m, one Tyr CH), 2.68-2.63 (1H, m, one Tyr CH). δ_{C} (DMSO, 125 MHz): 172.5 (Tyr C=O), 171.4 (Ser C=O), 156.2 (fluorenyl C=O), 144.3 (Tyr C $_q$), 144.2 (fluorenyl C $_q$), 141.1 (fluorenyl C $_q$), 130.6 (Tyr Ar CH), 128.6 (Tyr C $_q$), 128.0 (fluorenyl Ar CH), 127.5 (fluorenyl Ar CH), 125.7 (fluorenyl Ar CH), 120.5 (fluorenyl Ar CH), 115.2 (Tyr Ar CH), 66.1 (fluorenyl CH $_2$), 61.7 (Ser CH $_2$), 56.6 (Tyr C α), 55.1 (Ser C α), 52.3 (CH $_3$), 47.0 (fluorenyl CH), 37.1 (Tyr CH $_2$). MS (ES $^+$): m/z 527, [M + Na] $^+$. HRMS for C $_{28}$ H $_{29}$ O $_7$ N $_2$: expected 505.1975, found 505.1969. HPLC: > 99 % pure by HPLC analysis. Elemental analysis for C $_{28}$ H $_{29}$ O $_7$ N $_2$: expected C: 66.66 %, H: 5.59 %, N: 5.55 %; found C: 65.68 %, H: 5.40 %, N: 5.43 %.

8.3.3 Synthesis of Fmoc-YT-OMe

Fmoc-Y-OH (0.5 g, 1.24 mmol), T-OMe hydrochloride salt(0.252 g, 1.489 mmol), HBTU (0.564 g, 1.489 mmol) and DIPEA (539 μ L, 3.1 mmol) were dissolved in anhydrous dimethylformamide (15 mL) and left to stir overnight. The dimethylformamide was removed by evaporation *in vacuo*. The resulting mixture was dissolved in ethyl acetate (40 mL) and washed with equal volumes of saturated sodium bicarbonate, brine, hydrochloric acid (1 M) and brine. The organic layer was then dried with magnesium sulphate. The ethyl

acetate was then removed by evaporation *in vacuo*. The resulting solid was washed with diethyl ether to gain the product as a white powder (0.604 g, 94.0 %).

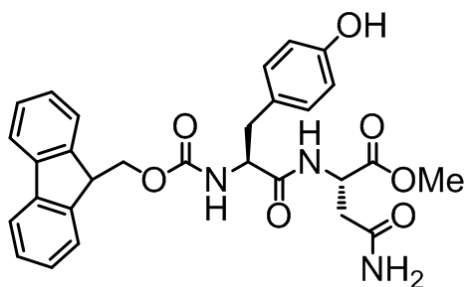


δ_{H} (DMSO, 500 MHz): 8.05 (1H, d, $J = 8.4$ Hz, Tyr NH), 7.86 (2H, d, $J = 7.5$ Hz, fluorenyl Ar CH), 7.64 – 7.57 (3H, m, fluorenyl Ar CH, Thr NH), 7.41 – 7.37 (2H, m, fluorenyl Ar CH), 7.32 – 7.26 (2H, m, fluorenyl Ar CH), 7.13 (2H, d, $J = 8.4$ Hz, Tyr Ar CH), 6.66 (2H, d, $J = 8.4$ Hz, Tyr Ar CH), 5.02 (1H, d, $J = 5.3$ Hz, Tyr OH), 4.34 – 4.30 (2H, m, Tyr C_{α} H, Thr CH), 4.18 – 4.10 (4H, m, fluorenyl CH_2 , fluorenyl CH, thr C_{α} H), 3.61 (3H, s, methyl ester CH_3), 2.95 – 2.92 (1H, m, one Tyr CH), 2.68 – 2.63 (1H, m, one Tyr CH), 1.06 (3H, d, $J = 6.3$ Hz, Thr CH_3). δ_{C} (DMSO, 125 MHz): 172.8 (Tyr C=O), 171.5 (Thr C=O), 156.2 (fluorenyl C=O), 144.2 (Tyr C_{α}), 144.1 (fluorenyl C_{α}), 141.1 (fluorenyl C_{α}), 130.6 (Tyr Ar CH), 128.6 (Tyr C_{α}), 128.0 (fluorenyl Ar CH), 127.5 (fluorenyl Ar CH), 125.7 (fluorenyl Ar CH), 120.5 (fluorenyl Ar CH), 115.2 (Tyr Ar CH), 66.6 (Thr CH), 66.1 (fluorenyl CH_2), 58.2 (Thr C_{α}), 56.8 (Tyr C_{α}), 52.2 (methyl ester CH_3), 47.0 (fluorenyl CH), 37.0 (Tyr CH_2), 20.6 (Thr CH_3). MS (ES⁺): m/z 541, $[\text{M} + \text{Na}]^+$. HRMS for $\text{C}_{29}\text{H}_{31}\text{O}_7\text{N}_2$: expected 519.2131, found 519.2126. HPLC: > 99 % pure by HPLC analysis. Elemental analysis for $\text{C}_{29}\text{H}_{31}\text{O}_7\text{N}_2$: expected C: 67.17 %, H: 5.83 %, N: 5.40 %; found C: 65.39 %, H: 5.69 %, N: 5.29 %.

8.3.4 Synthesis of Fmoc-YN-OMe

N(Trt)-OH (1 g, 2.67 mmol) was dissolved in methanol (25 mL). The reaction mixture was cooled to 0 °C followed by the drop-wise addition of thionyl chloride (0.968 mL, 0.014 mol). The reaction was allowed to warm to room temperature and then stirred overnight. The solvent was removed by evaporation *in vacuo*, remaining thionyl chloride was removed by the addition of diethyl ether and further evaporation. TLC analysis (5:95 v:v methanol: chloroform) of the isolated product N(Trt)-OMe indicated the presence of one spot (R_f 0.29) which was used without further purification. Fmoc-Y-OH (0.5 g, 1.24 mmol), N(Trt)-OMe

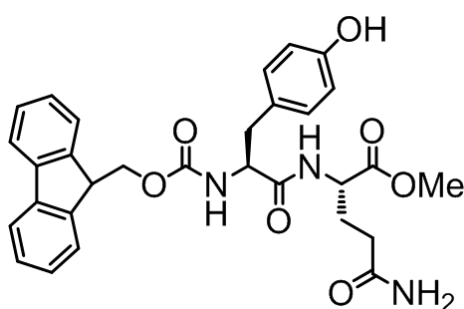
(0.579 g, 1.489 mmol), HBTU (0.565 g, 1.489 mmol) and DIPEA (539 μ L, 3.1 mmol) were dissolved in anhydrous dimethylformamide (15 mL) and left to stir overnight. The dimethylformamide was removed by evaporation *in vacuo*. The resulting mixture was dissolved in ethyl acetate (40 mL) and washed with equal volumes of saturated sodium bicarbonate, brine, hydrochloric acid (1 M) and brine. The organic layer was then dried with magnesium sulphate. The ethyl acetate was then removed by evaporation *in vacuo*. The resulting solid Fmoc-YN(Trt)-OMe was 95 % pure by HPLC analysis and was used without further purification. Fmoc-YN(Trt)-OMe (0.866 g, 1.2 mmol) was dissolved in 90:10 v:v trifluoroacetic acid: water (10 mL) and the reaction stirred overnight. The solvents were then removed by evaporation *in vacuo*, excess trifluoroacetic acid was removed by azeotropic distillation with toluene. The crude product was then recrystallised from diethyl ether. TLC analysis (10:90 v:v methanol: chloroform) of the isolated product indicated the presence of one spot (R_f 0.36), Fmoc-YN-OMe as an off-white solid (0.404 g, 68 %).



δ_H (DMSO, 500 MHz): 8.35 (1H, d, $J = 7.3$ Hz, NH), 7.86 (2H, d, $J = 7.5$ Hz, fluorenyl Ar CH), 7.65 – 7.61 (2H, m, fluorenyl Ar CH), 7.53 (1H, d, $J = 8.8$ Hz, NH), 7.41 - 7.38 (3H, m, fluorenyl Ar CH, one Asn NH), 7.32 – 7.27 (2H, m, fluorenyl Ar CH), 7.32 – 7.27 (2H, m, fluorenyl Ar CH), 7.08 (2H, d, $J = 8.3$ Hz, Tyr Ar CH), 6.92 (1H, s, one Asn NH), 6.62 (2H, d, $J = 8.3$ Hz, Tyr Ar CH), 4.63 – 4.59 (1H, m, Tyr C_{α} H), 4.21 – 4.09 (4H, m, Asn C_{α} H, fluorenyl CH_2 , fluorenyl CH), 3.58 (3H, s, CH_3), 2.93 – 2.86 (1H, s, one Tyr CH), 2.66 – 2.52 (3H, m, one Tyr CH, Asn CH_2). δ_C (DMSO, 125 MHz): 172.0 (Asn side chain C=O), 172.1 (Tyr C=O), 171.2 (Asn C=O), 156.1 (fluorenyl C=O), 144.2 (Tyr C_q), 144.1 (fluorenyl C_q), 141.1 (fluorenyl C_q), 130.6 (Tyr Ar CH), 128.5 (Tyr C_q), 128.0 (fluorenyl Ar CH), 127.5 (fluorenyl Ar CH), 125.8 (fluorenyl Ar CH), 120.5 (fluorenyl Ar CH), 115.2 (Tyr Ar CH), 66.1 (fluorenyl CH_2), 56.7 (Tyr C_{α}), 52.3 (CH_3), 49.1 (Asn C_{α}), 47.0 (fluorenyl CH), 37.1 (Tyr CH_2), 37.0 (Asn CH_2). MS (ES⁺): m/z 532, $[M + H]^+$. HRMS for $C_{29}H_{30}O_7N_3$: expected 532.2084, found 532.2078. HPLC: >95 % pure by HPLC analysis. Elemental analysis for $C_{29}H_{30}O_7N_3$: expected C: 65.53 %, H: 5.50 %, N: 7.91 %; found C: 62.85 %, H: 5.40 %, N: 7.53 %.

8.3.4 Synthesis of Fmoc-YQ-OMe

Q(Trt)-OH (1 g, 2.57 mmol) was dissolved in methanol (25 mL). The reaction mixture was cooled to 0 °C followed by the drop-wise addition of thionyl chloride (0.932 mL, 0.013 mol). The reaction was allowed to warm to room temperature and then stirred overnight. The solvent was removed by evaporation in vacuo, remaining thionyl chloride was removed by the addition of diethyl ether and further evaporation. TLC analysis (5:95 v:v methanol: chloroform) of the isolated product Q(Trt)-OMe indicated the presence of one spot (R_f 0.18) which was used without further purification. Fmoc-Y-OH (0.5 g, 1.24 mmol), Q(Trt)-OMe (0.600 g, 1.489 mmol), HBTU (0.565 g, 1.489 mmol) and DIPEA (539 μ L, 3.1 mmol) were dissolved in anhydrous dimethylformamide (15 mL) and left to stir overnight. The dimethylformamide was removed by evaporation *in vacuo*. The resulting mixture was dissolved in ethyl acetate (40 mL) and washed with equal volumes of saturated sodium bicarbonate, brine, hydrochloric acid (1 M) and brine. The organic layer was then dried with magnesium sulphate. The ethyl acetate was then removed by evaporation *in vacuo*. The resulting solid Fmoc-YQ(Trt)-OMe was 96 % pure by HPLC analysis and was used without further purification. Fmoc-YQ(Trt)-OMe (0.712 g) was dissolved in 90:10 v:v trifluoroacetic acid: water (10 mL) and the reaction stirred overnight. The solvents were then removed by evaporation in vacuo, excess trifluoroacetic acid was removed by azeotropic distillation with toluene. The crude product was then recrystallised from diethyl ether. Fmoc-YQ-OMe was a white solid (0.343 g, 70 %).



δ_H (DMSO, 500 MHz): 8.41 (1H, d, $J = 7.3$ Hz, NH), 7.86 (2H, d, $J = 7.5$ Hz, fluorenyl Ar CH), 7.65 – 7.61 (2H, m, fluorenyl Ar CH), 7.50 (1H, d, $J = 8.7$ Hz, NH), 7.42 – 7.38 (2H, m, fluorenyl Ar CH), 7.32 – 7.25 (3H, m, fluorenyl Ar CH, one Gln NH), 7.09 (2H, d, $J = 8.4$ Hz, Tyr Ar CH), 6.77 (1H, s, one Gln NH), 6.64 (2H, d, $J = 8.4$ Hz, Tyr Ar CH), 4.25 – 4.08 (5H, m, fluorenyl CH_2 , fluorenyl CH, Tyr C_α , Gln C_α), 3.61 (3H, s, CH_3), 2.94 – 2.87 (1H, m, one Tyr CH), 2.67 – 2.62 (1H, m, one Tyr CH), 2.16 – 2.13 (2H, t, $J = 7.9$ Hz, Gln CH_2), 1.99 – 1.93 (1H,

m, one Gln CH), 1.84 – 1.79 (1H, m, one Gln CH). δ_c (DMSO, 125 MHz): 173.7 (Gln side chain C=O), 172.7 (Gln C=O), 172.5 (Tyr C=O), 156.2 (fluorenyl C=O), 144.3 (Tyr C_q), 144.2 (fluorenyl C_q), 141.1 (fluorenyl C_q), 130.6 (Tyr Ar CH), 128.6 (Tyr C_q), 128.0 (fluorenyl Ar CH), 127.5 (fluorenyl Ar CH), 125.8 (fluorenyl Ar CH), 120.5 (fluorenyl Ar CH), 115.3 (Tyr Ar CH), 66.1 (fluorenyl CH₂), 56.6 (Tyr C_α), 52.3 (Gln C_α), 52.1 (CH₃), 47.0 (fluorenyl CH₂), 37.1 (Tyr CH₂), 31.5 (Gln CH₂), 27.0 (Gln CH₂). MS (ES+): m/z 568, [M + Na]⁺. HRMS for C₃₀H₃₂O₇N₃: expected 546.2240, found 546.2235. HPLC: >96 % pure by HPLC analysis. Elemental analysis for C₃₀H₃₂O₇N₃: expected C: 64.04 %, H: 5.73 %, N: 7.10 %; found C: 64.19 %, H: 5.77 %, N: 7.10 %.

8.3.5 Subtilisin catalysed hydrolysis of Fmoc-peptide methyl ester protected starting materials

To Fmoc-YX-OMe (10 mM) subtilisin from *Bacillus licheniformis* (20 μL) (Sigma-Aldrich, batch 056K1213) was added and the sample vortexed for approximately one minute to form a pellet. Sodium phosphate buffer (1 mL, 0.1 M, pH 8) was added and the mixture was sonicated for 15 minutes. The sample was then heated at 55 °C for one hour and then cooled to 20 °C over a period of 210 minutes controlled using an oil bath. Samples were then allowed to rest at 20 °C for 24 hours before further analysis was carried out.

8.3.6 Reaction progress by HPLC

Aliquots of each sample (25 μL) were diluted to 500 μL with 50 % acetonitrile (Sigma-Aldrich) solution in water containing 0.1 % trifluoroacetic acid (Sigma-Aldrich). Then, an aliquot (10 μL) of sample was injected on a Dionex P680 system operating with a Macherey-Nagel 250 Å, 4.6 × 250 mm, C18 column was used for reversed phase HPLC. The mobile phase was comprised of water and acetonitrile ramped from 20 – 80 % ACN over 35 minutes at a flow rate of 1 mL min⁻¹. Detection of the Fmoc- peptide amphiphiles was carried out using a UVD170U UV-Vis detector at a 300 nm wavelength.

8.3.7 Fluorescence spectroscopy

Fluorescence emission spectra were recorded from 300-600 nm, exciting at 295 nm, using slit settings of 3 nm, medium sensitivity and a scan speed of 500 nm min⁻¹, on a Jasco FP-6500 spectrofluorimeter. Samples were prepared in PMMA cuvettes (from Fisher Scientific). Experimental data was acquired in triplicate and the average data shown.

8.3.8 Circular dichroism

Circular dichroism (CD) spectra were measured on a Jasco J600 spectropolarimeter in a 0.1 mm pathlength cylindrical cell, with 1 s integration, step resolution of 1 nm, response of 0.5 s, bandwidth of 1 nm and slit width of 1 mm. Samples were added to the cell using a pipette. Experimental data was acquired in triplicate and the average data shown.

8.3.9 Infra-red spectroscopy

FTIR spectra were acquired using a Bruker Vertex spectrometer with a spectral resolution of 2 cm⁻¹. The spectra were obtained by averaging 32 interferograms for each sample. Measurements were performed in a standard IR cuvette (Harrick Scientific), in which the sample was contained between two CaF₂ windows (thickness, 2 mm) separated by a 25 μm PTFE spacer. All sample manipulations were performed in a glove box to minimize interference from atmospheric water vapour; D₂O (Sigma-Aldrich) was used as the solvent for all the infrared spectral measurements.

8.3.10 Rheology

Rheological properties were assessed using an Malvern Kinexus rheometer with temperature controlled at 20 °C using a 20 mm parallel plate geometry with a gap of 0.9 mm. Viscometry measurements were taken by monitoring the viscosity and shear stress over controlled shear rates from 0.1 - 100 s⁻¹. The dynamic moduli of the hydrogel were measured as a function of frequency in the range of 0.1 – 100 rad s⁻¹ with constant strain value. To ensure the measurements were made in the linear viscoelastic regime, amplitude

sweeps were performed at constant frequency of 1 Hz, from shear strain 0.01 – 100 %, where no variation in G' or G'' was observed up to a strain of 0.8 % for Fmoc-YS-OMe, and 0.4 % for Fmoc-YN-OMe (see supporting information). Experimental data was acquired in triplicate and the average data shown.

8.3.11 Transmission electron microscopy

Carbon-coated copper grids (200 mesh) were glow discharged in air for 30 seconds. The support film was touched onto the gel surface for 3 seconds and blotted down using filter paper. Negative stain (20 μ L, 1 % aqueous methylamine vanadate obtained from Nanovan; Nanoprobes) was applied and the mixture blotted again using filter paper to remove excess. The dried specimens were then imaged using a LEO 912 energy filtering transmission electron microscope operating at 120kV fitted with 14 bit/2 K Proscan CCD camera.

8.3.12 Dynamic light scattering

Dynamic Light Scattering was performed on an AVL/LSE-5004 light scattering electronics and multiple tau digital correlator. 3 mL of sample was transferred into glass tubes and analysed using a 3 DDLS instrument at a temperature of 25 °C, with an angle of 20 °, 90 ° and 120 °. Dynamic light scattering experiments records intensity autocorrelation functions $g_2(\tau)-1$. The autocorrelation functions were analyzed by means of the cumulant method in order to determine the initial decay rate and the corresponding average apparent diffusion coefficient D . The decay of the autocorrelation function was modeled as $g_1(\tau) = (g_2(\tau)-1)^{1/2} = \exp(-\Gamma \tau)$, where Γ is the decay rate ($\Gamma = D Q^2$), $Q = (4\pi n/\lambda)\sin(\theta/2)$ is the scattering vector magnitude, n is the refractive index of the solvent and λ is the wavelength of the laser. The average hydrodynamic radius r_H can be calculated from the Stokes-Einstein equation, $r_H = k_B T / 6\pi\eta D$, where k_B is the Boltzmann constant, T is the absolute temperature and η is the solvent viscosity at the given temperature.

8.3.13 Heat/Cool Cycles

Samples were heated to 55 °C for 1 hour, and then cooled to 20 °C over 3.5 hours. Samples were allowed to stand at room temperature for 24 hours prior to analysis. This process was repeated until the samples reached a constant value was reached for the peak ratio of 450 nm:320 nm monitored using fluorescence.

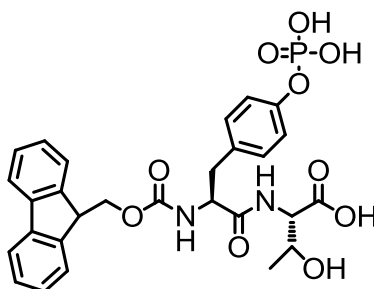
8.4 Methods and materials associated with the comparative *In vivo* studies of alkaline phosphatase catalysed self-assembly of aromatic peptide amphiphiles (discussed in Chapter 6.0).

All commercial reagents were used as supplied. Thin layer chromatography (TLC) was performed on aluminium sheets coated with 60 F₂₅₄ silica. Sheets were visualised using a UV light source (254 nm). ¹H and ¹³C nuclear magnetic resonance (NMR) spectra were recorded on Bruker AV500 spectrometer (¹H: 500 MHz and ¹³C: 125 MHz) in the deuterated solvent stated and interpreted with the aid of COSY spectra. ¹³C multiplicities were assigned using a DEPT sequence. All chemical shifts (δ) are quoted in ppm and coupling constants (J) given in Hz. Residual signals from the solvents were used as an internal reference. HPLC was carried out by injecting an aliquot (10 μ L) of sample on a Dionex P680 system operating with a Macherey-Nagel 250 Å, 4.6 \times 250 mm, C18 column for reversed phase HPLC. The mobile phase was comprised of water and acetonitrile ramped from 20 – 80 % ACN over 35 minutes at a flow rate of 1 mL min⁻¹. Detection of the Fmoc- peptide amphiphiles was carried out using a UVD170U UV-Vis detector at a 300 nm wavelength.

8.4.1 Synthesis of Fmoc-YpT-OH

Fmoc-Tyr(PO(NME₂)₂)-OH (0.5 g, 0.93 mmol), H-Thr(tBu)-OtBu (0.257 g, 1.11 mmol), HBTU (0.423 g, 1.11 mmol) and DIPEA (420 μ L, 2.3 mmol) were dissolved in anhydrous dimethylformamide (15 mL) and left to stir overnight. The dimethylformamide was removed by evaporation *in vacuo*. The resulting mixture was dissolved in ethyl acetate (50 mL) and washed with equal volumes of saturated sodium bicarbonate, brine, hydrochloric acid (1 M) and brine. The organic layer was then dried with magnesium sulphate. The ethyl acetate was then removed by evaporation *in vacuo*. The resulting solid was purified by

column chromatography using 20:1 chloroform/methanol mixture as eluent (yield is 0.660 g, 94 %). Then the deprotection of t-Bu and PO(NME₂)₂ groups were done by the overnight reaction of with 10 mL trifluoroacetic acid followed by addition of 1 mL of water and again an overnight stirring. The TFA and water was then removed by evaporation *in vacuo*. The excess TFA was removed by dissolving the solid in toluene followed by evaporation as azeotropic mixture. The resulting solid was washed with diethyl ether to gain the product as a white powder (yield is 0.42 g, 82 %).

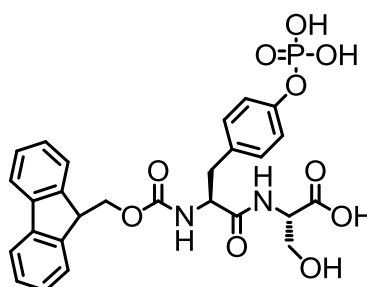


δ_{H} (DMSO, 400 MHz): 8.84 (3H, s, OPO₃H₂ and COOH), 7.98 (1H, d, $J = 9.2$ Hz, Tyr NH), 7.94 (2H, d, $J = 7.2$ Hz, fluorenyl Ar CH), 7.73 – 7.72 (3H, m, fluorenyl Ar CH, Thr NH), 7.48 – 7.45 (2H, m, fluorenyl Ar CH), 7.40 – 7.35 (2H, m, fluorenyl Ar CH), 7.3 (2H, d, $J = 8.4$ Hz, Tyr Ar CH), 7.1 (2H, d, $J = 8.4$ Hz, Tyr Ar CH), 4.48 – 4.42 (1H, m, Tyr C _{α} H), 4.29 – 4.24 (5H, m, fluorenyl CH₂, fluorenyl CH, Thr CH, thr C _{α} H), 3.07 – 3.04 (1H, m, one Tyr CH), 2.86 – 2.8 (1H, m, one Tyr CH), 1.1 (3H, d, $J = 6$ Hz, Thr CH₃). δ_{C} (DMSO, 100 MHz): 172.1 (Tyr C=O), 171.9 (Thr C=O), 155.7 (fluorenyl C=O), 143.8 (Tyr C _{q}), 143.7 (fluorenyl C _{q}), 140.6 (fluorenyl C _{q}), 129.9 (Tyr Ar CH), 129.8 (Tyr C _{q}), 127.6 (fluorenyl Ar CH), 127.1 (fluorenyl Ar CH), 125.3 (fluorenyl Ar CH), 120.0 (fluorenyl Ar CH), 119.8 (Tyr Ar CH), 66.2 (Thr CH), 65.6 (fluorenyl CH₂), 57.6 (Thr C _{α}), 56.2 (Tyr C _{α}), 46.4 (fluorenyl CH), 36.6 (Tyr CH₂), 20.3 (Thr CH₃). Purity by HPLC: 96 %.

8.4.2 Synthesis of Fmoc-YpS-OH

Fmoc-Tyr(PO(NME₂)₂)-OH (0.5 g, 0.93 mmol), H-Ser(tBu)-OtBu (0.242 g, 1.11 mmol), HBTU (0.423 g, 1.11 mmol) and DIPEA (420 μ L, 2.3 mmol) were dissolved in anhydrous dimethylformamide (15 mL) and left to stir overnight. The dimethylformamide was removed by evaporation *in vacuo*. The resulting mixture was dissolved in ethyl acetate (50 mL) and washed with equal volumes of saturated sodium bicarbonate, brine, hydrochloric

acid (1 M) and brine. The organic layer was then dried with magnesium sulphate. The ethyl acetate was then removed by evaporation *in vacuo*. The resulting solid was purified by column chromatography using 20:1 chloroform/methanol mixture as eluent (yield is 0.670 g, 93 %). Then the deprotection of t-Bu and PO(NME₂)₂ groups were done by the overnight reaction of with 10 mL trifluoroacetic acid followed by addition of 1 mL of water and again an overnight stirring. The TFA and water was then removed by evaporation *in vacuo*. The excess TFA was removed by dissolving the solid in toluene followed by evaporation as azeotropic mixture. The resulting solid was washed with diethyl ether to gain the product as a white powder (yield is 0.45 g, 86 %).

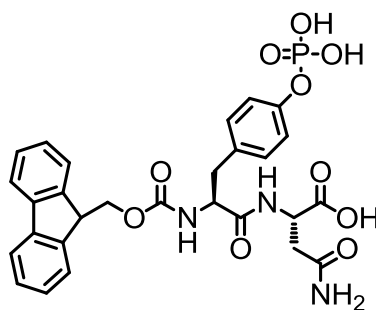


δ_{H} (DMSO, 400 MHz): 8.7 (3H, s, OPO₃H₂ and COOH), 8.31 (1H, d, $J = 7.6$ Hz, Tyr NH), 7.94 (2H, d, $J = 7.6$ Hz, fluorenyl Ar CH), 7.75 – 7.72 (2H, m, fluorenyl Ar CH), 7.68 – 7.66 (1H, d, $J = 8.4$ Hz, Ser NH), 7.47 – 7.45 (2H, m, fluorenyl Ar CH), 7.40 – 7.35 (2H, m, fluorenyl Ar CH), 7.31 (2H, d, $J = 8.4$ Hz, Tyr Ar CH), 7.11 (2H, d, $J = 8.4$ Hz, Tyr Ar CH), 4.41 – 4.34 (2H, m, Tyr C α H, Ser C α H), 4.28 – 4.22 (3H, m, fluorenyl CH₂, fluorenyl CH), 3.86 – 3.77 (1H, m, one Ser CH₂), 3.72 – 3.68 (1H, m, one Ser CH₂), 3.07 – 3.03 (1H, m, one Tyr CH), 2.85 – 2.78 (1H, m, one Tyr CH). δ_{C} (DMSO, 100 MHz): 172.1 (Tyr C=O), 171.7 (Thr C=O), 155.8 (fluorenyl C=O), 143.8 (Tyr C $_q$), 143.7 (fluorenyl C $_q$), 140.6 (fluorenyl C $_q$), 129.9 (Tyr Ar CH), 129.8 (Tyr C $_q$), 127.6 (fluorenyl Ar CH), 127.1 (fluorenyl Ar CH), 125.4 (fluorenyl Ar CH), 120.1 (fluorenyl Ar CH), 119.76 (Tyr Ar CH), 65.7 (fluorenyl CH₂), 61.4 (Thr CH), 56.2 (Tyr C α), 54.7 (Ser C α), 46.6 (fluorenyl CH), 36.8 (Tyr CH₂). Purity by HPLC: 98 %.

8.4.3 Synthesis of Fmoc-YpN-OH

Fmoc-Tyr(PO(NME₂)₂)-OH (0.5 g, 0.93 mmol), H-Asn-OtBu hydrochloride salt (0.250 g, 1.11 mmol), HBTU (0.423 g, 1.11 mmol) and DIPEA (420 μ L, 2.3 mmol) were dissolved in anhydrous dimethylformamide (15 mL) and left to stir overnight. The dimethylformamide

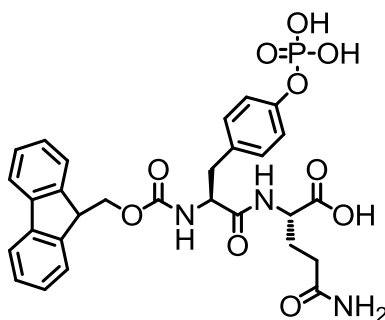
was removed by evaporation *in vacuo*. The resulting mixture was dissolved in ethyl acetate (50 mL) and washed with equal volumes of saturated sodium bicarbonate, brine, hydrochloric acid (1 M) and brine. The organic layer was then dried with magnesium sulphate. The ethyl acetate was then removed by evaporation *in vacuo*. The resulting solid was purified by column chromatography using 20:1 chloroform/methanol mixture as eluent (yield is 0.620 g, 88 %). Then the deprotection of t-Bu and PO(NME₂)₂ groups were done by the overnight reaction of with 10 mL trifluoroacetic acid followed by addition of 1 mL of water and again an overnight stirring. The TFA and water was then removed by evaporation *in vacuo*. The excess TFA was removed by dissolving the solid in toluene followed by evaporation as azeotropic mixture. The resulting solid was washed with diethyl ether to gain the product as a white powder (yield is 0.410 g, 79 %).



δ_{H} (DMSO, 400 MHz): 8.6 (3H, s, OPO₃H₂ and COOH), 8.3 (1H, d, $J = 7.6$ Hz, Tyr NH), 7.9 (2H, d, $J = 7.6$ Hz, fluorenyl Ar CH), 7.71 – 7.67 (2H, m, fluorenyl Ar CH), 7.64 – 7.62 (1H, d, $J = 8.4$ Hz, Asn NH), 7.44 – 7.41 (3H, m, fluorenyl Ar CH, one Asn CONH₂), 7.36 – 7.3 (2H, m, fluorenyl Ar CH), 7.25 (2H, d, $J = 8.4$ Hz, Tyr Ar CH), 7.06 (2H, d, $J = 8.4$ Hz, Tyr Ar CH), 6.86 (1H, s, one Asn CONH₂), 4.59 – 4.54 (1H, m, Tyr C α H), 4.29 – 4.23 (1H, m, Asn C α H), 4.18 (3H, m, fluorenyl CH₂, fluorenyl CH), 3.0 – 2.96 (1H, m, one Tyr CH), 2.78 – 2.71 (1H, m, one Tyr CH). δ_{C} (DMSO, 100 MHz): 172.8 (Tyr C=O), 171.4 (Asn C=O), 171.1 (Asn CONH₂), 155.8 (fluorenyl C=O), 143.8 (Tyr C $_q$), 143.7 (fluorenyl C $_q$), 140.7 (fluorenyl C $_q$), 130.0 (Tyr Ar CH), 129.8 (Tyr C $_q$), 127.6 (fluorenyl Ar CH), 127.1 (fluorenyl Ar CH), 125.3 (fluorenyl Ar CH), 120.0 (fluorenyl Ar CH), 119.6 (Tyr Ar CH), 65.7 (fluorenyl CH₂), 56.1 (Tyr C α), 48.7 (Ser C α), 46.6 (fluorenyl CH), 36.7 (Tyr CH₂), 36.5 (Asn CH). Purity by HPLC: 96 %.

8.4.4 Synthesis of Fmoc-YpQ-OH

Fmoc-Tyr(PO(NME₂)₂)-OH (0.5 g, 0.93 mmol), H-Gln-OtBu hydrochloride salt (0.261 g, 1.11 mmol), HBTU (0.423 g, 1.11 mmol) and DIPEA (420 μ L, 2.3 mmol) were dissolved in anhydrous dimethylformamide (15 mL) and left to stir overnight. The dimethylformamide was removed by evaporation *in vacuo*. The resulting mixture was dissolved in ethyl acetate (50 mL) and washed with equal volumes of saturated sodium bicarbonate, brine, hydrochloric acid (1 M) and brine. The organic layer was then dried with magnesium sulphate. The ethyl acetate was then removed by evaporation *in vacuo*. The resulting solid was purified by column chromatography using 20:1 chloroform/methanol mixture as eluent (yield is 0.610 g, 90 %). Then the deprotection of t-Bu and PO(NME₂)₂ groups were done by the overnight reaction of with 10 mL trifluoroacetic acid followed by addition of 1 mL of water and again an overnight stirring. The TFA and water was then removed by evaporation *in vacuo*. The excess TFA was removed by dissolving the solid in toluene followed by evaporation as azeotropic mixture. The resulting solid was washed with diethyl ether to gain the product as a white powder (yield is 0.43 g, 83 %).



δ_{H} (DMSO, 300 MHz): 8.99 (3H, s, OPOH₂ and COOH), 8.19 (1H, d, $J = 7.6$ Hz, Tyr NH), 7.97 (2H, d, $J = 7.2$ Hz, fluorenyl Ar CH), 7.81 – 7.76 (2H, m, fluorenyl Ar CH), 7.67 (1H, d, $J = 8.4$ Hz, Gln NH), 7.52 – 7.49 (3H, m, fluorenyl Ar CH, one Gln CONH₂), 7.43 – 7.39 (2H, m, fluorenyl Ar CH), 7.24 (2H, d, $J = 8.4$ Hz, Tyr Ar CH), 7.11 (2H, d, $J = 8.4$ Hz, Tyr Ar CH), 6.86 (1H, s, one Gln CONH₂), 4.37 – 4.22 (5H, m, Tyr C_αH, Asn C_αH, fluorenyl CH₂, fluorenyl CH), 3.0 – 2.95 (1H, m, one Tyr CH), 2.9 – 2.84 (1H, m, one Tyr CH), 2.2 (2H, t, Gln CH₂), 2.06-1.97 (1H, m, one Gln CH₂), 1.88 - 1.81 (1H, m, one Gln CH₂). δ_{C} (DMSO, 100 MHz): 173.6 (Tyr C=O), 173.5 (Gln C=O), 171.4 (Asn CONH₂), 155.7 (fluorenyl C=O), 143.9 (Tyr C_q), 143.8 (fluorenyl C_q), 140.6 (fluorenyl C_q), 129.7 (Tyr Ar CH), 127.6 (fluorenyl Ar CH), 127.3 (Tyr C_q), 127.1 (fluorenyl Ar CH), 125.4 (fluorenyl Ar CH), 121.4 (fluorenyl Ar CH), 120.0 (Tyr Ar CH),

65.7 (fluorenyl CH₂), 56.3 (Tyr C_α), 51.8 (Ser C_α), 46.6 (fluorenyl CH), 37.0 (Tyr CH₂), 31.4 (Gln CH₂), 27.2 (Gln CH₂). Purity by HPLC: 97 %.

8.4.5 alkaline phosphatase catalysed dephosphorylation of phosphorylated Fmoc-dipeptide protected starting materials *in vitro*

10 mM of phosphorylated precursor (Fmoc-YpX-OH synthesised as discussed in 7.4.1 – 7.4.2, Fmoc-FYp-OH from CSbio) was dissolved in 0.5 mL of 0.6 M sodium phosphate buffer pH 8. 50 µL of alkaline phosphatase from bovine intestinal mucosa (Sigma-Aldrich, batch 1001084595) was added and the solution diluted to 1.0 mL in the same solvent. Samples were then allowed to stand at room temperature for 24 hours before further analysis was carried out.

8.4.6 Reaction progress by HPLC analysis (*in vitro* studies)

A Dionex P680 system operating with a Macherey-Nagel 250 Å, 4.6 x 250 mm, C18 column was used for reversed phase HPLC. 10 µL of sample was injected. The mobile phase was comprised of water and acetonitrile ramped from 20-80 % over 35 minutes at a flow rate of 1 mL min⁻¹. Detection of the peptide amphiphiles was carried out using a UVD170U UV-Vis detector at a 300 nm wavelength.

8.4.7 Fluorescence

Fluorescence emission spectra were measured on a Jasco FP-6500 spectrofluorometer with light measured orthogonally to the excitation light with a scanning speed of 200 nm min⁻¹. Excitation light at 280 nm and emission data range between 300 nm and 600 nm. The emission spectra were measured with a bandwidth of 3 nm with a medium response and a 1 nm data pitch. Spectra were normalised to maximum intensity.

8.4.8 Infra-Red Spectroscopy

FTIR spectra were acquired using a Bruker Vertex spectrometer with a spectral resolution of 2 cm^{-1} . The spectra were obtained by averaging 32 interferograms for each sample. Measurements were performed in a standard IR cuvette (Harrick Scientific), in which the sample was contained between two CaF_2 windows (thickness, 2 mm) separated by a $25\text{ }\mu\text{m}$ PTFE spacer. All sample manipulations were performed in a glove box to minimize interference from atmospheric water vapour; D_2O (Sigma-Aldrich) was used as the solvent for all the infrared spectral measurements.

8.4.9 Transmission electron microscopy (*in vitro* studies)

Carbon-coated copper grids (200 mesh) were glow discharged in air for 30 seconds. The support film was touched onto the gel surface for 3 seconds and blotted down using filter paper. Negative stain ($20\text{ }\mu\text{L}$, 1 % aqueous methylamine vanadate obtained from Nanovan; Nanoprobes) was applied and the mixture blotted again using filter paper to remove excess. The dried specimens were then imaged using a LEO 912 energy filtering transmission electron microscope operating at 120kV fitted with 14 bit/2 K Proscan CCD camera.

8.4.10 Preparation of the E.Coli MC-1000 stock solution

10.0024 g of LB broth (Sigma-Aldrich) dissolved in distilled water and diluted to 500 mL with the same solvent. The solution was then autoclaved at $121\text{ }^\circ\text{C}$ for 20 minutes to sterilise and cooled to room temperature. A 100 mL aliquot was then sampled into a sterilised conical flask. An inoculation loop was sterilised over an open flame, then cooled. The inoculation loop was then dipped into E.Coli MC-1000 (donated from Dr. Charles Knapp, Dept. of Civil Engineering, University of Strathclyde, stored at $-60\text{ }^\circ\text{C}$), and then immediately into the 100 mL LB broth. The flask was then incubated at $37\text{ }^\circ\text{C}$ for 24 hours at 150 rpm. Stock solution stored in fridge.

8.4.11 Preparation of Growth Medium

Two formulations of growth media were prepared (Medium A and Medium B), based on the recipes described by Csopek *et.al.*, where the inclusion of inosine was shown to promote the expression of alkaline phosphatase in Medium B.¹⁵⁰ Each of the Ingredients for a 5x stock solution of the culture medium were weighed into a 1 L flask, with the exception of glucose, and dissolved in approximately 500 mL of distilled water (see Table 8.1 and 8.2). All reagents were of analytical grade from commercial suppliers. The pH of the resulting solution was adjusted to pH 7.80 using hydrochloric acid (Sigma-Aldrich) and solutions then diluted to 1 L using distilled water. Note: glucose is added (sterile) into the solution after autoclaving as it will caramelize at elevated temperatures (see Section 8.4.12)

Medium A	Concentration	Mass per 1L (g)	Mass per 5L stock (g)
tris	0.12 M	14.5368	72.684
KCl	0.08 M	4.6752	23.376
NaCl	0.02 M	1492	7.46
KCl	0.02 M	1.0698	5.349
NH ₄ Cl	0.003 M	1.426	2.1306
Na ₂ SO ₄	0.001 M	0.20331	1.01655
MgCl ₂	2.0 x 10 ⁻⁴ M	0.0294	0.147
ZnCl ₂	2.0 x 10 ⁻⁵ M	2.7258 x 10 ⁻⁴	0.00136
Glucose	0.50%	5	25
Difco Bactopeptone	0.50%	5	25
Inosine	-	-	-

Table 8.1 – Composition of cell culture medium A.

Medium B	Concentration	Mass per 1L (g)	Mass per 5L stock (g)
tris	0.12 M	14.5368	72.684
KCl	0.08 M	4.6752	23.376
NaCl	0.02 M	1492	7.46
KCl	0.02 M	1.0698	5.349
NH ₄ Cl	0.003 M	1.426	2.1306
Na ₂ SO ₄	0.001 M	0.20331	1.01655
MgCl ₂	2.0 x 10 ⁻⁴ M	0.0294	0.147
ZnCl ₂	2.0 x 10 ⁻⁵ M	2.7258 x 10 ⁻⁴	0.00136
Glucose	0.50%	5	25
Difco Bactopeptone	0.50%	5	25

Table 8.2 - Composition of cell culture medium B.

8.4.12 Preparation of E.Coli MC-1000 Cultures

100mL the 5x stock medium solution (discussed in Section 7.4.11) was diluted to 500 mL with distilled water. Solutions were then autoclaved at 121 °C for 20 minutes, and cooled to room temperature. 5 mL of a 0.5 g/mL glucose solution was syringe filtered (0.2 µm pore size) into the Medium. 50 mL of medium was transferred into a sterile conical flask. An innoculation loop was sterilised over an open flame, then cooled. The inoculation loop was then dipped into E.Coli MC-1000 stock solution (see Section 7.4.10), and then immediately into the growth medium.

Samples were incubated at 37 °C, at 150 rpm.

8.4.13 E.Coli Growth Curves

At selected timepoints, 250 µL of the culture was sampled into a 96 well plate. The absorbance was monitored at 590 nm (as per Csopek *et al.*¹⁵⁰), on a BioTek Epoch spectrofluorimeter.

Controls prepared; (1) media with no bacteria, and; (2) positive *E. Coli* samples.

8.4.14 Alkaline Phosphatase Activity Assay

The E.Coli alkaline phosphatase activity was modified from the Worthington enzyme manual.¹⁵⁵ 1 mL of 1.5 M tris buffer (VWR) was added to 0.5 mL of 0.003M p-nitrophenyl phosphate (PNP) solution (sigma-aldrich). 0.05 mL of *E. Coli* culture was added and mixed. (A gradual change from a clear to yellow solution indicates active alkaline phosphatase). 250 µL of the solution was then transferred to a 96 well plate. The absorbance at 410 nm was monitored every minute over 10 minutes on a BioTek Epoch spectrofluorimeter to monitor the rate of production of p-nitrophenol.

Controls prepared; (1) absence of PNP; (2) absence of sample.

8.4.15 Sample preparation for HPLC monitoring the reaction progress *in vivo*

E.coli cultures were prepared in media 24 hours before sample preparation. 20 mL of culture was then transferred to a sterile centrifuge tube. 13 mg of Fmoc-Fyp-OH was then added, and incubated for 24 hours at 37 °C, 150 rpm. Samples were then centrifuged at 8000 rpm for 4 min.

Media Samples: The superlatent was then syringe filtered through a 0.2 µm pore sized filter. A 250 µL aliquot of the solution was then diluted to 500 µL using a 50 % solution of acetonitrile containing 0.1 % trifluoroacetic acid.

Cell Samples: The residue was then washed 3 times using 0.6 M phosphate buffer pH8, and all organic matter dissolved in 2 mL of acetonitrile. Again, the solution was syringe filtered through a 0.2 µm pore sized filter. A 25 µL aliquot of the solution was then diluted to 500 µL using a 50 % solution of acetonitrile containing 0.1 % trifluoroacetic acid.

Contents of samples and controls prepared are summarised in Table 8.3.

Sample Name	Contents		
	Media	E coli	Fmoc-Fyp-OH
A-	A	-	-
A- Fmoc-Fyp	A	-	✓
A+	A	✓	-
A+ Fmoc-Fyp	A	✓	✓
B-	B	-	-
B- Fmoc-Fyp	B	-	✓
B+	B	✓	-
B+ Fmoc-Fyp	B	✓	✓

Table 8.3 - Contents of each sample and control.

8.4.15 Reaction progress *in vivo* using HPLC

An aliquot (20 µL) of each sample was injected on a Dionex P680 system operating with a Macherey-Nagel 250 Å, 4.6 × 250 mm, C18 column was used for reversed phase HPLC. The mobile phase was comprised of water and acetonitrile ramped from 20 – 80 % over 35

minutes at a flow rate of 1 mL min⁻¹. Detection of the Fmoc- peptide amphiphiles was carried out using a UVD170U UV-Vis detector at a 300 nm wavelength.

8.4.15 Live/Dead® cell staining

Ecoli samples were grown in media (either A or B) over 24 hours, 37 °C, 150 rpm. A 20 mL sample was then treated with the 2×10^{-5} mols of Fmoc-dipeptide (approximately 13 mg) and incubated at 37 °C, 150 rpm, for 24 hours. Samples were then concentrated by centrifugation at 8000 rpm for 10 minutes and resuspended in 2 mL of 0.85 % NaCl in de-ionised water. 1 mL of the suspension was then added to 20 mL of 0.85 % NaCl solution and incubated at room temperature for 1 hour, mixing every 15 mins. The sample was then concentrated by centrifugation at 8000 rpm for 10 minutes, washed once with 20 mL 0.85 % NaCl solution, and resuspended in 10 mL of 0.85 % NaCl.

50 µL of component A (1.67 mM SYTO 9 dye/ 1.67 mM Propidium iodide solution) was added to 50 µL of component B (1.67 mM SYTO 9 dye / 18.3 mM Propidium iodide solution (both Invitrogen Detection Technologies)). 3 µL of the dye mix was then added to 1 mL of the bacterial suspension and incubated in the dark for 15 minutes.

A 2x dilution of the sample was prepared immediately before imaging using a 0.85 % NaCl solution. 5 µL of the stained and diluted bacterial sample was trapped between a glass slide and a coverslip and imaged on a Zeiss Axioimager Z1 fluorescent optical microscope at 40x magnification, through rhodium (excitation: 546/12 nm, emission: 575 – 640 nm) and FTIC (excitation: 450 – 490 nm, emission 515 – 565 nm) filters.

Controls; (1) Media, (2) Media treated with Fmoc-dipeptide (no *E. Coli*), and (3) 0.85 % NaCl solution.

8.4.16 Transmission electron microscopy (*in vivo* studies)

Carbon-coated copper grids (200 mesh) were glow discharged in air for 30 seconds. 20 µL of the bacterial sample was transferred to the support film and blotted down after 3 seconds using filter paper. Negative stain (10 µL, 0.5 % urinal acetate solution) was applied and the mixture blotted again using filter paper to remove excess. The dried specimens were then

imaged using a LEO 912 energy filtering transmission electron microscope operating at 120kV fitted with 14 bit/2 K Proscan CCD camera.

9.0 References

9.1 References

1. M. Hughes, H. Xu, P. W. J. M. Frederix, A. M. Smith, N. T. Hunt, T. Tuttle, I. A. Kinloch and R. V. Ulijn, *Soft Matter*, 2011, **7**, 10032.
2. M. Hughes, P. W. J. M. Frederix, J. Raeburn, L. S. Birchall, J. Sadownik, F. C. Coomer, I. H. Lin, E. J. Cussen, N. T. Hunt, T. Tuttle, S. J. Webb, D. J. Adams and R. V. Ulijn, *Soft Matter*, 2012, **8**, 5595.
3. M. S. Lamm, N. Sharma, K. Rajagopal, F. L. Beyer, J. P. Schneider and D. J. Pochan, *Advanced Materials*, 2008, **20**, 447.
4. N. Sharma, A. Top, K. L. Kiick and D. J. Pochan, *Angewandte Chemie-International Edition*, 2009, **48**, 7078.
5. M. Zhou, A. M. Smith, A. K. Das, N. W. Hodson, R. F. Collins, R. V. Ulijn and J. E. Gough, *Biomaterials*, 2009, **30**, 2523.
6. E. F. Banwell, E. S. Abelardo, D. J. Adams, M. A. Birchall, A. Corrigan, A. M. Donald, M. Kirkland, L. C. Serpell, M. F. Butler and D. N. Woolfson, *Nature Materials*, 2009, **8**, 596.
7. H. Shao and J. R. Parquette, *Chemical Communications*, 2010, **46**, 4285.
8. H. Xu, A. K. Das, M. Horie, M. S. Shaik, A. M. Smith, Y. Luo, X. Lu, R. Collins, S. Y. Liem, A. Song, P. L. A. Popelier, M. L. Turner, P. Xiao, I. A. Kinloch and R. V. Ulijn, *Nanoscale*, 2010, **2**, 960.
9. Y. Gao, Y. Kuang, Z.-F. Guo, Z. Guo, I. J. Krauss and B. Xu, *Journal of the American Chemical Society*, 2009, **131**, 13576.
10. G. Liang, Z. Yang, R. Zhang, L. Li, Y. Fan, Y. Kuang, Y. Gao, T. Wang, W. W. Lu and B. Xu, *Langmuir*, 2009, **25**, 8419.
11. J. Naskar, G. Palui and A. Banerjee, *Journal of Physical Chemistry B*, 2009, **113**, 11787.
12. R. V. Ulijn and A. M. Smith, *Chemical Society Reviews*, 2008, **37**, 664.
13. M. Reches and E. Gazit, *Current Nanoscience*, 2006, **2**, 105.

14. A. L. Boyle and D. N. Woolfson, *Chemical Society Reviews*, 2011, **40**, 4295.
15. M. R. Ghadiri, J. R. Granja, R. A. Milligan, D. E. McRee and N. Khazanovich, *Nature*, 1993, **366**, 324.
16. S. G. Zhang, T. Holmes, C. Lockshin and A. Rich, *Proceedings of the National Academy of Sciences of the United States of America*, 1993, **90**, 3334.
17. J. B. Guilbaud, E. Vey, S. Boothroyd, A. M. Smith, R. V. Ulijn, A. Saiani and A. F. Miller, *Langmuir*, 2010, **26**, 11297.
18. S. G. Zhang, T. C. Holmes, C. M. Dipersio, R. O. Hynes, X. Su and A. Rich, *Biomaterials*, 1995, **16**, 1385.
19. A. Aggeli, I. A. Nyrkova, M. Bell, R. Harding, L. Carrick, T. C. B. McLeish, A. N. Semenov and N. Boden, *Proceedings of the National Academy of Sciences of the United States of America*, 2001, **98**, 11857.
20. A. Aggeli, M. Bell, N. Boden, J. N. Keen, P. F. Knowles, T. C. B. McLeish, M. Pitkeathly and S. E. Radford, *Nature*, 1997, **386**, 259.
21. V. Castelletto, I. W. Hamley, P. J. F. Harris, U. Olsson and N. Spencer, *Journal of Physical Chemistry B*, 2009, **113**, 9978.
22. K. Lu, J. Jacob, P. Thiyagarajan, V. P. Conticello and D. G. Lynn, *Journal of the American Chemical Society*, 2003, **125**, 6391.
23. M. J. Krysmann, V. Castelletto, J. E. McKendrick, L. A. Clifton, I. W. Hamley, P. J. F. Harris and S. A. King, *Langmuir*, 2008, **24**, 8158.
24. S. Nautiyal, D. N. Woolfson, D. S. King and T. Alber, *Biochemistry*, 1995, **34**, 11645.
25. S. A. Potekhin, T. N. Melnik, V. Popov, N. F. Lanina, A. A. Vazina, P. Rigler, A. S. Verdini, G. Corradin and A. V. Kajava, *Chemistry & Biology*, 2001, **8**, 1025.
26. M. J. Pandya, G. M. Spooner, M. Sunde, J. R. Thorpe, A. Rodger and D. N. Woolfson, *Biochemistry*, 2000, **39**, 8728.
27. M. G. Ryadnov and D. N. Woolfson, *Nature Materials*, 2003, **2**, 329.

28. D. Papapostolou, A. M. Smith, E. D. T. Atkins, S. J. Oliver, M. G. Ryadnov, L. C. Serpell and D. N. Woolfson, *Proceedings of the National Academy of Sciences of the United States of America*, 2007, **104**, 10853.
29. A. M. Smith, R. J. Williams, C. Tang, P. Coppo, R. F. Collins, M. L. Turner, A. Saiani and R. V. Ulijn, *Advanced Materials*, 2008, **20**, 37.
30. V. Jayawarna, M. Ali, T. A. Jowitt, A. E. Miller, A. Saiani, J. E. Gough and R. V. Ulijn, *Advanced Materials*, 2006, **18**, 611.
31. C. Tang, A. M. Smith, R. F. Collins, R. V. Ulijn and A. Saiani, *Langmuir*, 2009, **25**, 9447.
32. A. Mahler, M. Reches, M. Rechter, S. Cohen and E. Gazit, *Advanced Materials*, 2006, **18**, 1365.
33. D. M. Ryan, T. M. Doran, S. B. Anderson and B. L. Nilsson, *Langmuir*, 2011, **27**, 4029.
34. S. Debnath, A. Shome, D. Das and P. K. Das, *Journal of Physical Chemistry B*, 2010, **114**, 4407.
35. L. Chen, K. Morris, A. Laybourn, D. Elias, M. R. Hicks, A. Rodger, L. Serpell and D. J. Adams, *Langmuir*, 2010, **26**, 5232.
36. E. K. Johnson, D. J. Adams and P. J. Cameron, *Journal of Materials Chemistry*, 2011, **21**, 2024.
37. G. Cheng, V. Castelletto, C. M. Moulton, G. E. Newby and I. W. Hamley, *Langmuir*, 2010, **26**, 4990.
38. D. Bardelang, F. Camerel, J. C. Margeson, D. M. Leek, M. Schmutz, M. B. Zaman, K. Yu, D. V. Soldatov, R. Ziessel, C. I. Ratcliffe and J. A. Ripmeester, *Journal of the American Chemical Society*, 2008, **130**, 3313.
39. C. Tang, R. V. Ulijn and A. Saiani, *Langmuir*, 2011, **27**, 14438.
40. Z. M. Yang, H. W. Gu, D. G. Fu, P. Gao, J. K. Lam and B. Xu, *Advanced Materials*, 2004, **16**, 1440.

41. H. Wang, C. Ren, Z. Song, L. Wang, X. Chen and Z. Yang, *Nanotechnology*, 2010, **21**, 225606.
42. H. Wang, Z. Wang, D. Song, J. Wang, J. Gao, L. Wang, D. Kong and Z. Yang, *Nanotechnology*, 2010, **21**, 155602.
43. J. Gao, W. Zheng, D. Kong and Z. Yang, *Soft Matter*, 2011, **7**, 10443.
44. Q. Wang, Z. Yang, Y. Gao, W. Ge, L. Wang and B. Xu, *Soft Matter*, 2008, **4**, 550.
45. A. K. Das, R. Collins and R. V. Ulijn, *Small*, 2008, **4**, 279.
46. A. R. Hirst, S. Roy, M. Arora, A. K. Das, N. Hodson, P. Murray, S. Marshall, N. Javid, J. Sefcik, J. Boekhoven, J. H. van Esch, S. Santabarbara, N. T. Hunt and R. V. Ulijn, *Nature Chemistry*, 2010, **2**, 1089.
47. L. Chronopoulou, S. Lorenzoni, G. Masci, M. Dentini, A. R. Togna, G. Togna, F. Bordi and C. Palocci, *Soft Matter*, 2010, **6**, 2525.
48. D. Koda, T. Maruyama, N. Minakuchi, K. Nakashima and M. Goto, *Chemical Communications*, 2010, **46**, 979.
49. Z. Yang, P.-L. Ho, G. Liang, K. H. Chow, Q. Wang, Y. Cao, Z. Guo and B. Xu, *Journal of the American Chemical Society*, 2007, **129**, 266.
50. S. Toledano, R. J. Williams, V. Jayawarna and R. V. Ulijn, *Journal of the American Chemical Society*, 2006, **128**, 1070.
51. A. K. Das, A. R. Hirst and R. V. Ulijn, *Faraday Discussions*, 2009, **143**, 293.
52. L. M. Randolph, M.-P. Chien and N. C. Gianneschi, *Chemical Science*, 2012, **3**, 1363.
53. M. E. Hahn and N. C. Gianneschi, *Chemical Communications*, 2011, **47**, 11814.
54. S. Roy and R. V. Ulijn, in *Enzymatic Polymerisation*, ed. A. R. A. H. A. Palmans, 2010, **237**, 127.
55. K. Thornton, A. M. Smith, C. L. R. Merry and R. V. Ulijn, *Biochemical Society Transactions*, 2009, **37**, 664.
56. Z. Yang, G. Liang and B. Xu, *Soft Matter*, 2007, **3**, 515.

57. R. J. Williams, R. J. Mart and R. V. Ulijn, *Biopolymers*, 2010, **94**, 107.
58. R. J. Williams, A. M. Smith, R. Collins, N. Hodson, A. K. Das and R. V. Ulijn, *Nature Nanotechnology*, 2009, **4**, 19.
59. M. Reches and E. Gazit, *Science*, 2003, **300**, 625.
60. G. A. Silva, C. Czeisler, K. L. Niece, E. Beniash, D. A. Harrington, J. A. Kessler and S. I. Stupp, *Science*, 2004, **303**, 1352.
61. M. Reches and E. Gazit, *Nano Letters*, 2004, **4**, 581.
62. R. Djalali, J. Samson and H. Matsui, *Journal of the American Chemical Society*, 2004, **126**, 7935.
63. W. Helen, P. de Leonardis, R. V. Ulijn, J. Gough and N. Tirelli, *Soft Matter*, 2011, **7**, 1732.
64. L. Chen, J. Raeburn, S. Sutton, D. G. Spiller, J. Williams, J. S. Sharp, P. C. Griffiths, R. K. Heenan, S. M. King, A. Paul, S. Fuzeland, D. Atkins and D. J. Adams, *Soft Matter*, 2011, **7**, 9721.
65. J. M. A. Carnall, C. A. Waudby, A. M. Belenguer, M. C. A. Stuart, J. J. P. Peyralans and S. Otto, *Science*, 2010, **327**, 1502.
66. X. Zhao, F. Pan, H. Xu, M. Yaseen, H. Shan, C. A. E. Hauser, S. Zhang and J. R. Lu, *Chemical Society Reviews*, 2010, **39**, 3480.
67. I. W. Hamley, *Soft Matter*, 2011, **7**, 4122.
68. M. Zelzer and R. V. Ulijn, *Chemical Society Reviews*, 2010, **39**, 3351.
69. G. E. Ozin, Arsenault, A.C, Cadematiri, L., *Nanochemistry II: A Chemical Approach to Nanomaterials*, The Royal Society of Chemistry, Cambridge, 2009.
70. E. Gazit, *Plenty of Room for Biology at the Bottom*, Imperial College Press, London, 2007.
71. J. Gao and B. Xu, *Nano Today*, 2009, **4**, 37.
72. E. Gazit, *NanoBioTechnology*, 2005, **1**, 286.

73. G. L. Hornyak, Tibbals, F., Dutta, J., Moore, J. J., *Introduction to Nanoscience and Nanotechnology*, CRC Press, Boca Raton, 2009.
74. P. C. Champe, Harvey, R. A., Ferrier, D. R., *Biochemistry*, Lippincott Williams and Wilkins, Baltimore/Philadelphia, 2005.
75. L. A. Moran, Horton, H. R., Scrimgeour, K. G., Perry, M. D., *Principles of Biochemistry*, Pearson Education Ltd., New Jersey, 2006.
76. S. G. Zhang, D. M. Marini, W. Hwang and S. Santoso, *Current Opinion in Chemical Biology*, 2002, **6**, 865.
77. L. Pauling and R. B. Corey, *Proceedings of the National Academy of Sciences of the United States of America*, 1951, **37**, 251.
78. L. Pauling, Corey, R.B., Branson, H.R., *Proceedings of the National Academy of Sciences of the United States of America*, 1951, **37**, 205.
79. F. H. C. Crick, *acta crystallograpy*, 1953, **6**, 689.
80. S. G. Zhang, *Nature Biotechnology*, 2003, **21**, 1171.
81. F. Chiti and C. M. Dobson, in *Annual Review of Biochemistry*, 2006, **75**, 333.
82. P. B. Harbury, T. Zhang, P. S. Kim and T. Alber, *Science*, 1993, **262**, 1401.
83. Z. M. Yang, G. L. Liang, L. Wang and B. Xu, *Journal of the American Chemical Society*, 2006, **128**, 3038.
84. Z. Yang, G. Liang, M. Ma, Y. Gao and B. Xu, *Small*, 2007, **3**, 558.
85. Z. M. Yang, H. W. Gu, Y. Zhang, L. Wang and B. Xu, *Chemical Communications*, 2004, **2**, 208.
86. D. J. Adams, *Macromolecular Bioscience*, 2011, **11**, 160.
87. J. D. Hartgerink, E. Beniash and S. I. Stupp, *Science*, 2001, **294**, 1684.
88. J. P. Schneider, D. J. Pochan, B. Ozbas, K. Rajagopal, L. Pakstis and J. Kretsinger, *Journal of the American Chemical Society*, 2002, **124**, 15030.

89. S. A. Stpierre and R. S. Hodges, *Biochemical and Biophysical Research Communications*, 1976, **72**, 581.
90. T. N. Melnik, V. Villard, V. Vasiliev, G. Corradin, A. V. Kajava and S. A. Potekhin, *Protein Engineering*, 2003, **16**, 1125.
91. E. Gazit, *Chemical Society Reviews*, 2007, **36**, 1263.
92. C. Valery, F. Artzner and M. Paternostre, *Soft Matter*, 2011, **7**, 9583.
93. H. A. Behanna, J. Donners, A. C. Gordon and S. I. Stupp, *Journal of the American Chemical Society*, 2005, **127**, 1193.
94. J. D. Hartgerink, E. Beniash and S. I. Stupp, *Proceedings of the National Academy of Sciences of the United States of America*, 2002, **99**, 5133.
95. S. E. Paramonov, H. W. Jun and J. D. Hartgerink, *Journal of the American Chemical Society*, 2006, **128**, 7291.
96. S. Vauthey, S. Santoso, H. Y. Gong, N. Watson and S. G. Zhang, *Proceedings of the National Academy of Sciences of the United States of America*, 2002, **99**, 5355.
97. S. Santoso, W. Hwang, H. Hartman and S. G. Zhang, *Nano Letters*, 2002, **2**, 687.
98. M. Reches and E. Gazit, *Nature Nanotechnology*, 2006, **1**, 195.
99. W. A. Petka, J. L. Harden, K. P. McGrath, D. Wirtz and D. A. Tirrell, *Science*, 1998, **281**, 389.
100. Y. Zimenkov, S. N. Dublin, R. Ni, R. S. Tu, V. Breedveld, R. P. Apkarian and V. P. Conticello, *Journal of the American Chemical Society*, 2006, **128**, 6770.
101. L. A. Haines, K. Rajagopal, B. Ozbas, D. A. Salick, D. J. Pochan and J. P. Schneider, *Journal of the American Chemical Society*, 2005, **127**, 17025.
102. Z. Yang, K. Xu, Z. Guo, Z. Guo and B. Xu, *Advanced Materials*, 2007, **19**, 3152.
103. Z. Yang, G. Liang and B. Xu, *Accounts Chem. Res.*, 2008, **41**, 315.
104. J. Gao, H. Wang, L. Wang, J. Wang, D. Kong and Z. Yang, *Journal of the American Chemical Society*, 2009, **131**, 11286.

105. S. Dos Santos, A. Chandravarkar, B. Mandal, R. Mimna, K. Murat, L. Saucedo, P. Tella, G. Tuchscherer and M. Mutter, *Journal of the American Chemical Society*, 2005, **127**, 11888.
106. K. J. C. van Bommel, M. C. A. Stuart, B. L. Feringa and J. van Esch, *Organic & Biomolecular Chemistry*, 2005, **3**, 2917.
107. P. T. Corbett, J. Leclaire, L. Vial, K. R. West, J.-L. Wietor, J. K. M. Sanders and S. Otto, *Chemical Reviews*, 2006, **106**, 3652.
108. S. J. Rowan, S. J. Cantrill, G. R. L. Cousins, J. K. M. Sanders and J. F. Stoddart, *Angewandte Chemie-International Edition*, 2002, **41**, 898.
109. E. Alsberg, E. Feinstein, M. P. Joy, M. Prentiss and D. E. Ingber, *Tissue Engineering*, 2006, **12**, 3247.
110. J. Cornelissen, A. E. Rowan, R. J. M. Nolte and N. Sommerdijk, *Chemical Reviews*, 2001, **101**, 4039.
111. P. Jonkheijm, P. van der Schoot, A. Schenning and E. W. Meijer, *Science*, 2006, **313**, 80.
112. S. A. Latt, B. Holmquist and B. L. Vallee, *Biochemical and Biophysical Research Communications*, 1969, **37**, 333.
113. F. W. Dahlquist, J. W. Long and W. L. Bigbee, *Biochemistry*, 1976, **15**, 1103.
114. M. A. Holmes and B. W. Matthews, *Journal of Molecular Biology*, 1982, **160**, 623.
115. H. Matsubar, *Biochemical and Biophysical Research Communications*, 1966, **24**, 427.
116. S. Blumberg and B. L. Vallee, *Biochemistry*, 1975, **14**, 2410.
117. B. Holmquist, S. Blumberg and B. L. Vallee, *Biochemistry*, 1976, **15**, 4675.
118. G. Morgan and J. S. Fruton, *Biochemistry*, 1978, **17**, 3562.
119. M. Pank, O. Kirret, N. Paberit and A. Aaviksaar, *Febs Letters*, 1982, **142**, 297.
120. S. I. Wayne and J. S. Fruton, *Proceedings of the National Academy of Sciences of the United States of America-Biological Sciences*, 1983, **80**, 3241.

121. M. A. Holmes and B. W. Matthews, *Biochemistry*, 1981, **20**, 6912.
122. Y. Isowa and T. Ichikawa, *Bulletin of the Chemical Society of Japan*, 1979, **52**, 796.
123. T. Oka and K. Morihara, *Journal of Biochemistry*, 1980, **88**, 807.
124. L. Haines-Butterick, K. Rajagopal, M. Branco, D. Salick, R. Rughani, M. Pilarz, M. S. Lamm, D. J. Pochan and J. P. Schneider, *Proceedings of the National Academy of Sciences of the United States of America*, 2007, **104**, 7791.
125. H. Cui, T. Muraoka, A. G. Cheetham and S. I. Stupp, *Nano Letters*, 2009, **9**, 945.
126. A. Aggeli, M. Bell, N. Boden, J. N. Keen, T. C. B. McLeish, I. Nyrkova, S. E. Radford and A. Semenov, *Journal of Materials Chemistry*, 1997, **7**, 1135.
127. D. J. Adams, K. Holtzmann, C. Schneider and M. F. Butler, *Langmuir*, 2007, **23**, 12729.
128. S. Matsumura, S. Uemura and H. Mihara, *Chemistry-a European Journal*, 2004, **10**, 2789.
129. K. T. Nam, S. A. Shelby, P. H. Choi, A. B. Marciel, R. Chen, L. Tan, T. K. Chu, R. A. Mesch, B.-C. Lee, M. D. Connolly, C. Kisielowski and R. N. Zuckermann, *Nature Materials*, 2010, **9**, 454.
130. A. Barth and C. Zscherp, *Quarterly Reviews of Biophysics*, 2002, **35**, 369.
131. H. Yokoi, T. Kinoshita and S. G. Zhang, *Proceedings of the National Academy of Sciences of the United States of America*, 2005, **102**, 8414.
132. P. Zhu, X. Yan, Y. Su, Y. Yang and J. Li, *Chemistry-a European Journal*, 2010, **16**, 3176.
133. W. Wang and Y. Chau, *Soft Matter*, 2009, **5**, 4893.
134. R. de La Rica, K. I. Fabijanic, A. Baldi and H. Matsui, *Angewandte Chemie-International Edition*, 2010, **49**, 1447.
135. F. Patolsky, Y. Weizmann and I. Willner, *Nature Materials*, 2004, **3**, 692.
136. N. Ostrov and E. Gazit, *Angewandte Chemie-International Edition*, 2010, **49**, 3018.

137. T. Lefevre and M. Subirade, *International Journal of Food Science and Technology*, 1999, **34**, 419.
138. A. J. Geddes, K. D. Parker, E. D. T. Atkins and E. Beighton, *Journal of Molecular Biology*, 1968, **32**, 343.
139. C. L. Ruben Diaz-Avalos, Eric Fontano, Melinda Balbirnie, Robert Grothe, David Eisenberg, Donald D.L. Caspar, *Fibre Diffraction Review*, 2003, **11**, 79.
140. K. Halverson, P. E. Fraser, D. A. Kirschner and P. T. Lansbury, *Biochemistry*, 1990, **29**, 2639.
141. E. D. Eanes and G. G. Glenner, *Journal of Histochemistry & Cytochemistry*, 1968, **16**, 673.
142. D. J. Adams, L. M. Mullen, M. Berta, L. Chen and W. J. Frith, *Soft Matter*, 2010, **6**, 1971.
143. M. Philipp and M. L. Bender, *Molecular and Cellular Biochemistry*, 1983, **51**, 5.
144. R. Bott, M. Ultsch, A. Kossiakoff, T. Graycar, B. Katz and S. Power, *Journal of Biological Chemistry*, 1988, **263**, 7895.
145. J. D. Robertus, R. A. Alden, J. J. Birktoft and J. Kraut, *Biochemistry*, 1972, **11**, 4293.
146. C. R. Martinez and B. L. Iverson, *Chemical Science*, 2012, DOI: 10.1039/C2SC20045G.
147. L. S. Birchall, S. Roy, V. Jayawarna, M. Hughes, E. Irvine, G. T. Okorogheye, N. Saudi, E. De Santis, T. Tuttle, A. A. Edwards and R. V. Ulijn, *Chemical Science*, 2011, **2**, 1349.
148. Z. M. Yang, G. L. Liang, M. L. Ma, Y. Gao and B. Xu, *Small*, 2007, **3**, 558.
149. Z. Yang, G. Liang, Z. Guo, Z. Guo and B. Xu, *Angewandte Chemie-International Edition*, 2007, **46**, 8216.
150. H. Csopak, G. Garellick and B. Hallberg, *Acta Chemica Scandinavica*, 1972, **26**, 2401.
151. Chappelle.D, M. Iwatsubo and Lazdunsk.M, *Biochemistry*, 1974, **13**, 3754.
152. H. N. Fernley, *Nature-New Biology*, 1973, **241**, 110.

153. B. Stec, K. M. Holtz and E. R. Kantrowitz, *Journal of Molecular Biology*, 2000, **299**, 1303.
154. J. W. Sadownik, J. Leckie and R. V. Ulijn, *Chemical Communications*, 2011, **47**, 728.
155. V. Worthington, *Worthington Enzyme Manual*, Worthington Biochemical Corporation, Lakewood, 1993.
156. M. A. Thompson, WA Planaria Software LLC, Seattle, 2004.
157. J. C. Phillips, R. Braun, W. Wang, J. Gumbart, E. Tajkhorshid, E. Villa, C. Chipot, R. D. Skeel, L. Kale and K. Schulten, *Journal of Computational Chemistry*, 2005, **26**, 1781.
158. B. R. Brooks, C. L. Brooks, III, A. D. Mackerell, Jr., L. Nilsson, R. J. Petrella, B. Roux, Y. Won, G. Archontis, C. Bartels, S. Boresch, A. Caflich, L. Caves, Q. Cui, A. R. Dinner, M. Feig, S. Fischer, J. Gao, M. Hodoscek, W. Im, K. Kuczera, T. Lazaridis, J. Ma, V. Ovchinnikov, E. Paci, R. W. Pastor, C. B. Post, J. Z. Pu, M. Schaefer, B. Tidor, R. M. Venable, H. L. Woodcock, X. Wu, W. Yang, D. M. York and M. Karplus, *Journal of Computational Chemistry*, 2009, **30**, 1545.
159. W. Humphrey, A. Dalke and K. Schulten, *Journal of Molecular Graphics*, 1996, **14**, 33.

Appendices

Appendix I – List of abbreviations

Ac	acetyl
ACN	acetonitrile
AP	alkaline phosphatase
ATP	Adenosine-5'-triphosphate
cryoTEM	cryo-transmission electron microscopy
DCL	dynamic combinatorial library
DIPEA	N,N-Diisopropylethylamine
DMSO	dimethyl sulfoxide
E.Coli	escherichia coli
Fmoc	fluorenyl-9-methoxycarbonyl
HBTU	O-Benzotriazole-N,N,N',N'-tetramethyl-uronium-hexafluoro-phosphate
HPLC	high performance liquid chromatography
MMP-7	matrix metalloproteinase-7
Nap	naphthalene
NDI	1,4,5,8-naphthalenetetracarboxylic acid diimide
OMe	methyl ester
Pal	palmitoyl
PEG	polyethylene glycol
PNP	para-nitrophenyl phosphate
TEM	transmission electron microscopy

TFA	trifluoroacetic acid
Tris	tris(hydroxymethyl)aminomethane
WAXS	wide angle x-ray scattering

Appendix 2 – List of amino acid abbreviations

Amino Acid	1 Letter Code	3 Letter Code
valine	V	Val
tyrosine	Y	Tyr
tryptophan	W	Trp
threonine	T	Thr
serine	S	Ser
proline	P	Pro
phenylalanine	F	Phe
methionine	M	Met
lysine	K	Lys
leucine	L	Leu
isoleucine	I	Ile
histadine	H	His
glycine	G	Gly
glutamine	Q	Gln
glutamic acid	E	Glu
cysteine	C	Cys
aspartic acid	D	Asp
asparagine	N	Asn
arginine	R	Arg
alanine	A	Ala

